Ventilative Cooling

by

Guilherme Carrilho da Graça

Licenciado in Engineering Physics
Instituto Superior Técnico, Lisbon, Portugal, 1995

Submitted to the Department of Architecture in
Partial Fulfillment of the Requirements for the
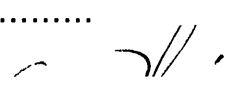Degree of

Master of Science in Building Technology

at the

Massachusetts Institute of Technology

June 1999

Signature of Author ....

Department of Architecture
May 07, 1999

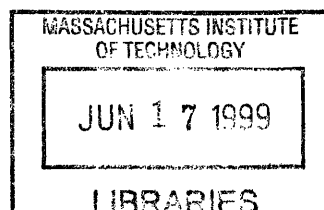Certified by ....

Qingyan Chen
Associate Professor of Building Technology
sis Supervisor

Accepted by ....

Stanford Anderson
Chairman, Department Committee on Graduate Students
Head, Department of Architecture

1

Ventilative Cooling

by

Guilherme Carrilho da Graça

Submitted to the Department of Architecture

on May 7, 1999 in Partial Fulfillment of the
Requirements for the Degree of

Master of Science in Building Technology

Abstract

This thesis evaluates the performance of daytime and nighttime passive ventilation cooling strategies for Beijing, Shanghai and Tokyo. A new simulation method for cross-ventilated wind driven airflow is presented. This method decouples the airflow model from the thermal model allowing for fast real weather simulation of the building thermal performance.

The simulation is performed on a six-story, isolated, suburban apartment building, considered to be typical of the three cities. The performance of the two natural ventilation strategies on this building is compared. The impact on the performance of different types of construction is assessed for the night cooling ventilation strategy.

The results show that night cooling is superior to daytime ventilative cooling in the three cities. Night cooling can successfully replace air conditioning systems for a significant part of the cooling season in Beijing and Tokyo. For Shanghai, neither of the two passive ventilation systems can be considered successful. In both Beijing and Tokyo the application of night cooling may cause condensation in partitions. The use of heavyweight partitions does not show a noticeable improvement over normal construction (using 10cm concrete partitions). On the other hand, the lightweight case shows a noticeable degradation in system performance. Therefore, the normal structural system is the best option. The use of carpet has a very negative impact on night cooling performance, and is therefore not advised.

Thesis Supervisor: Qingyan Chen
Title: Associate Professor of Building Technology

Acknowledgments

To Rita.

Table of Contends.

Introduction

One of the functions of a residential building is to protect its occupants from the climate. Because of this protected environment, buildings also tend to contain the internally generated heat as well as the solar and conductive heat gained through the façade. In the warmer months of the year, this generally leads to overheating, creating a need for a cooling system. Active cooling systems require a large energy input. One way of avoiding this energy expense is to use naturally driven cooling systems. One of the most common techniques is wind driven passive cooling.

In many areas of the globe, the potential to use wind-driven cooling of buildings is not fully explored. From a situation where buildings had to be designed in harmony with their surroundings we, in many cases, evolved into highly energy-inefficient designs. The same energy intensive design concepts, such as the glass façade tower, were applied independently of the climate. This design approach was made possible through the widespread use of HVAC equipement. These systems can ensure adequate temperature and humidity levels independently of outside conditions. The use of these systems largely contributes to the increased energy consumption and running costs of today's buildings.

There is a need to understand the process of wind driven ventilative cooling. A better understanding of the phenomena involved should lead to a more widespread use of these systems. This would reduce the environmental impact of building cooling.

This thesis presents a study of the performance of two wind-driven ventilative cooling strategies when applied to a six-story apartment building in three different locations in Asia. The passive cooling techniques studied are daytime wind-driven ventilation and nighttime wind-driven structural cooling. Detailed models are used to predict the response of the three components of the system: thermal response of the building structure, ventilation performance and occupant thermal comfort.

The work presented here was developed in the context of the "Energy-Efficient Buildings in Developing Countries" and "Tokyo Half Emissions" projects. One common goal of these two projects is to reduce the emission of energy production related pollutants into the atmosphere. One way of achieving this goal is to reduce the cooling energy need of buildings.

This study is done for three cities, two in China (Beijing and Shanghai) and one in Japan (Tokyo). These two countries are in different stages of economic development. China is currently undergoing a phase of strong economic development. As part of this development effort, considerable construction is occurring, and will continue to occur as more Chinese families move to the city suburbs. This high construction volume creates both a need and an opportunity to promote and implement energy efficient buildings. China is responsible for one quarter of the world coal consumption (ASHRAE 1997). More effective energy use in Chinese buildings will have a positive impact on the local economy (lower investments in energy). Also the earth's environment will benefit from lower emissions of energy production related pollutants (residential and commercial buildings represent 20% of the US energy consumption, ASHRAE 1997).).

Tokyo is one of the largest cities in the world. It has several problems directly related to its dimension and activity level: pollution, heat island effect, construction density, etc. The use of air conditioning in buildings is quite generalized. This is due both to high living standards and to the fact that in, the summer months, high temperature (32°C) and relative humidity levels (90%) can occur.

In the following paragraphs, a description of several passive-cooling systems is presented. The choice to do a detailed study of the performance of two of these systems studied is then justified.

In the warmer months of the year, buildings generally need a cooling system in order to achieve acceptable comfort conditions. This need is due to the effect of one or more of the following heat sources:

-Internal heat sources, such as: occupants, lighting systems and appliances (for a four persons apartment unit these gains are typically around 600W).
- Heat gains through the building envelope. These gains are due to conduction and convection with the outside and to absorption of solar radiation.
-Heat gains by ventilation.
-Direct solar heat gains by fenestration (direct solar gains can be as high as 800 W/m^2).

In order to remove these heat gains it is necessary to use at least one of the heat sinks available in nature. These are: the atmosphere, the ground and large water masses (rivers, ponds underground water etc...). These heat sinks have a large heat capacity and a temperature lower than the building (in the case of the atmosphere this may only occur during the night). Passive cooling strategies accomplish the transfer of internal energy into these heat sinks with limited or no use of mechanical systems.

Passive cooling systems can be grouped into five main types (adapted from Givoni 1994):

Comfort Ventilation (or Daytime Ventilation). This is the most common passive cooling strategy. Thermal comfort is obtained by increased convective heat removal in the warmer hours of the day. This is done using outside air that goes through the building. Generally, the air movement is wind-driven although stack effect ventilation and simple fan assisted systems also belong to this group. In order for this strategy to be effective, outside air cannot be too hot (above 32°C) or too humid (above 80%). In this system, the atmosphere is the cooling source.

Nighttime Ventilative Cooling (also named Night Cooling). In this type of system, cold night air (around 18-22°C) is circulated through the building. The building structure is consecutively cooled during the night and is a heat sink for the internal gains during the day. In this system, the atmosphere is again the heat sink and the building structure is an intermediate medium.

Radiative Cooling. In this case, long-wave radiative heat exchange with the night sky is the cooling mechanism. Again, this is a system that releases heat to the atmosphere during the night.

Ground Coupled Cooling. In this system, the soil is used as heat sink. This cooling method takes advantage of the relatively low and stable soil temperature. These systems usually have an active heat exchanger between the building and the cooler soil.

Evaporative Cooling. These systems cool the air by increasing its water content. The air provides the latent heat of evaporation and therefore lowers its temperature. This system is not adequate for humid climates due to the reduced ability of high relative humidity air to absorb water. Also further increasing the high humidity levels that already exist will cause thermal discomfort.

All of these passive-cooling techniques, when applicable, have several advantages when compared to mechanical cooling systems: low energy spending, low maintenance requirements, low construction costs and low environmental impact.

In theory, all the passive cooling systems mentioned could be applied to the cities studied. Still, some should be expected to be more effective and therefore were chosen for this study.

The use of evaporative cooling is limited by the rather high humidity levels (in the majority of days above 70%, reaching peaks above 95% during humidity waves) encountered in these climates. These systems become almost ineffective during humidity waves (for this type of climate these are some of the periods of greater

heat stress). The application of radiant cooling systems to apartment buildings is very hard. A large surface must be exposed to the sky in order for significant heat transfer to occur. Usually this surface is the roof. This imposes a geometry constraint that makes the system only usable in low-rise buildings. Ground coupled passive cooling can be a rather expensive option. This is due to high construction costs. There is also a need for an active heat exchanger system in order to dump heat into the ground. In this case, it can be more cost effective to use ground-coupled heat pumps since they require smaller heat exchangers (both with the ground and with the room air).

The last two passive cooling options are ventilative cooling and night cooling. Both have a low implementation cost due to the simplicity of operation. The only specific needs for applying these techniques is a building plan with possibility for cross ventilation as well as large operable windows. Still, one obvious problem with the two approaches is their dependence on the ventilation level of the building and on the wind potential available. If enough airflow cannot be obtained (either during the night or during the day) then these systems will not function. As we know, the ventilation levels obtained in a building depend not only on its particular geometry but also on the building location and microclimate.

One positive point when applying a night cooling system in China is the fact that Chinese buildings traditionally have heavy internal partitions. In Japan, ventilative cooling has been used for many centuries. Naturally ventilated open designs are common in traditional houses. In all the three cities studied, apartment buildings are the most common residential building type. Six stories is the height limit for buildings with no elevator in China. The cost of the elevator is important in the building budgets in China. For this reason, there are a large number of low-rise six story apartment buildings in China. In order to increase the generality of this work a six-story building was studied. The goal of this study is then to understand whether daytime ventilative cooling and night cooling can be effective in removing the heat load for an apartment building.

These two passive strategies differ in their use of thermal mass and sensitivity to daytime outdoor temperature. In figure 1 (see next page), we can see the basic operation procedure for a night cooling strategy. This passive strategy takes advantage of the lower temperature of the outside night air to cool the building

thermal mass. The cooled walls then function as heat sinks during the day, absorbing the internal heat gains. In order to reduce the heat gains during the day, the windows should be kept closed. During the day, outside air infiltration (for a leaky house, 1.5 ACH/hour) is usually sufficient to provide adequate amounts of fresh air (10 l/s per occupant, ASHRAE (1997)). The occupant cooling effect that is provided by this system has two sources. One is the increased radiative heat transfer with the cooler high thermal mass elements. The other source is increased convective heat exchange with inside air that is cooled by the cold high thermal mass elements. In order to make this system more effective, indoor air circulation and mixing should be promoted during the day (one good way

Night Time

Walls Release Heat, Maximum Ventilation

Day Time

Walls Absorb Heat, Minimum Ventilation

Figure 1.

The two modes of a night cooling strategy

of promote this circulation is to use ceiling fans). The higher the difference between day and night the more effective this passive cooling system will be. For this system to be effective the night air temperature must be below 23°C. If the night air temperature is too high the system will perform poorly since the walls cannot release the heat accumulated during the day.

Compared with night cooling, comfort ventilation is simpler to implement. In this strategy, outside air is used to remove the internal heat load and to cool the occupants (see figure 2). In order to use this strategy, we must have mild outside temperature. If the outside temperature is too high, the convective internal gains can still be removed. However, the warm air will heat up the building and cause discomfort to the occupants. The cooling effect is obtained from increased convective and evaporative heat loss. Indoor velocities as high as 2 m/s can be
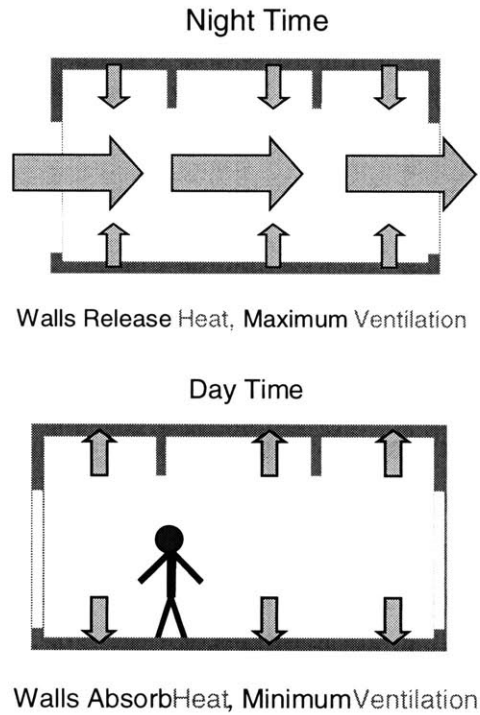
16

used in these systems (Givoni (1998), in a field study in Japan, Tanabe (1988), found a preferred velocity of 1.6 m/s).

Passive cooling systems are dependent on outside whether conditions and can only handle a limited heat load. Therefore, to successfully apply these cooling strategies the internal gains should be as low as possible and the wall and floor surfaces (the high thermal mass elements) should be fully exposed to nighttime airflow.

Air Flow Removes Heat From the Occupants

Figure 2.

Day Time Comfort Ventilation

One way of achieving this is by using properly designed external shading devices. External shading can eliminate more than 50% of the direct solar gains (depending on the shading system).

We have now seen how the two ventilative cooling strategies work and why it is important to study their performance for our application case. We now proceed to describe the analysis methodology used. The present work builds on previous research on several aspects of building and passive cooling systems simulation.

Research in low energy buildings had a great boost after the energy crisis in the mid-1970s. In the late 70s and early eighties there was an increased interest on passive architecture in the US (see the work of Givoni (1994) and Chandra (1984)). In Europe a major research effort was recently completed (the PASCOOL project, as reviewed by Santamouris, 1997). As a product of the research developed all over the world in night cooling techniques many purpose designed software tools are available. Balaras (1996) presents an extensive review of these tools. All of the reviewed tools are intended to be used in an early phase of passive ventilation systems design. They provide fast results and require reduced data input (see part 1.3 for further details). Their reduced level of precision makes them inadequate for the present study. It should be pointed that for stack driven ventilation, and as long as the correct semi-empirical coefficients are provided, very close prediction of temperature variation in a day (within 1.5 K precision) can be obtained with simple modeling tools. One good example is LESOCOOL (Van der Maas, (1991) and Roulet and Florentzou, (1997)). The problem with this particular tool is the need to
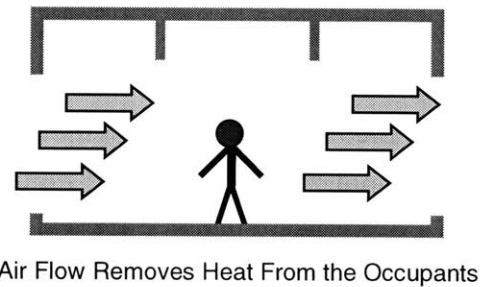
provide the right area of thermal mass surface that is exposed to the flow field. This is almost impossible to do, for most users in most cases, since the stagnant flow areas depend on the airflow pattern, which is unknown. In addition, limitations in the analytical model used to predict thermal mass heat storage interdicts the use of this tool short analysis periods (a maximum of three or four-days). It is important to be able to test passive systems using real weather for long periods. Only in this way is it possible to effectively assess the impact of these cooling strategies, specifically in handling the warm days or weeks of the year.

For the reasons mentioned above simple tools are not adequate for the present study. A high level of precision is necessary in order to accurately predict the performance of the two passive ventilative cooling systems.

On the other end of the precision spectrum, we find a set of more precise building thermal analysis tools (such as DOE, BLAST, TRNSYS, etc.) that could be used for this study. Still, in order to adequately model the convective heat removal from each wall, considerable adaptation of the source code would be necessary. In this context, the choice was made to use a simple, case-specific thermal code.

In a very interesting study on ventilative cooling, Kammerud (1984) uses one of these detailed thermal programs (BLAST v3.0) to study the advantages of using a night ventilation strategy for a typical house in several locations of the US. He points out two main problems encountered in his work: difficulty in modeling the natural ventilation flow in the building and consequent incorrect estimation of the convective heat transfer coefficients (these coefficients depend on the flow velocity). Due to this difficulty, he supposed fan-assisted airflow. The accurate study of the ventilation performance of the building that is done in the present work tries to address the first problem. A detailed numerical approach (computational fluid dynamics, CFD) is used to predict the airflow in and around the building. The use of an experimentally obtained correlation (Chandra, 1984) for the convective heat transfer coefficients addresses the second problem. The use of this correlation is possible due to the increased precision provided by CFD. In this way, more precise modeling of the convective heat transfer is possible.

For the ventilative cooling system, the prediction of the airflow field is even more crucial. In this system, occupant cooling is done by convective heat transfer between the body and wind driven airflow. The thermal behavior of the structure is

18

also important but the prediction of the indoor air velocities for given outside wind conditions is the main component. Therefore, particular attention is dedicated in this study to the ventilation analysis method.

A CFD program (PHOENICS v.3.1) is used to predict the flow in the apartment units for given wind conditions on an hourly basis. The increased precision in the airflow prediction is then used to improve the accuracy of the convective heat transfer coefficients as well as the comfort level predictions (airflow velocities are predicted inside the apartments using a grid accuracy of approximately 0.5 meters).

Increasing the precision and reliability of the analysis methods is a fundamental step in increasing the use of passive ventilative cooling techniques. One of the arguments for the use of mechanical cooling systems is their reliability. Due to the uncertainty of wind conditions and the complexity of modeling cross ventilation airflow, passive ventilation systems are more complex to design. Generally, their performance is considered more unreliable. The analysis methods that have been used so far for ventilative cooling are too simple and inaccurate and cannot provide accurate predictions. One example is the simple aperture equation models that are commonly used. These models can be very imprecise (100% difference) even for the simplest single room cases (Persily (1986)). The precision of the CFD approach used in this study has been conformed in several cases (predictions are within 20% of measured cases, see review in part 1.3). It should allow for a more reliable result that can contribute to the more widespread use of ventilative cooling systems.

This thesis is composed of two parts: part one introduces the basic modeling approaches and procedures used in predicting ventilative cooling performance, part two presents the results of the application of ventilative cooling strategies to three cities in Asia.

Part one is subdivided in four sections: the first section describes the physical processes governing building thermal response as well as the assumptions used in the modeling process. The second section introduces the basic concepts used in predicting occupant thermal comfort. Both the adaptive and Fanger comfort theories are presented and briefly compared. The third section, several approaches used to model building ventilation are described and the use of CFD for the present analysis is discussed. Finally, in section 1.4 the integrated model used in this

analysis is presented. The details of the integration between the models presented in the previous sections are described.

Part two is divided in three sections. The first section presents an analysis of the climate conditions of the three locations studied. In the second section, the case being studied is described, as well as the variations considered. In section four the

results of the analysis are presented. This thesis finally presents two Low-Energy Systems that can be Used for Lowering Temperatures in Summer.

Part I

In order to predict the efficiency of the two passive cooling systems it is essential to accurately model the building thermal response to outdoor climate conditions and internal heat loads. This thermal response, in conjunction with the thermal comfort and ventilation models (to be presented in parts 1.2 and 1.3 respectively), will determine when there is need for cooling, and how high is this need. If the analysis determines that there is no need for cooling the passive systems can be considered successful in replacing mechanical cooling systems.

1.1-Building Thermal Response.

In this section, the fundamental concepts involved in modeling building thermal response are presented. The components of the building thermal model used for this study are described.

The three modes of heat transfer (conduction, convection and radiation) are present in a building. They all influence the building thermal performance, in conjunction with the geometry and properties of the building envelope and internal partitions. Accurate modeling of the three heat transfer modes is then essential to successfully predict a building's thermal response. Detailed modeling of radiative heat transfer allows us to correctly take into account the solar heat gains as well as the radiative exchange between internal partition elements. Conduction heat exchange occurs in the façade and in the process of heat storage in the building thermal mass. Finally, the heat transfer between the air and the building elements (walls

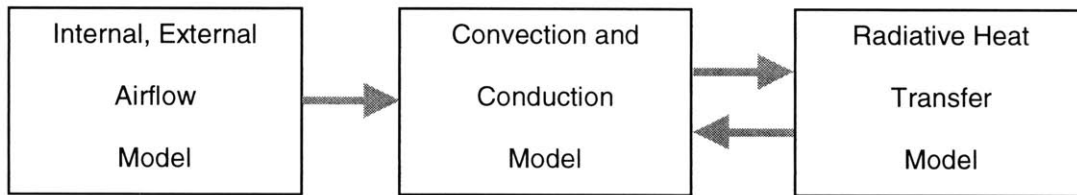| Internal, External Airflow Model		Convection and Conduction Model		Radiative Heat Transfer Model

Figure 1.1.1

Three main components of the building thermal response model

floors and windows) is mainly convective and highly dependent on the air flow characteristics (velocity and turbulence level). Convective and radiative heat transfer processes are also responsible for the interaction between the occupants and the building (skin mass transfer is also an important factor in this interaction, see part 1.2). Finally, the lighting and equipment heat gains are transmitted to the building through conduction, convection and radiation.

Building thermal behavior influences night cooling and daytime ventilation in different ways. Of the two ventilative cooling systems, night cooling is the most sensitive to the thermal behavior of the building. Performance of a night cooling strategy is deeply interrelated with the building's thermal mass. Success is achieved when this thermal mass is cold enough after the night hours so that it can absorb the daytime heat gains. Daytime heat removal by natural ventilation is less dependent on the building thermal mass and more sensitive on the outdoor climate conditions that exist when the building temperature goes above comfort level. In this case, the airflow field is more important because airflow is the main cooling source.

For both passive-cooling systems, the interaction between the different physical phenomena described above plays an important role. The process of modeling the coupled behavior of these phenomena can be divided in three main components: conduction and heat storage in the building fabric, radiative exchange and airflow. In figure 1.1.1 (above), we can see these three main components of the building thermal response model.

These three components exchange information in the way depicted by the gray arrows in the figure. The airflow model supplies flow conditions to the thermal model and is considered to be independent of the thermal conditions (see part 1.3 for details). This approximation is possible because for the design analyzed there are no vertical connections between the units. The flow is wind dominated and mostly horizontal (the opposite case would be the vertical, buoyancy dominated, flow that occurs in a chimney). The airflow can then be modeled as isothermal. The goal being to obtain the air change rates and the velocities near the surfaces of the building structure. These flow rates and near wall velocities greatly influence the conduction and heat storage process. This approximation is consistent with the experimental results of Chandra (1984). The correlation obtained by this researcher will be used to model the convective heat transfer process that occurs at the walls.

The radiative heat transfer model is presented as a single box in the figure. There are two components in this model. They address radiative exchange in two parts of the spectrum: the short wave (which is present due to the solar gains) and the infrared. The short wave part of the radiation exchange model only gives information to the convection and heat conduction/thermal storage model (in this case the gains due to solar radiation for each surface of the building). The infrared part of the radiative heat transfer model has two way information exchanges with the thermal model. Infrared energy emission by the internal surfaces depends on their temperature (arrow pointing to the right in figure 1.1.1) and their infrared radiative exchange is calculated by the radiative exchange model (arrow pointing to the left in figure 1.1.1).

The center and the right hand side boxes in figure 1.1.1 form the thermal part of the model used in this study. This section presents the thermal part of the model and is divided in three subsections. In subsection 1.1.1, the convective and conductive heat transfer processes are described. In subsection 1.1.2, the radiative heat transfer model is presented. Finally, in subsection 1.1.3, the way in which the internal heat gains are modeled is explained. The internal gains are both convective and radiative.

It is useful to present here an overview of the first part of this thesis. In section 1.2 the model used for human comfort prediction is explained. In section 1.3, the model used for internal and external airflow (computational fluid dynamics, using the K-ϵ turbulence model) is described.

Finally, in section 1.4 the interaction between the three main components of the physical model with the thermal comfort model is explained. The incorporation of outside weather conditions in the model is described. The general sequence of calculation of the coupled model is presented and discussed.

1.1.1-Modeling Conduction Heat Transfer and Heat Storage.

When modeling heat conduction processes in a building structure it is generally adequate to use a one-dimensional heat flow approximation. This simplification is acceptable because the building internal partitions and envelope elements (floors, walls doors and windows) have two dimensions much larger than the third (their thickness). If the surfaces of these partition and envelope elements are isothermal, then conduction heat transfer processes can be modeled as occurring only in the third direction (thickness). Heat transfer is then one dimensional (see figure 1.1.2).

Many different numerical calculation methods and tools can be applied to building thermal simulation. These methods are usually based on three different approaches: finite difference or finite element discretization of the heat equation, wall transfer function methods (using convolution principles and z-transforms), and finally, a set of simpler methods, that use more approximations and pre-calculated transient thermal response (in some cases thermal inertia is ignored). These simple methods are only accurate for lightweight buildings, where thermal storage phenomena are not important in their thermal response.

In this study, finite difference discretization of the one-dimensional heat equation is used. This method was chosen because it is easy to implement, robust and can be as precise as necessary (see comparison between the finite difference code used and the semi-infinite in appendix A). This numerical approach is
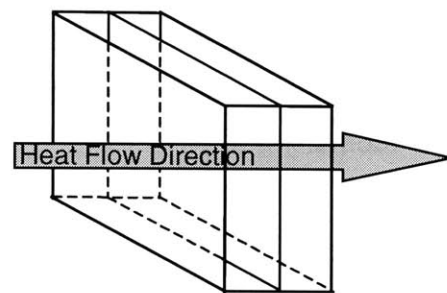

Figure 1.1.2

The one-dimensional approximation to heat transfer. This approximation is adequate for flat partition elements.

more versatile and easy to use than the other methods mentioned. Due to the increased availability of computer power, this approach is becoming increasingly popular (see, for example, Blomberg (1996)).

When using this numerical approach to predict transient thermal response there are two possible numerical solution methods: explicit or implicit. The explicit method is simpler to implement since it requires no iterations, the solution being obtained by sequentially calculating the system temperatures in time steps. This method is computationally more demanding than the implicit method (which uses iteration to reach the solution for each time step) since a small time step is required in order to achieve stability (see equation 1.1.4 below). In the implicit method, much larger time steps can be used, but the solution process is more complex, the method not having a clear stability condition like the explicit method.

In this study, the explicit method is used. The choice of this method was based on two criteria: it is straightforward to implement and calculation time is not a critical factor.

The application of this one-dimensional approach to model wall thermal storage and conduction in a building has the underlying approximation that each partition or floor in a room has an isothermal surface. This approximation can fail in several situations:

There are non-uniform radiative gains in different parts of the wall (in a building this will occur when there are direct solar gains through the windows). In section 2.2 we can see that for the cases under study the windows have external shading that prevents direct solar gains into the rooms.

One part of the wall is exposed to very high thermal gains. In our case strong internal heat sources are not expected to be present.

High thermal stratification occurs inside a room. In this case, the surface can be subject to varying conduction boundary conditions in the vertical direction. In the case being studied stagnation does not occur except for

26

some windless hours in the nighttime (during the day ceiling fans are used, see part 2.2).

We now present the details of the application of this method to this study. The expressions presented below were taken from Mills (1996). Adaptations were done whenever necessary.

When using this method to model building thermal conduction the walls and floors are divided in layers of small thickness (in this case 0.02m). If we consider a finite wall or floor layer of width Δx (see figure 1.1.3), the increase in energy (ΔU) per square meter due to the heat flux Q in the time interval Δt is:

$$\Delta U = \dot{Q}\Delta t \quad 1.1.1$$

This increase in internal energy implies a temperature increase at point m between time steps i and i+1 (ρ is the air density and c is the thermal capacity of air):

$$\Delta U = \rho c(\Delta x)(T_m^{i+1} - T_m^i) \quad 1.1.2$$

Figure 1.1.3

Finite layer notation used for one dimensional heat transfer numerical calculation.

The conduction fluxes form the East and West faces (labeled I_E and I_W in the expression) of the layer are given by (k is the thermal conductivity):

$$\dot{Q}_x \, I_W \, \Delta t = -k(T_m^i - T_{m-1}^i)\Delta x^{-1}\Delta t$$

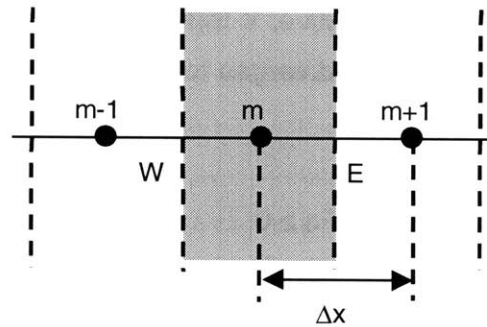$$\dot{Q}_x \, I_E \, \Delta t = -k(T_{m+1}^i - T_m^i)\Delta x^{-1}\Delta t \quad 1.1.3$$

Dividing equation 1.1.3 by Δt and using equations 1.1.1 and 1.1.2 we obtain:

$$T_m^{i+1} = Fo(T_{m-1}^i + T_{m+1}^i) + (1 - 2Fo)T_m^i$$

$$Fo = \alpha \Delta t / \Delta x^2 \qquad 1.1.4$$

This is the explicit formula for the temperature of node m at time step i+1. This temperature is a function of the surrounding temperatures and the temperature in that point in the previous time step. This expression is used in all the inner wall points in the building structure thermal analysis model.

By analyzing equation 1.1.4, we realize that for this numerical method to be numerically stable, the factor that multiplies the previous time step temperature must be positive. If this factor becomes negative numerical oscillations appear and the solution diverges to infinite values. Therefore, we have to observe the following criterion:

$$1 - 2Fo \geq 0 \qquad 1.1.5$$

In a building, a surface is normally subject to a boundary condition composed of a two parts:

A radiative heat flux (due to solar gains and infrared radiation exchange, see the next subsection).

A conductive and convective heat flux (a single coefficient is used for the two processes, using a correlation that spans from stagnation to surface velocities of 3 m/s, see section 2.2 for more details).

A point at the surface of a wall or floor (see figure 1.1.4, point T_0), subject to a convective boundary condition (in our case the room air, with temperature T_{Air} and convective heat transfer coefficient h_c) and a known heat flux (q_s^i, the solar heat gain plus the radiative transfer from the other surfaces), we have the following explicit formula for the temperature of node m at time step i+1:

$$T_0^{i+1} = 2Fo(T_1^i + BiT_{Air}^i + q_s^i \Delta x / k) + (1 - 2Fo - 2FoBi)T_0^i, \; Bi = h_c \Delta x / k \qquad 1.1.6$$

For this case, the stability criteria is again obtained by forcing the second term on the right-hand side of the equation to be always positive:

$$Fo \le (2(1 + Bi))^{-1} \qquad 1.1.7$$

Equation 1.1.6 is the basic formula used for the boundary conditions in the internal partitions.
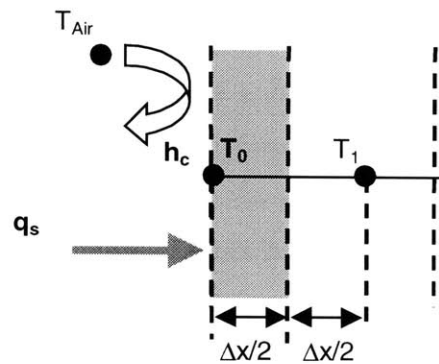
Figure 1.1.4
Simultaneous convective and radiative heat flux boundary condition.

Convective heat transfer coefficient: h_c.
Radiative heat flux: q_s.

1.1.2-Radiative Heat Transfer

The previous section presented the numerical heat transfer approach used in this study. Radiative heat transfer, in conjunction with conduction and convection, is responsible for the heat transfer between the several building envelope and internal partition elements.

Radiative heat transfer in a building occurs between the structural elements, the windows and furniture. All the building components exchange thermal radiation. Besides this radiative exchange, there are also the solar radiative gains that enter through the windows. This radiation can be direct and diffuse or just diffuse in case the windows are shaded.

Shading is one of the most effective summer energy saving measures. A properly designed external shading system can avoid most of the direct solar gains. In this case, the windows can be approximated as diffuse light sources. The radiative gain is then much smaller (for the building in this study, it is typically 40% smaller). Still this gain is important and must be correctly accounted for.

In a typical case, light entering a room will encounter a building internal surface where it will be partially absorbed by the building material, the rest of the radiation being reflected. This reflected radiation will hit another building element and again be partially absorbed and reflected. This complex process can be accurately modeled using the energy balance method described below.

The application of the energy balance method makes use of several theoretical concepts:

J - radiosity, is all the radiation that comes from a body (in the case of a wall, J will be the sum of its thermal emissions plus the reflected radiation).

G - irradiation, is all the radiation that a surface is exposed to (due to emission and reflection from the other surfaces).

F_{ij}- view factor between surface i and surface j.

E_{bi} - the black body emissive power of surface i. This emission is usually called thermal radiation. It is proportional to the fourth power of the object's temperature (in kelvin) according to the following expression:

$$E_{bi}(T) = \varepsilon \sigma T^4 \qquad 1.1.8$$

Where ε is the infrared emissivity of the object and σ is the Stefan-Boltzmann constant.

Using these definitions, the radiation that goes into surface i from all other surfaces in a room is given by:

$$G_i = \sum_{k=1}^{n} J_k F_{ik} \qquad 1.1.9$$

The radiation that is emitted by surface i is then:
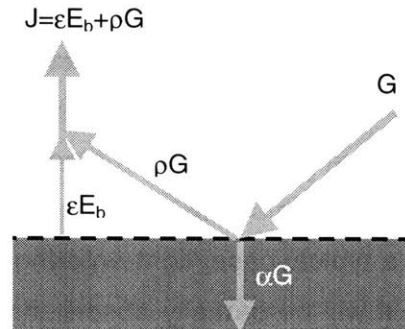
Figure 1.1.5

Energy balance in a room surface.

$$J_i = \varepsilon_i E_{bi} + (1 - \alpha_i) \sum_{k=1}^{n} J_k F_{ik} \qquad 1.1.10$$

32

This defines a system of n equations for the n surfaces of a room. After obtaining the radiosities, we can calculate the heat fluxes using:

$$\dot{Q}_i = \frac{\varepsilon_i A_i}{1 - \alpha_i} (E_{bi} - J_i) \qquad 1.1.11$$

There are particular aspects to applying these general formulas to model building radiative exchange balance. These aspects will now be explained.

At room temperature, thermal emission occurs in the infrared region. In this region, it is a good approximation to consider that partitions behave as gray surfaces (emissivity is equal to the absorptivity and does not vary with temperature). For this reason in equations 1.1.10 and 1.1.11, $\varepsilon = \alpha$ is used.

In a room, radiative heat transfer occurs in two wavelength regions, short-wave (due to solar radiation, wavelengths close to the visible) and the infrared (due to thermal radiation emission by all the objects inside the building). When calculating radiative heat transfer, two sets of energy balances must be considered: one for short wave and another for infrared. This separation is necessary because the absorptive and emissive properties of the room surfaces are different in these two wavelength regions. Fortunately, adequate accuracy can be obtained when using constant values for these properties in these two wavelengths regions (Mills 1995, ASHRAE 1997).

When applying these equations for the short-wave part of the spectrum, a different value should be used for ε and α. In addition, the $\varepsilon_i E_{bi}$ (equation 1.1.8) term should be zero for all the surfaces except the windows (the emission of thermal radiation in the visible part of the spectrum by objects at room temperature is negligible). For a window, we set the emission term (equation 1.1.8) equal to the solar radiation heat flux through that window.

View Factor Calculation

The amount of radiative heat exchange between two surfaces is linearly dependent on the fraction of the radiative flux leaving the first surface that is intercepted by the second surface. Rigorous determination of this quantity involves the calculation of generally complex surface integrals. For simple configurations, there are formulas available. In the case being studied, it is not possible to accurately obtain all the view factors using simple formulas.

Therefore, a numerical calculation routine is used in conjunction with the flowing simple relations (see figure 1.1.6):

$$A_B F_{BC} = A_C F_{CB} \quad 1.1.12$$

Where A_B and A_C are the surface areas. For all the surfaces of an enclosure,

$$\sum_{j=1}^{n} F_{ij} = 1 \quad 1.1.13$$

The view factors used here were calculated using dedicated software. The calculation was done using the program "FFACTOR.EXE", which calculates the exchange area matrix of the system. This program does not account for occlusion between surfaces, but that does not occur in the cases considered.

Figure 1.1.6

34
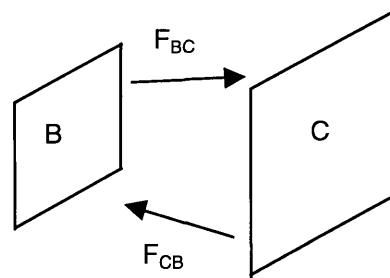
The exchange area matrix has the following form.

$$S = \begin{bmatrix} S_{11} & \cdots & S_{1N} \\ \vdots & \ddots & \vdots \\ S_{N1} & \cdots & S_{NN} \end{bmatrix} = \begin{bmatrix} A_1 F_{11} & \cdots & A_1 F_{1N} \\ \vdots & \ddots & \vdots \\ A_N F_{N1} & \cdots & A_N F_{NN} \end{bmatrix}$$

Where A_i is the area of element i, F_{ij} is the view factor from surface i to surface j, and S_{ij} is the exchange area between surfaces i and j.

Given the reciprocity relationship,

$$S_{ij} = A_i F_{ij} = A_j F_{ji} = S_{ji} \qquad 1.1.14$$

we can see that the exchange area matrix is symmetrical. The form factor matrix is then obtained by

$$F = \begin{bmatrix} F_{11} & \cdots & F_{1N} \\ \vdots & \ddots & \vdots \\ F_{N1} & \cdots & F_{NN} \end{bmatrix} = \begin{bmatrix} \dfrac{1}{A_1} & \cdots & 0 \\ \vdots & \ddots & \vdots \\ 0 & \cdots & \dfrac{1}{A_N} \end{bmatrix} \begin{bmatrix} S_{11} & \cdots & S_{1N} \\ \vdots & \ddots & \vdots \\ S_{N1} & \cdots & S_{NN} \end{bmatrix}$$

The FFACTOR.EXE program calculates the exchange areas by performing an approximation on a form of the standard expression for the exchange area between two surfaces (Siegel, 1981):

$$S_{ij} = \frac{1}{\pi} \int_{A_i} \int_{A_j} \frac{\cos \theta_i \cos \theta_j}{D^2} dA_i \, dA_j \qquad 1.1.15$$

where dA_i and dA_j are elements of A_i and A_j, respectively, D is the distance between dA_i and dA_j, θ_i and θ_j are the angles between the normals of surfaces i and j, respectively, and the direction where D is measured. This integral can be put into a

form which is more convenient from the computational point of view (DiLaura, 1997),

$$S_{ij} = \frac{1}{2\pi} \oint_{\Gamma_i} \oint_{\Gamma_j} (1 - \cot\theta) d\bar{\gamma}_i \cdot \hat{\psi}\hat{\psi} \cdot d\bar{\gamma}_j \qquad 1.1.16$$

where Γ_i and Γ_j are the contours of elements i and j, $d\gamma_1$ and $d\gamma_2$ are elements of those contours, θ is the angle between the normal to i and the direction from $d\gamma_1$ to $d\gamma_2$, and ψ is the azimuthal versor around the normal to i.

The program "FFACTORS.EXE" implements this last expression, by dividing the contour of each surface into small, finite segments, and performing a summation instead of an integral.

36

1.1.3-Estimation of the Internal Heat Gains

Reasonable estimation of the internal heat gains is essential to accurately model real buildings. In the case being studied (a residential apartment building), these gains are generated by a combination of occupants, machinery and lighting. There are considerable uncertainties in this parameter, both in the magnitude and in the type of gains. For a given warm object, the percentage of the heat that is transferred to the building by radiation and convection depends on the geometry of the object and type of source. For example, a gas stove is predominantly convective, whereas a radiator is predominantly radiative.

In this study, the values proposed by ASHRAE (1997) are used. Due to the fact that we are studying an apartment unit, we use a metabolic rate for each occupant of 0.8 met (for comfort calculations 1.2 met is used, see section 1.2), which for an exposed area of 1.8 m^2 gives a heat gain of 85 W per occupant. According to ASHRAE recommendations, this heat gain should be considered as being 70% radiative and 30% convective (similar to the proportion obtained for a heated vertical cylinder with an emissivity of 0.8 and a 10°C temperature difference). The machine and appliance heat gains are considered to be 470 W (single family house). Due to the difficulty in determining the exact nature of these gains, we use a similar distribution as in the case of the occupant heat loads.

In the present study the effects of furniture are ignored due to the complexity and uncertainty involved in doing rigorous calculations of its effect on the several components of the model.

We have now defined the basic concepts used to model the building thermal response. The next section presents the model used for occupant thermal comfort prediction.

1.2-Predicting Occupant Thermal Comfort

The final goal of an indoor climate control system is to provide thermal comfort and acceptable indoor air quality to the building occupants, with minimum cost and environmental impact. Predicting the occupants' thermal comfort is therefore an essential part of simulating the performance of an indoor environment control strategy.

In this section, human thermal comfort concepts are presented. The most widely accepted and used thermal comfort model, the Fanger comfort equations, is presented. The basic assumptions of this model are then explained and the principles involved in achieving comfort through ventilation are illustrated. A brief review of the most recent ideas and concepts of adaptive thermal comfort is also presented.

In the introduction of section 1.1, the three main components of the building thermal performance model were presented. In this section, a fourth component is introduced. This part of the model predicts the occupant's thermal stress for given indoor conditions, metabolic rate and clothing level.

Simple concepts of thermal comfort for warm environments have been used for a long time in architecture. In order to make warm periods tolerable to the building occupants; designers avoid direct sun exposition (with external and internal shading devices). In addition, many traditional designs provide opportunities for convective cooling by air movement (by designing with operable external windows and floor plans that allow for cross-ventilation). In many warm locations in the world, thermal mass is used as moderator of indoor climate. In some cases, this thermal mass is a source of radiative cooling (whenever the thermal mass is ground coupled or passively cooled during the night).

In the last fifty years extensive research has been done on indoor thermal comfort. This research effort has led the development of models for the heat transfer process that occurs between the occupants and the indoor environment. Laboratory studies using human test subjects were performed (Fanger, 1980, 1982 and 1985), which were used to develop models that relate human thermal stress sensation with the different forms of heat exchange with the indoor climate.

The work of Fanger became a reference for indoor thermal comfort prediction when it was adopted by ASHRAE (Standard 55) and by ISO (Standard 7730) in the definition of the summer and winter thermal comfort conditions. These standards have a considerable impact not only in the US and EU but also in other parts of the globe were air conditioning is becoming more widespread.

The adoption of these comfort standards, developed in the western world, in different parts of the world has been increasingly criticized, most recently by Humphreys (1998) and De Dear (1998). These criticisms are based on the idea that cultural and genetic factors influence thermal comfort sensations, which, in their view, is a justification for the need to develop local comfort standards.

The existence of comfort standards that are stricter than necessary leads to higher energy consumption in buildings. If in the summer the indoor temperature set point is raised, the building temperature becomes closer to the outside temperature average in the building location, and a reduction in the cooling energy consumption can be achieved. The same can be done in the winter (although in the opposite direction of heat transfer). In different parts of the world, people are exposed to diverse outside conditions, and therefore relaxing the indoor temperature settings is a reasonable step towards making buildings more integrated with the environment.

The fact that these standards impose a narrow comfort window on the indoor conditions works as a deterrent for the more widespread use of passive heating and cooling techniques. In this context, the ongoing studies in adaptive thermal comfort are very relevant and can have a significant impact on building energy consumption. Unfortunately, adaptive theory is still too qualitative at this stage (see part 1.2.2), and therefore cannot be used in this type of quantitative study.

Although the theory of Fanger has several limitations (explained below), it is still the simplest modeling approach that quantitatively relates indoor conditions,

40

metabolic rates and clothing levels to the occupant's thermal comfort. For this reason, the Fanger equations are used in this study.

1.2.1-The Fanger Comfort Model

In 1982, Fanger published a set of formulas that constituted what later came to be known as the Fanger comfort model. These formulas take as input the occupants' activity and clothing levels, establishing a relation between indoor environment variables and the thermal comfort sensation. This was done by adapting and simplifying previous work on heat transfer between the human body and outside environment. Fanger connected the predicted heat imbalance for a given set of indoor conditions with the qualitative responses of human test subjects under similar conditions.

This section introduces a set of basic concepts forming the base for the Fanger comfort model.

From a thermodynamic point of view, the relationship between the human body and the indoor environment is similar to the relationship between the building and its surroundings. The metabolic rate is the amount of energy that the human metabolic system produces at given time. It is similar to a building's internal gains, and just like these, it has to be transferred to the outside so that the body thermal system remains in optimal thermal balance.

The heat production is given by the metabolic heat generation minus the work produced. The efficiency of the human body is close to zero for most activities (ASHRAE 1997). For this reason, it is usual to neglect the contribution of the work production for the heat production:

$$\text{Heat Production} = (M-W) \approx M \qquad 1.2.1$$

The thermal load on the human body can then be calculated by imposing thermal balance between the body and its surroundings:

L(Load on Body)=Heat Production - Heat Loss   1.2.2

The total heat lost by the human body is the sum of the losses through the body interface and through respiration. The interface is composed of skin or skin plus clothes, depending on the body part. The different insulating properties of the body interface are taken into account by different values of the clothing factor variable (f_{cl}, see below).

Fanger proposes the following formula to calculate the heat loss through the body interface:

$$\text{Heat Loss} = 3.96\text{x}10^{-8}f_{cl}((t_{cl}+273)^4 - (\bar{t}_r + 273)^4) + f_{cl}h_c(t_{cl}-t_a) +$$
$$+ 0.42\text{x}(M-58.15) + 3.05(5.73 - 0.007\text{x}M - p_a) \qquad 1.2.3$$
$$+ 0.0173\text{x}M\text{x}(5.87 - p_a) + 0.0014M(34 - t_a)$$

Where:

f_{cl} – Clothing area factor is defined as the ratio between the clothed area and the body surface. The clothing level is measured in clo units. One clo is 0.155 m^{2}K/W (the clo values for different clothing combinations can be found in ASHRAE 1997, for example, walking shorts plus a short-sleeve shirt have a clo value of 0.36). The clothing area factor then varies with the clo level according to:

$$f_{cl} = \begin{cases} 1.0 + 0.2I_{cl} & I_{cl} < 0.5\text{clo} \\ 1.05 + 0.1I_{cl} & I_{cl} > 0.5\text{clo} \end{cases} \qquad 1.2.4$$

t_{cl} – Clothing temperature, obtained by iterative calculation using the formula presented below.

t_r – Average temperature of the surrounding surfaces.

44

h_c − Convective heat transfer coefficient between the human body and the environment. The convective heat transfer coefficient depends on the relative strength of the human thermal plume effect and the forced convection due to room air movement (velocity V):

$$h_c = \begin{cases} 2.38(t_{cl} - t_a)^{0.25} & 2.38(t_{cl} - t_a)^{0.25} > 12.1\sqrt{V} \\ 12.1\sqrt{V} & 2.38(t_{cl} - t_a)^{0.25} < 12.1\sqrt{V} \end{cases} \qquad 1.2.5$$

M − Metabolic rate, in W/m^2, of body heat transfer surface.

t_a − Indoor air temperature.

p_a − Water vapor pressure in kPa.

The first term on the right hand side of equation 1.2.3 accounts for radiative heat transfer. Fanger uses an average infrared emissivity of 0.7 for the exposed surface ($\sigma x \varepsilon = 3.96 \times 10^{-8}$). The second term is a simple convective heat transfer formula (see the definition of h_c above).

The third term gives the ideal value of the evaporative heat loss from the skin for a given metabolic rate (ASHRAE 1997). The remaining terms of equation 1.2.3 account for corrections due to evaporative heat loss for varying humidity levels.

It is important to note that Fanger greatly simplified the modeling the evaporative heat loss process in two aspects:

1 - The skin wetness factor is not present due to the fact that Fanger does not consider sweat accumulation (this factor is the ratio between the portion of body wetted surface over the total skin surface). This assumption limits the application of these equations to conditions where the skin wetness factor is close to zero. This excludes modeling very hot climate conditions or high metabolic rate levels (which generally imply high skin wetness).

2 - The indoor air velocity has no influence in the mass transfer factor for evaporative heat loss, which is a further assumption that Fanger uses for the global evaporative heat loss.

Fanger defined a scale that the laboratory test subjects used to express their thermal comfort sensations.

The main outcome of is work was then to produce the following expression to predict a subject's thermal sensation (given its thermal load (L) and metabolic rate (M)):

$$PMV = (0.303xe^{-0.036M} + 0.028)xL \qquad 1.2.6$$

This expression gives us the predicted mean vote (PMV). Given this value, Fanger proposed a second formula that gives the percentage of people that will express thermal dissatisfaction (Predicted Percentage of Dissatisfied occupants):

$$PPD = 100 - 95xe^{-(0.03353PMV^4 + 0.2179PMV^2)} \qquad 1.2.7$$

Using the Fanger formulas is relatively straight forward, except that in the calculation process the clothing temperature must be calculated in an iterative way by solving the following equation (notice the fact that f_{cl} and h_c depend on t_{cl}):

$$t_{cl} = (35.7 - 0.028(M - W)) - R_{cl}(39.6x10^{-9}f_{cl}((t_{cl} + 273)^4 - (\bar{t}_r + 273)^4) \\ + f_{cl}h_c(t_{cl} - t_a)) \qquad 1.2.8$$

R_{cl} is the clothing resistance, given by:

$$R_{cl} = 0.155xI_{cl} \qquad 1.2.9$$

The first term in equation 1.2.8 gives the comfort skin temperature for a given metabolic rate. The remaining terms take into account the effects on clothing temperature of the heat transfer process between the clothes and the environment.

46

Using the Fanger comfort equations involves a sequence of steps. For a given set of conditions (M, I_{cl}, t_r, t_a and p_a), the first step is to calculate t_{cl}. The following step is to use expression 1.2.2 to obtain the thermal load (L). This thermal load is then used to calculate PMV and finally PPD. The percentage of people dissatisfied is the most commonly used measure for thermal comfort; it is easier to qualitatively understand than the PMV value.

The Fanger comfort theory is most known for being the base for the definition of the ASHRAE and ISO indoor thermal comfort criteria. Still, its application to measure the cooling effect of ventilative cooling strategies is valid (ASHRAE 1997). The physical processes of body heat transfer are the same as in air-conditioned buildings.

The two cooling systems being studied rely on different cooling methods. In the case of daytime ventilation cooling, the increased heat removal from the body is obtained by increased convection (see the lower part of the right hand side of formula 1.2.5, the convective heat transfer coefficient increases with the square root of the velocity of the airflow surrounding the body).

In the case of night cooling the increased heat removal comes from lowering the indoor mean radiative temperature (due to lower surface temperature). The structural elements of the building are cooled by the night air and cool the daytime indoor air by convection and conduction. This colder air, in conjunction with the low surface temperature, is responsible for removing the heat from the occupants.

In Figures 1.2.1 to 1.2.4 (in the next page), we can see the PMV and PPD for typical indoor conditions for the apartment units being studied. Figure 1.2.2 illustrates the cooling effects obtained when increasing the indoor air velocity (the basic principle used in ventilative cooling). As the indoor air velocity increases, the improvement in thermal comfort becomes smaller. When this velocity goes above (approximately) 1.2 m/s the improvement in thermal comfort is close zero. This result is only indicative and should not mean that no improvement is obtained with higher air velocities (in fact, when skin wetness is higher, high air velocities can be effective (Givoni 1996)).
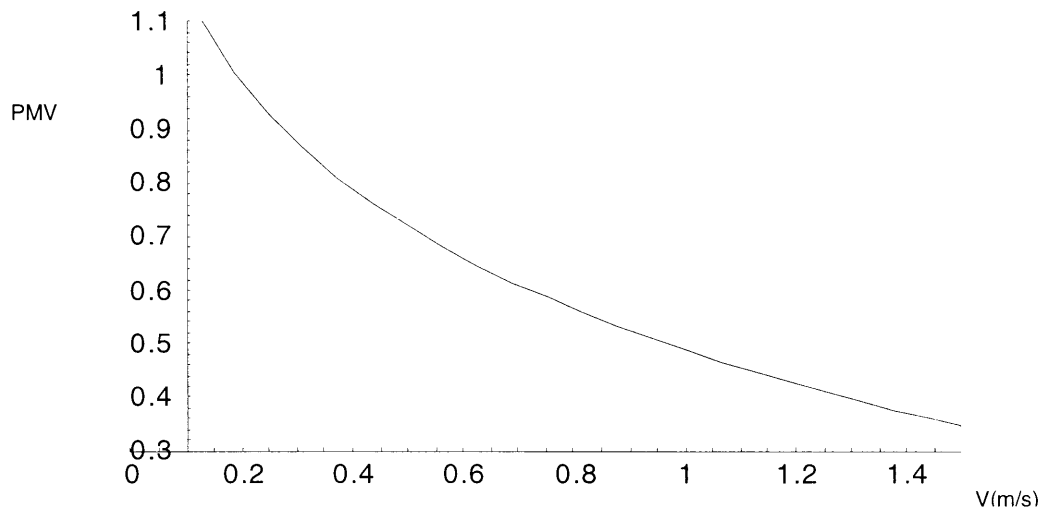
Figure 1.2.1

Sensitivity of the PMV value to variations of the indoor air velocity (t_a=28°C, tr=28°C, M=1.2 met, Icl=0.5 clo, RH=70%).
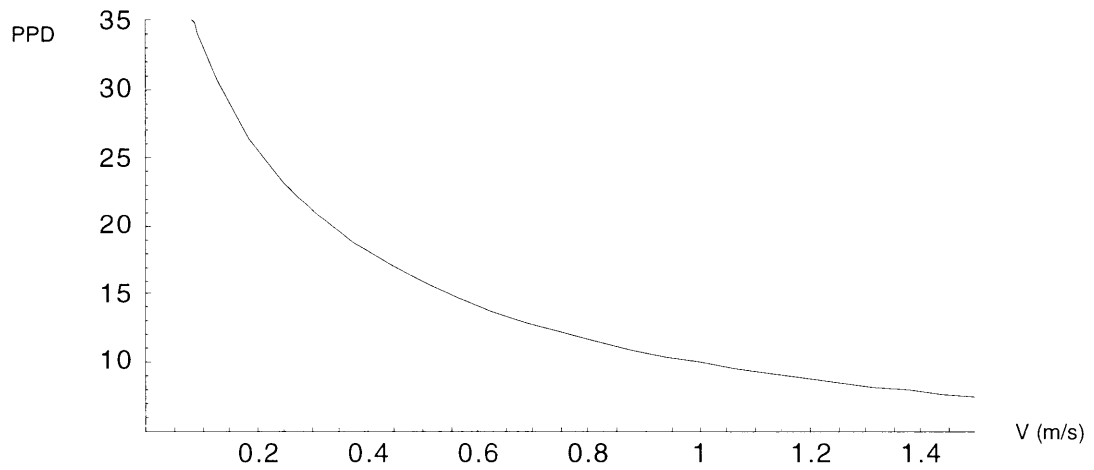
Figure 1.2.2

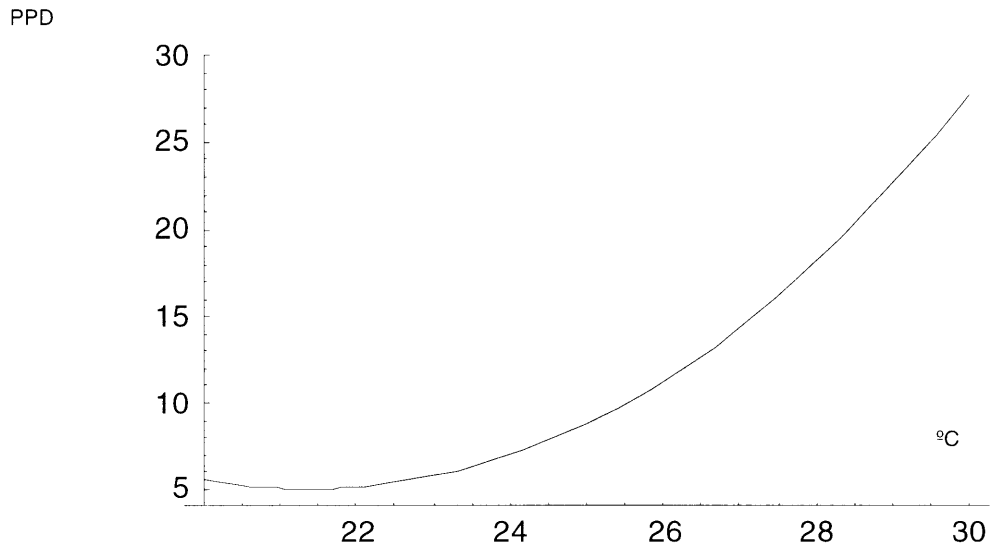Sensitivity of the PPD value to variations of the indoor air velocity (t_a=28°C, tr=28°C, M= 1.2met, Icl=0.5 clo, RH=70%).

48

PPD

Figure 1.2.3

Sensitivity of the PPD value to variations of the room surface temperatures (t_a=28ºC, M=1.2 met, Icl=0.5 clo, V=0.4 m/s).
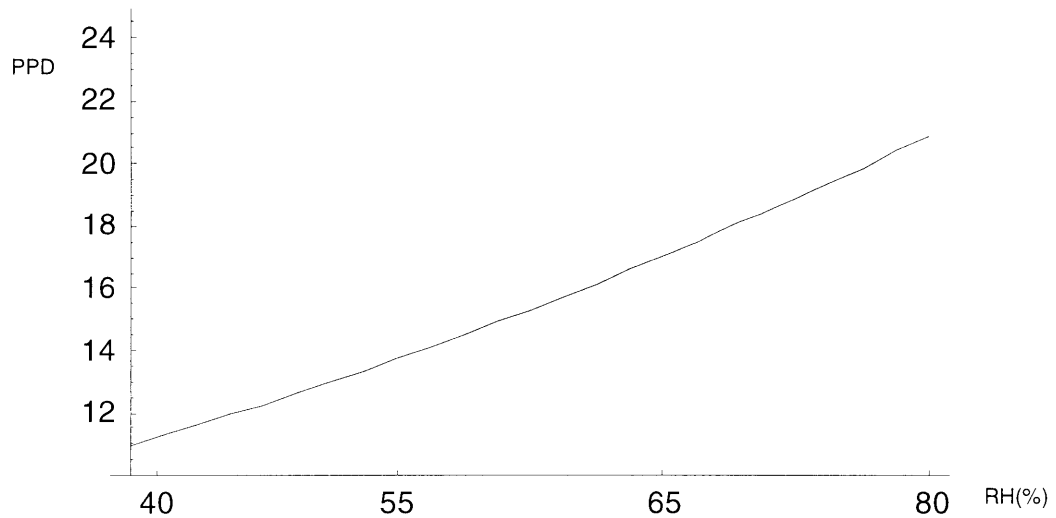

Figure 1.2.4

Sensitivity of the PPD value to variations of the indoor humidity level (t_a=28ºC, tr=28ºC, M=1.2 met, Icl=0.5 clo, V=0.4 m/s).

49

1.2.2-The adaptive approach to thermal comfort

Human beings have a considerable ability to adapt to different conditions and situations. In the particular aspect of adapting to different climate conditions, three types of adaptations generally occur: behavioral, psychological and physiological. Currently used comfort standards fail to model the impact of both psychological and physiological adaptations. The adaptive theory of human thermal comfort analyzes the impact of all adaptive human behaviors in thermal comfort expectations.

With the widespread use of air conditioning came the ability to have a high degree of control over the indoor environment. In many existing air-conditioned buildings the user has very limited control over the indoor climate conditions. In many cases the design concept does not reflect or take advantage of the particular outside environment. This practice leads to highly energy intensive buildings that rely heavily on mechanical and electrical systems (indoor lighting is another area were there were similar developments). In these buildings, considerable energy is wasted to maintain excessively controlled indoor conditions. This waste can occur both due to excessive control and due to a too high or too low temperature set point. Due to there being a belief in the existence of universally accepted ideal conditions, the user is given limited control over the indoor environment, which greatly limits the positive impact of behavioral adaptation.

The argument of the researchers pursuing the implementation of adaptive comfort standards is that the current, non-adaptive, standards almost completely ignore this fundamental ability of human beings. Several field surveys indicate that thermal comfort can occur in wider temperature ranges than that currently accepted (Baker (1996), de Dear (1998), Kwok (1998) and Oseland (1998)).

In his paper of 1998, Humphreys (one of the first authors to introduce the adaptive ideas to thermal comfort) presents an extensive review of the adaptive thermal comfort theory. He described how different human adaptive behaviors have particular impacts on thermal comfort perception:

Psychological adaptation refers to the ability of controlling expectations (people tend to be more tolerant to changing indoor conditions in a building with no air conditioning) and to reduce the psychological response induced by a stimulus as a consequence of previous exposition to a similar stimulus.

Behavioral adaptation includes all the changes that a human being can make in order to achieve the best possible thermal balance with the environment. These changes can involve controlling different aspects: the activity level (therefore changing the metabolic rate), the clothing level, the activity period, and the indoor environment conditions (controlling windows, air conditioning, lighting, etc...).

Physiological adaptation consists of permanent physical changes that may increase tolerance to climate conditions. These adaptations can occur in different time scales: adaptation to a particularly warm week, adapting to living in a warmer or colder climate and finally genetic adaptation that occurs after generations of living in certain climate conditions.

Research in adaptive thermal comfort is still in the stage of showing that there is a need for applying these principles, fighting the ideas prevailing after years of application of the current standards. Several field studies have been done with the goal of showing that these adaptations have an impact in the perceived thermal comfort levels and also that increased tolerance exists for the so called free running buildings (non air-conditioned). The results so far are qualitative, with the exception of several proposed equations for the preferred indoor temperature as a function of the outdoor conditions, as well as proposed temperature ranges for free running buildings. These results are obtained from statistical treatment of field data. At this stage, there is still no connection between the proposed equations and particular building features or occupant activities.
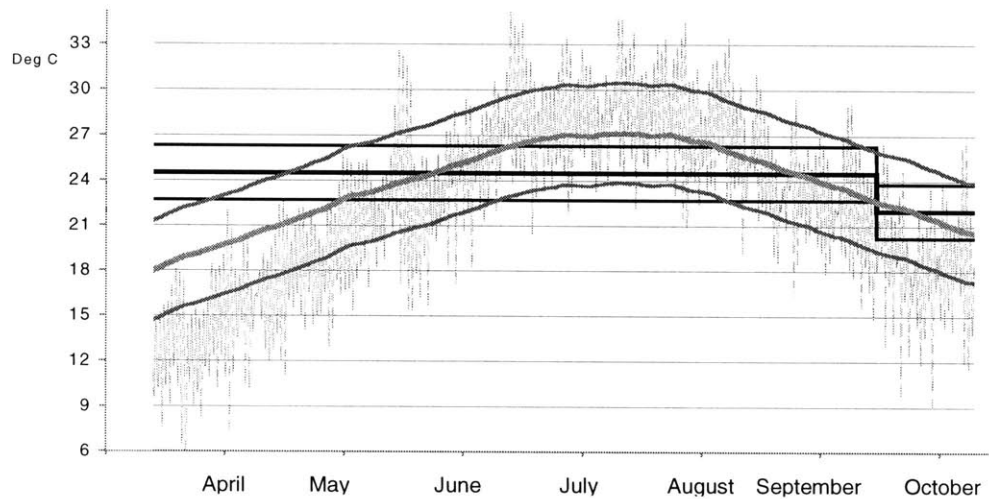
Figure 1.2.1
Comparison between ASHRAE (Standard 55) and an application of adaptive comfort standards for typical Shanghai weather.

Figure 1.2.1 is and illustration of the two different approaches when applied to the Shanghai outdoor temperature variation in a typical year (any of the other two cities in this study would have been suitable for this example). In this figure, The acceptability band used comes form statistical treatment of real measurements in free running buildings (de Dear 1998).

The thick gray line is obtained using the equation proposed by Humphreys (1998):

$$T_c = 11.9 + 0.534\,T_o \qquad 1.2.10$$

where T_c is the comfort temperature and T_o is the monthly average of the outdoor temperature. When presenting this formula, Humphreys does not give a value for the acceptable variation of the comfort temperature that will be still acceptable for the users. Therefore, in order to introduce an acceptability band in this comparative chart, the work of another researcher is used (de Dear (1998)). In his paper, de Dear presents an acceptability band that is an average of the acceptability bands found for thirty-four free running buildings worldwide. This acceptability band

obtained in this way is almost twice the size of the ASHRAE acceptable variation. It should be noted that the lowest value for the acceptable temperature range presented in this figure (13°C) is consistent with field measurements.

There is a real need to extend the current comfort equations in order to include psychological and physiological adaptations. It is important to note that current equations are already able to model most of the behavioral adaptations. For example, in the Fanger equations it is possible to vary the activity level, the clothing level and the changes in indoor conditions that might occur due to behavioral adaptation.

1.3- Modeling Airflow In and Around the Building.

In the previous two sections, two of the three parts that will be used to simulate the passive systems were presented. This section presents the third part. This part of the model calculates the airflow in and around the apartment analyzed in this thesis.

The performance of a wind driven cooling system is directly dependent on the magnitude of the airflow in the building. Air extracts heat from the building by convection. This convective heat removal process affects the occupants directly and indirectly (through the building thermal mass). For these reasons, accurate modeling of the wind driven airflow through the building is an important component in this simulation.

In this section, the model used for predicting airflow is introduced. The choice of the type of model used is justified. Finally, in the last part of this section, the use of measured wind data as an input of the model is discussed.

In a building air has an important role as an energy transport medium. Of the several physical processes that occur in a building airflow is the most difficult to model. The study of fluid flow is a major field in engineering. Fluids present a big challenge due to their complex behavior. This complexity is translated in the very complex nature of the equations that describe fluid flow (the Navier Stokes equations). In order to predict the behavior of gases the Navier Stokes equations must be solved, in conjunction with the fundamental conservation equations of mass and energy (for liquids the solution process are generally simpler).

With the increased availability of computers, engineering fluid mechanics is shifting from simplified analytical models and experimental correlations towards the use of numerical solution methods. Initially, precise solutions were only available for

a limited number of cases (the ones with analytical solution). Today, experimental correlations are mostly used to deal with the more complex phenomena (such as turbulent boundary layers or transient problems).

The development of building airflow models followed a parallel path of evolution. In this field detailed numerical solution, methods are also becoming more widespread. Simple modeling approaches and empirical correlation formulas (derived from experiment) are used whenever the solution of the equations is not feasible. These simple approaches can be adequate for many practical design problems.

Currently available building airflow models can be divided into three groups. The first group of models is based on experimentally obtained formulas that relate outside wind velocity to indoor velocity. These formulas are obtained by curve fitting a function to a set of experimentally obtained velocity points inside a scale model tested on a wind tunnel. These studies are done for a specific type of building geometry. The results are valid for a set of aperture areas and impinging flow angles. This modeling approach is geometry-specific and does not provide detailed information on the airflow pattern. Aynsley (1977) and Ernest (1991) are two researchers that worked on this type of approach.

The second type of models is based on the aperture equation and on mass and energy conservation principles. An excellent review of these models is presented by Feustel (1992). Some aspects of the geometry of the building are considered (outside pressure coefficients, internal/external aperture areas and height of the mid-point above a reference height). The influence of the building specific factors on the results is generally qualitatively correct. Still, the uncertainty in the results can be quite high (Persily (1986)). These models can be inadequate for multiple inlet configurations. For some of these cases, the results can even be qualitatively incorrect. Another situation when these models are not adequate is if there is conservation of the inflow momentum as the air goes through the building. This is due to limitations of the fundamental equation used in these models (the aperture equation, based on Bernoulli's law) when dealing with these cases (Murakami 1991).

Both of the two previous groups of models fail to provide information on internal flow patterns, making the accurate treatment of air to wall convective heat transfer

impossible. The third group of models is based on the numerical solution of the time-averaged Navier-Stokes equations. This type of models belongs to the field of computational fluid dynamics (CFD).

In these numerical methods, the momentum equation is solved in three directions (in Cartesian coordinates, x, y and z) in conjunction with the mass and energy conservation equations and turbulence model equations.

The simplest family of turbulence models uses corrected viscosity (usually known as turbulent viscosity) to account for the effects of turbulence on the flow field. There are several types of turbulence models that can be used for airflow in and around buildings (for a simple review of different effective viscosity turbulence models see the paper by Spalding at www.cham.co.uk). In the present study, the k-ε model is used. It is the most commonly used turbulence model (see Shaw (1992) for a good review of numerical turbulence modeling and the k-ε model in different applications). This two-equation model (one equation for the conservation of turbulent kinetic energy (k) and one for its dissipation (ε)) has been successfully applied to a wide range of engineering flows. In what regards building airflow there is a large amount of work analyzing the application of computational fluid dynamics with the kε model to natural ventilation cases (from now on just referred to as CFD).

In the last twenty years, extensive work has been done in applying CFD to building airflow (both indoor and outdoor). One interesting study was done by Tsutsumi et al (1996). In this study, comparison between full-scale measurements and wind tunnel tests for a cross-ventilated apartment building is presented. Reasonable agreement was found. Still, the main problem with measuring real buildings is always the control on the experimental conditions (transient effects of the local wind then have considerable influence on the results). There is extensive work comparing CFD simulations with wind tunnel experiments (among others, Freskos (1998), Lino (1998), and Karabuchi (1998)). In these studies, good agreement was found between the numerical model and experiment. In this context, the use of CFD in the present case seems to be the best option, although it should be noted that there are some problems with this approach. In his work on airflow around a cube, Murakami (1990) shows some of the limitations of the k-ε model when compared with rigorous laboratory measurements and results of a more precise turbulence modeling technique (large eddy simulation (LES)). These

problems are due to the assumption of isotropic turbulent viscosity (a common characteristic of all effective viscosity models). As computer performance increases, the use of more complex turbulence models should become possible. LES is one of the most promising techniques (see Murakami (1992) for a rigorous comparison between LES and experimental measurements in a cross-ventilation case).

In this study, CFD (with the k-ε turbulence model) is used to simulate the wind driven cross ventilation airflow through the building. Although there are more precise numerical approaches they remain too time consuming to make their use feasible (if LES was used each simulation would take approximately one month in a Pentium II 450MHz machine). In addition, the use of other approximations in this study (see sections 1.4 and 2.2) limits the overall precision of the model used. In this way the increased precision of, for example LES would probably not have a noticeable impact on the overall precision of the results. On the other side, the use of simple ventilation model is not adequate for this work because there is a need to obtain the airflow velocities near the surfaces of the thermal mass partition elements.

1.3.1- Using CFD to Simulate Wind Driven Cross-ventilation in an Apartment Building.

This subsection presents several important aspects of the application of CFD to study natural ventilation. The CFD simulation package (PHOENICS) used in this study is presented. The numerical discretization of the flow domain is also presented and justified.

When analyzing building ventilation it is common to separate inside from outside flow simulation. The outside conditions due to wind are obtained from either a separated simulation or a wind tunnel testing of scaled building models. In this way, the boundary conditions that are then supplied to the indoor airflow model are obtained. Experimental work by Straaten (1967) shows that whenever the building façade aperture area exceeds 20% of the total area, this uncoupled approach is not adequate. As can be seen in part 2.2, the building under study, when in cross-ventilation mode, has more than 20% aperture area. This makes a coupled indoor-outdoor simulation necessary.

The experimental findings by Straaten are a manifestation of a simple momentum conservation phenomenon. Since air goes through the highly porous cross-ventilated, building the amount of deflected impinging air is reduced. Due to the fact non-negligible amounts of air will flow across the building, the pressure coefficients on the windward side tend do be lower than the ones obtained from a closed model (Aynsley (1988)). When doing a cross-ventilation simulation, care must be taken to position the boundaries of the flow domain at a sufficient distance from the building so that real external flow conditions can be reproduced. When the inlet boundary is too close to the building, its influence on the results is higher than desirable. The case simulated then becomes closer to reproducing forced inlet
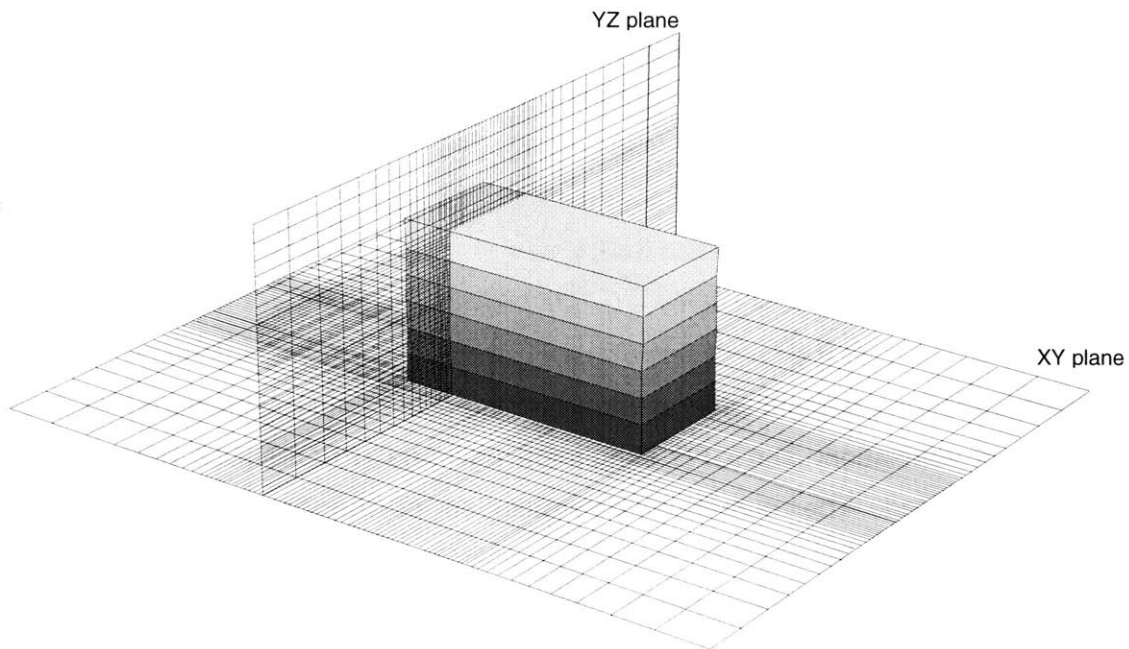
Figure 1.3.1

conditions than the external flow case under analysis. A survey of several simulation papers and a set of preliminary runs of the simulation model led to the adoption of the domain configuration that can be seen on figure 1.3.1. Distance between the inlet and the building is at least 25m (150% of the building height). The simulation domain is divided into a set of finite volumes. The number of volumes used and their distribution is finely tuned in order to obtain adequate spatial resolution and convergence of the numerical solution procedure. Still, the number of volumes must be kept as low as possible; otherwise, the simulation process demands excessive computational power. Computational fluid dynamics is highly demanding in computational power.

Inside the building (light gray rectangle in the picture), a constant grid density is used. The typical size of the discretization volumes inside the building is approximately 0.5 m. outside; the grid size is proportional to the distance from the

building. The total grid size used in this study is 74x58x45 points, which makes for a total of 2×10^5 grid points in the flow domain.

For isothermal three-dimensional flow, six coupled equations must be solved, the numerical solution procedure going trough each simulation grid point several times in each iteration (for an excellent review of the numerical procedure used in PHOENICS see Patankar (1980)). He proposes a very simple notation for all the equations that are used in the numerical model:

$$(\partial / \partial t)(\rho\phi) + \nabla.(\rho\vec{v}\phi) = \nabla.(\Gamma\Delta\phi) + S \qquad 1.3.1$$

The six equations that are solved in the CFD numerical procedure are obtained by using the different forms for ϕ shown in table 1.3.1.

In this study, the commercial CFD package PHOENICS (version 3.1) is used. Extensive general and detailed technical information on the PHOENICS CFD package can be found on the company's web site (www.cham.co.uk).

A typical simulation run begins with all the variables (P, V_x, V_y, V_z, k, ϵ) set to an initial value (normally zero). Solution is then obtained by iteration. The different equations are solved individually (momentum conservation in the three axes, mass conservation and turbulence model equations). The simulation converges when the fractional error of the computed variables goes below a user-defined criterion. This criterion is the average percentage error. The error is weighted by the total source

Table 1.3.1

Equation	ϕ
Mass Conservation	1
Momentum in x	V_X
Momentum in y	V_Y
Momentum in z	V_Z
Turbulent Kinetic Energy	k
Turbulent Energy Dissipation	ϵ

strength for each solution variable in the domain. The pressure field is obtained by solving a modified version of the mass continuity equation. Therefore, for this variable, the total inlet mass flow rate is used as a weighting factor.

1.3.2-Using Hourly Wind Data in the Airflow Model.

Incorporating urban boundary layer airflow conditions into a building ventilation model is a complex task. Three characteristics of the external wind flow must be provided to the CFD simulation routine: wind direction, wind velocity and wind turbulence intensity. A set of approximations and assumptions is used when translating these variables into the model. In this subsection, the model used to account for real whether wind conditions is described.

Wind is by far the hardest meteorological factor to incorporate in a real weather building thermal model. In the process of using wind, hourly data as the input for an airflow model there are several potential sources of error. The weather station might not be in an area which has a wind profile similar to the building site (the site might be inner-city or urban and the weather station might be in open terrain conditions, like an airport area, etc...). An empirical formula, obtained by interpolating experimental data, must be used to extrapolate the variation of the wind velocity profile at the building location.

The wind velocity and direction data that is used in this study is measured in weather stations at the standard reference height of 10 meters. The location of the weather stations is usually chosen so that the influence of surrounding obstacles on the measured wind is limited. There was no information available about the location of the weather stations for any of the files used in this study.

In the atmospheric boundary layer, mean wind velocity increases with height. This is a consequence of friction between the layer of moving air and the ground. This friction reduces the mean wind velocity and increases turbulence in the near-ground region. The size of this boundary layer depends on the roughness of the ground surface. For wind, flowing over flat, unobstructed areas the typical value of
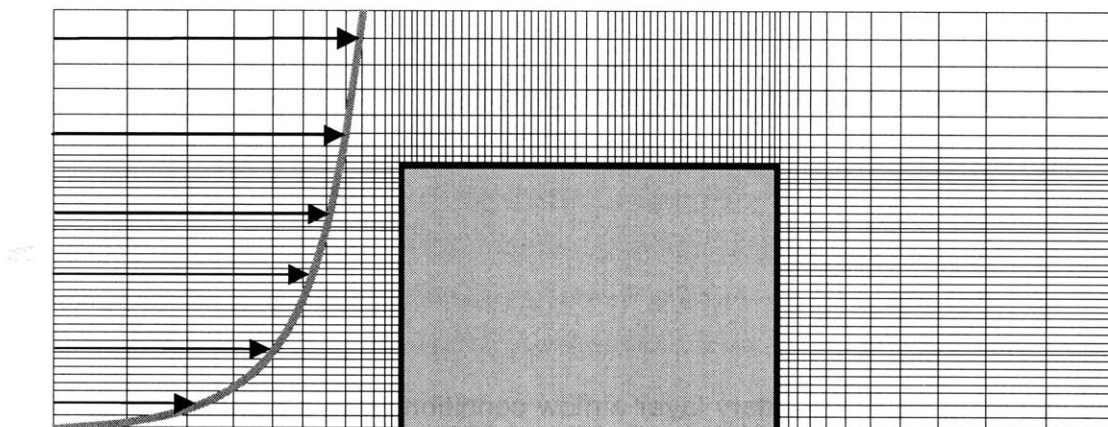
Figure 1.3.2

Ilustration of the urban wind profile approaching the building.

The wind is a continuous field and must be discretized in order to be used as a boundary condition for the CFD simulation

the height of the boundary layer is 210 m (ASHRAE (1997)). This value is proportional to the typical roughness size of the ground surface. The roughness size in the urban area is the typical size of buildings. For urban area roughness, the height of the boundary layer is twice the value of undisturbed areas (around 450m).

The two most commonly used empirical interpolations are the logarithmic (Landsberg, 1981) and the exponential (Davenport, 1960). The logarithmic model predicts zero velocity at typical obstacle height (in our case building height). For this reason, this model is not adequate for urban building airflow simulations. The exponential interpolation is then the most commonly adopted model. Davenport proposed the following formula:

$$V_h/V_g=(h/B_H)^a \qquad 1.3.1$$

In this model, different types of terrain are characterized by the exponent (a) and boundary layer thickness (B_H) values. In this study, the values adopted by ASHRAE (1997) are used. When modeling a building site, an assumption must be made on what is the prevailing wind profile in the area. There are several possibilities for the wind profile. In our case we are studying an isolated apartment
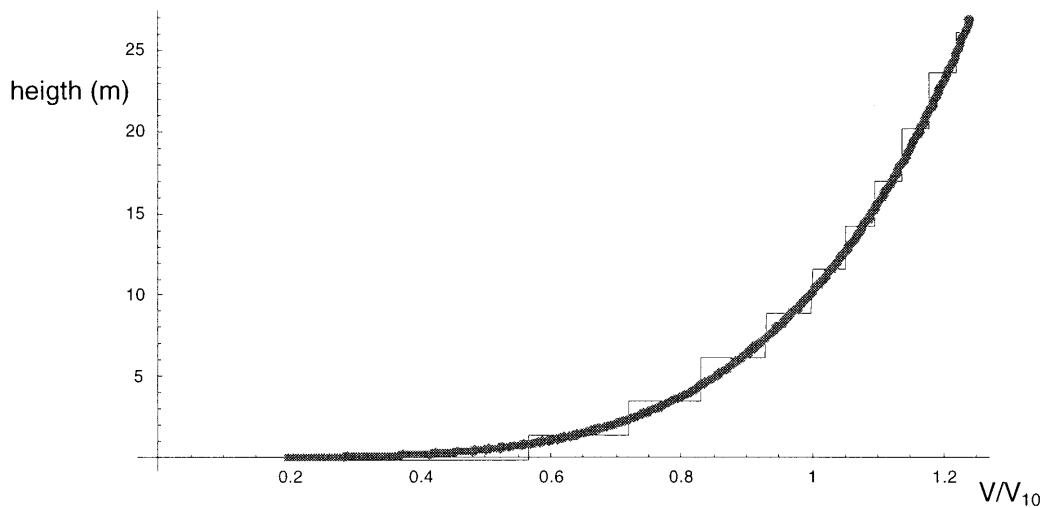
Figure 1.3.4

Discretization of the power law for urban wind velocity profile.

building in an urban area so exponent and boundary layer thickness values of urban/suburban area are used (a=0.22 and B_H=370 m).

We have seen how the urban boundary layer velocity profile is modeled. Two other variables remain the wind direction and the turbulence intensity. The wind direction is measured in intervals of 22.5°. This discrete measurement procedure is introduces a further approximation (this time at the source).

The value of the turbulent kinetic energy intensity is a boundary condition that must be provided to the turbulence model. It influences the calculated flow field through the effective turbulent viscosity parameter.

It is important to note that even when measured wind velocity and turbulent intensity are used in the model the real wind conditions are still not correctly taken into account. This is due not only to difficulties in reproducing the wind velocity variation with height but also to the steady state approach used in the CFD model. The CFD approach used is steady state; real wind flow is a transient process. Wind fluctuates in both direction and velocity, small intensity wind gusts constantly occur. This large-scale turbulence has an impact on the flow rates and on building ventilation that is not considered in the CFD model used in this work. The turbulence intensity parameter models small-scale turbulence (the turbulence scale that can be modeled by artificially changing the fluid viscosity).

For the atmospheric boundary layer, the turbulent intensity can be adequately modeled as constant. This is true whenever mechanically generated turbulence (the other possibility being buoyancy generated turbulence) prevails in the lower part of the atmospheric boundary layer (Panofsky, 1984). In an urban area with wind, this approximation is therefore adequate. This assumption fails when there is no wind and high buoyancy forces are present. In this study, the flow model is not applied when there is no wind. In no wind conditions, an average heat transfer coefficient of $5W/m^2K$ is used for external walls (therefore adopting an average buoyancy heat transfer coefficient). For internal walls a value of . When wind is present, the buoyancy forces inside the apartment can be neglected. This validity of this approximation can be tested by calculating the Archimedes number:

$$A_r = gL_0\Delta T/(V^2T) \qquad 1.3.2$$

Where g is the acceleration of gravity, L_0 is the typical length of the heated vertical plane where buoyancy is generated, ΔT is the average temperature difference between the surface and the air and V^2 is the typical velocity of the external flow. The Archimedes number is a relation between the buoyancy forces (in the numerator) and the inertial forces (in the denominator). In the present case and for indoor flow A_r will vary from 0.05-0.5 when the wind varies from 1-3m/s for typical internal wall conditions (wall-internal air ΔT of 5K and Lo=2.7m (the height of each apartment)). For external walls, this approximation is not adequate during the day when the walls heat up to temperatures above 40°C and the height for the buoyancy boundary layer to build up is the building height (16.5m). The consequence of this is that during the day the model underestimates the convective heat loss into the environment. This approximation reduces the heat loss from the apartment in the warm parts of the day making the obtained results worse than reality (it is a conservative approximation).

The value used for the inlet turbulence intensity was 16%. This value is similar to the one adopted by Haghighat (1991) and close to the one measured by Etheridge (1979).

In figure 1.3.1 (gray line), we can see the urban wind profile used. Numerical models use a discrete grid of points in each of the three spatial directions. Therefore, it is necessary to discretize this wind profile.

When making the discretization of the exponential urban wind profile, care was taken in order to keep the relative discretization error below 5% for any point in the z-axis. In order to meet this criterion, there was a need to use finer subdivisions in the lower heights. Ten inlets were used, with each inlet having the velocity of the exponential formula at mid-height of the inlet.

The present section ends the description of the components of the models used in this study. The next section presents in detail the method used to couple the several components of the model.

1.4- The Integrated Model

This section presents the coupled building thermal simulation model. This coupled model will be used in the second part of this work to analyze the performance of the passive cooling systems. The three components of this model were presented in sections 1.1 to 1.3. These separate components must be coupled in order to take into account the interaction of the different thermal phenomena that occur in a building. In this way, we obtain a coupled model that for given outside weather conditions predicts the occupants thermal comfort. This section ends with the description of the two ventilation strategies that were studied.

Figure 1.4.1 (in the next page) shows the general operation procedure of the coupled model. The starting and end of the simulation process are displayed. On the left we can see the outside weather conditions, which are the starting point. This weather information is processed by the two components of the building coupled response model: on the upper box the airflow model; on the lower box the thermal model. At this point, the airflow model provides the airflow rates and the air velocities near the walls to the thermal model. Finally, both of these models supply indoor conditions to the thermal comfort model, reaching the end of the simulation process.

The thermal comfort model (described in section 1.2) is simple; given the indoor environment conditions it predicts the thermal comfort level. The most delicate point of the coupling between the three components of the model is therefore in the interaction between the airflow and the thermal model. As explained in section 1.3, the airflow model runs slowly. Even for the isothermal case used in this study, each flow simulation can take approximately 18 hours (using a Pentium II 450MHz). For this reason, it was necessary to devise a coupling method that does not require a
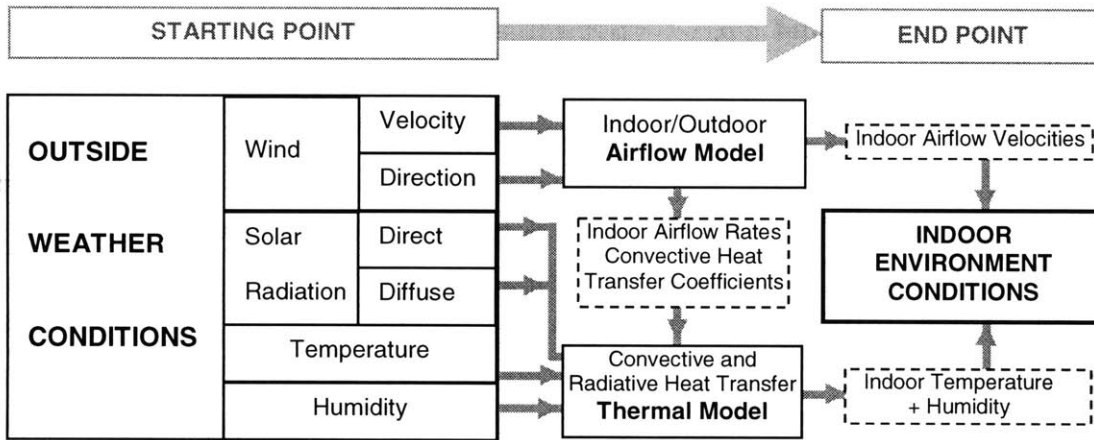
Figure 1.4.1

Components of the coupled model.

new airflow simulation. This is because the outside weather conditions change on an hourly basis.

The coupling approach used in this work is specific to cross-ventilation wind driven flows. It takes advantage of the characteristics of this type of flow to achieve a highly efficient coupled model. This is a priority since a simulation using real weather on an hourly basis over an extended period (five months) is to be performed. In the next subsection, the approach used in coupling the airflow with the thermal model is described.

1.4.1-Coupling of the Thermal and Airflow Models

All building simulation codes use a form of coupling between the air and the internal surfaces of the building. One common way of implementing this coupling is to approximate the air in each room of the building as isothermal, and the convective heat transfer coefficient as constant. DOE2, one of the most commonly used building simulation tools, uses these two approximations. A more precise coupling procedure is used in tools such as COMIS and TRANSYS. These programs can model thermal stratification inside a room, allowing for air temperature variation with height in each room of the building. The convective heat transfer coefficient for each surface now depends on whether the surface is in a current or stagnant flow zone. These simple coupling procedures work well for air-conditioned buildings and for determining heating and cooling annual loads. In the other extreme of building indoor environment simulation is the detailed treatment of the building airflow and thermal behavior using CFD (non-isothermal flow and detailed treatment of room boundary conditions). One example of this type of approach is the work of Chen (1988). Many other more recent examples are available (among others: Off (1996) and Nielsen (1998)).

In the present work, the main concept used in the coupling of the two models is actually decoupling. The airflow is simulated as isothermal and therefore does not receive information from the thermal model. For the case under analysis, this is because the apartments are horizontal and the maximum height in which the convective current can be formed is 2.7m. Wind driven flows for these low height configurations are much stronger than buoyancy flows (see discussion in part 1.3.2), and define the direction of the flow (Chandra (1984)).

With this approach, it is possible to prerun the flow simulations and create a database of flow cases that is accessed according to outside weather conditions.
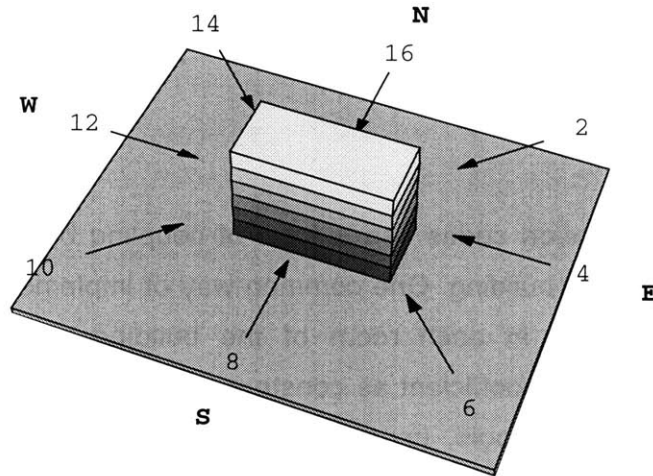
Figure 1.4.2

The apartment building in the CFD flow domain.
The numbers 2, 4...16 are the flow directions used in this study.

In figure 1.4.2 we can see the directions used in the flow simulation. The medium gray plane in this figure defines the boundaries of the flow domain (already discussed in part 1.3). This domain contains a single building (as opposed to containing the building studied and possible surrounding buildings). Therefore, in this study an isolated building in an urban area is considered. This option makes this simulation study more general, since no specific urban layout is used (the existence of surrounding buildings would have a considerable impact on the results). On the other hand, it can be argued that it makes the case analyzed less general, since isolated buildings are becoming less and less common.

Due to the symmetry of the building, only directions 8, 10, 12, 14 and 16 have to be calculated. The apartment unit analyzed was on the left-hand side (when looking at the building from south) of the fourth floor. The result for flow coming from direction 6 can be obtained from the result of the simulation for direction 10.
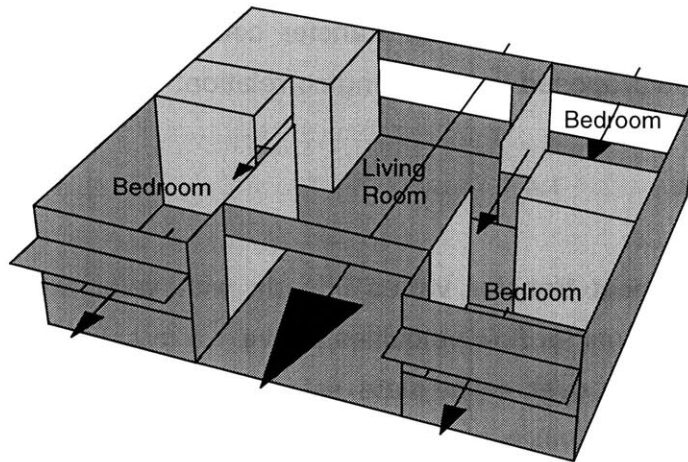
Figure 1.4.3
Airflow direction in the apartment for north winds.

This is done by using, for the left-hand side unit, the result of the right-hand side unit.

Preliminary runs for direction 12 showed a very low flow rate in all units (average inlet velocity inferior to 1/20 of the external wind velocity). For this reason, the wind driven airflow from this direction is taken as zero. In the model, this is equivalent to considering only infiltration (flow rates of 1.5 ACH/h). This approximation reduces the overall flow rate in the apartments during the warm season. For this reason, it makes the results slightly worse than reality (it is a conservative approximation). The flow rates obtained from these simulations are fed into the building thermal model. Other input used by this model are the flow velocities near each internal surface of the apartment (see figure 1.4.3). In this way, the convective heat transfer can be determined with greater accuracy. In order to determine the value of the convective heat transfer coefficient (h_c in W/m^2 K) an experimentally obtained correlation is used.

After an extensive survey of previous work, an experimentally determined correlation was found that is specific for convective heat transfer in wind dominated

cross-ventilation airflow in buildings (Chandra (1984)). In this work, Chandra used an experimental facility (real size). Under controlled conditions and using wind driven airflow, he measured the heat transfer coefficient for a set of near wall airflow velocities. He proposed the following correlation:

$$h_c(V) = 2.3 + 6.4 \times V \qquad 1.4.1$$

The convective heat transfer varies linearly with velocity. Chandra did not obtain any measurements for flow velocities above 1.6 m/s. Laboratory correlations obtained for forced flow over a flat plate extend this linear (or close to linear in some cases) behavior to much higher velocities (up to 40 m/s, Mills (1995)). For this reason, it was judged reasonable to extend Chandra's correlation up to 3 m/s (after this value all the velocities correspond to the h_c obtained using a velocity of 3 m/s).

The convective heat transfer between the building and the outside air is considered in detail. The direct and diffuse solar radiation incident on the external surfaces is considered, as well as the convective transfer at the outside surfaces (the same correlation used for the internal surfaces is applied; the average velocity at those surfaces is calculated with the CFD simulation results).

In figure 1.4.3, the basic layout of the apartment unit used in this study is displayed. The arrows represent the direction of airflow as observed in all the simulations for north wind directions (in figure 1.4.2, directions 14, 16 and 2). The direction of airflow for southern winds is reversed. The light gray volumes in the model are the restrooms and the kitchen. These compartments are not modeled in detail. The internal faces of the partitions of the restrooms are considered to be at living room temperature. The internal faces of the partitions of the kitchen are considered to be at outside temperature (the window of the kitchen is considered to be partially open at all times). The convective heat transfer coefficient used in this coupling was 5 W/m^2 K.

1.4.2-The Ventilation Strategies

One of the goals of this study is to compare the performance of two ventilative cooling strategies: night cooling and daytime ventilative cooling. In order to simulate the two ventilation strategies it is necessary to implement user behavior into the calculation routine (see Appendix B). The ventilation strategies, described in the introduction, are:

Comfort Ventilation (or Daytime Ventilation). Thermal comfort is obtained by increased convective heat removal in the warmer hours of the day. This is done using outside air that goes through the building. Generally, the air movement is wind-driven.

Nighttime Ventilative Cooling (also named Night Cooling). In this type of system, cold night air (around 18-22°C) is circulated through the building.

These are the general definitions. When using the two strategies users will regulate the opening of windows according to these basic rules and also a set of common sense actions:

- If outside air is colder than inside and the apartment is not too cold (below 24°C), users will open the windows.
- If at the end of the day the indoor temperature is below 24°C, the users will not open the windows during the following night.
- For daytime ventilation, if the apartment is warm (above 28°C) the users will open the windows to increase convective heat removal. Still, they will only do this if there is enough wind to drive airflow through the apartment.

Night Cooling Ventilation Strategy
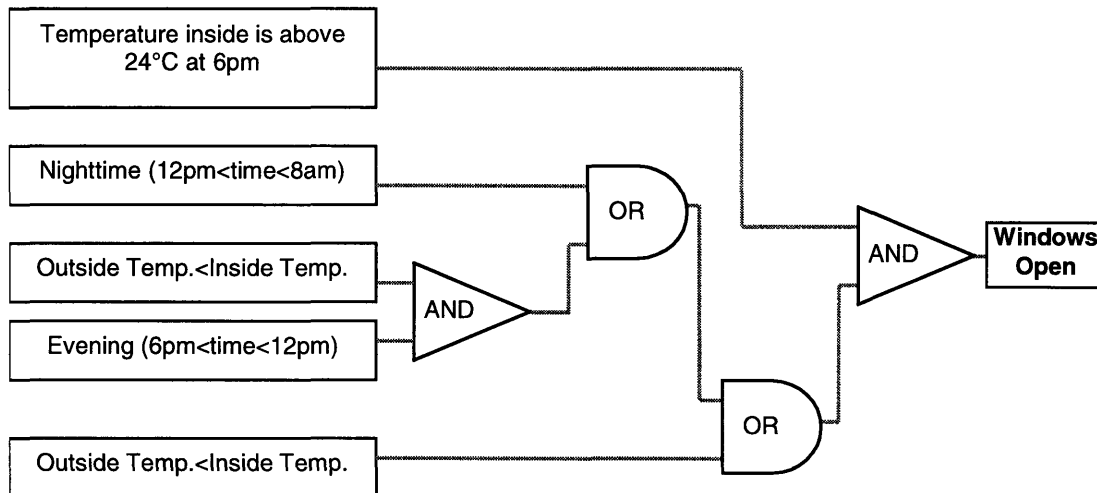
Figure 1.4.4

In figures 1.4.4 and 1.4.5, in the next page, we can see the general logic layout of the implementation of the user behavior for the two ventilation strategies.

Figure 1.4.4 represents the logic layout of the night cooling ventilation strategy. The determining condition is the one at the top: indoor temperature above 24°C at 6 p.m. From 8 a.m. to 6 p.m., whenever this condition is satisfied, the condition at the bottom of the figure ensures that the windows will be open whenever the indoor temperature is higher than the outdoor temperature. The next two from the bottom ensure that the same happens during the evening (6 p.m. to midnight). The following one means that the windows will be open throughout the night whenever the determining condition is satisfied.

Figure 1.4.5 represents the logic layout of the daytime ventilative cooling strategy. It is the same layout of figure 1.4.4, with two more conditions added. These ensure that, whenever the indoor temperature is above 28°C and the airflow generated in the living room by opening the windows is above 0.3 m/s, the windows will be opened (provided the determining condition is satisfied).

Daytime Ventilative Cooling Strategy
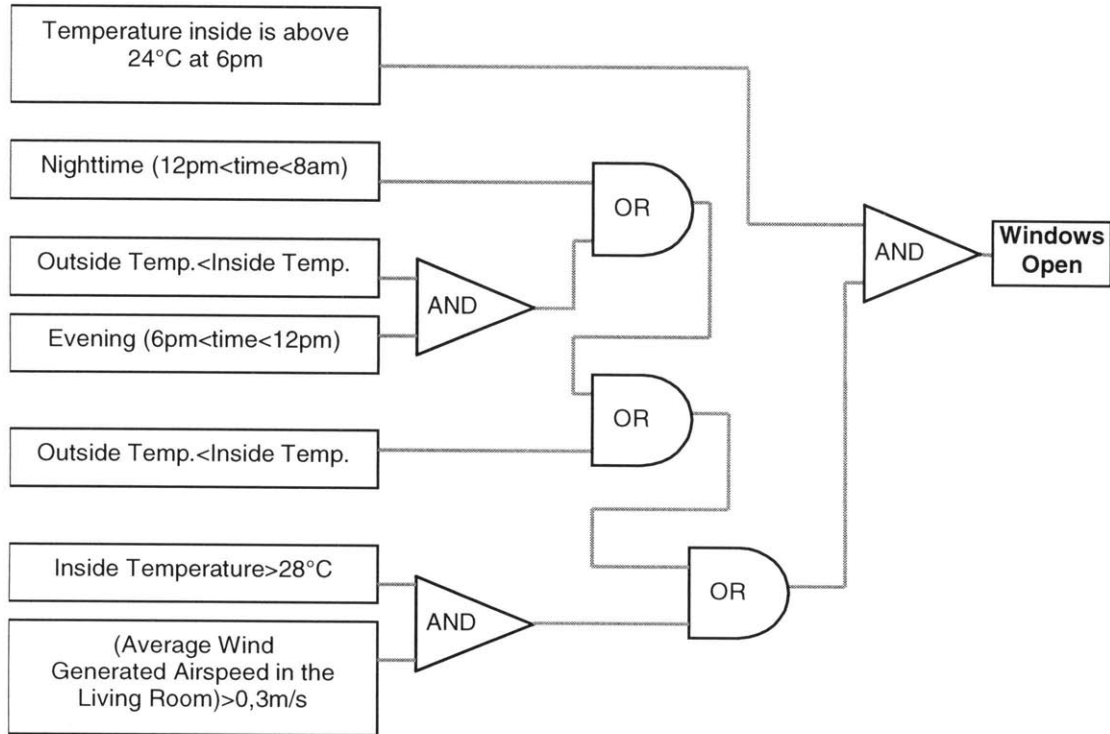
Figure 1.4.5

Day Time Comfort Ventilation

Part II

Part one of this thesis presented the theoretical concepts that are used to perform the coupled simulation that is the goal of this work. Part two of this thesis the coupled model described in section 1.4 is applied to study the performance of daytime ventilation and night cooling systems. Part two begins with a climate analysis of the three cities considered in this study. This climate analysis is essential to establish the starting point for the application of the two passive cooling systems. Section 2.2 presents the details of the case studied (a six story apartment building). The final section of this part presents the results of the simulations.

2.1-Climate Conditions in Beijing, Shanghai and Tokyo.

This section presents an analysis of the climate conditions of the three cities considered in this study. A climate analysis is necessary to detect the possible problems with these climates (the first one is weather there is need for cooling). After this first analysis, a more detailed study of additional climate parameters is presented. These additional parameters are specific to passive ventilative cooling systems.

When studying passive systems there is a need to do a more detailed weather analysis. To design with nature, one should have to take a closer look at nature, in this case the climate. In the next section, the heat capacity of the building materials and the heat transfer process between them are analyzed in detail. Again looking at natural processes in detail and using them to achieve a good building thermal performance and occupant thermal comfort.

The first step in this study was to obtain the weather information. In order to perform a building thermal simulation the following weather data is needed: dry bulb temperature, relative humidity, atmospheric pressure, wind velocity, wind direction, direct solar radiation and diffuse solar radiation. The files used in this study are TMY (typical mean year). It is essential to use a TMY file in order to avoid using a specific weather year (which could be too warm, too cold or too sunny etc...). For all the cities TMY files were used. For this study, a full summer external shading system is used. In this context, solar radiation is not a crucial factor (although it has a moderate influence in the results as will be shown in the next section). For this reason, insolation data was not used in the preliminary analysis presented in this section.

The weather file for the city of Tokyo was provided to our group by our counterparts in Japan. It is a typical weather year. For each of the Chinese cities, two TMY (Typical Mean Year) files were obtained from LBL.

In the case of Beijing, the TMY file did not contain wind direction information. In order to overcome this flaw, there was a need to use another source. In this case, Chinese building design handbook. In this handbook, we can find information about wind direction probability for summer, winter and whole year. Summer information is for June, July and August. This information was used to complete the TMY file. For every hour with a non-zero wind velocity, a wind direction was randomly assigned. A simple routine was written to randomly assign wind directions to each wind velocity point using the frequency distribution obtained from the handbook.

The comparison between the Chinese design handbook data and the TMY file shows good agreement both in the average velocity and the number of hours without wind (20% in the whole year, see table 2.1.1, see next page).

These two files, plus the file for the city of Tokyo, were used in the passive system performance analysis presented in the following sections. The quality of a system performance analysis is dependent on the quality of the data it uses. In the case of Beijing, the analysis can clearly be improved by using a complete, single source file.

When studying cooling needs in these climates winter and autumn are not important. The period of the year were buildings may need cooling is spring and summer. This study is done for the period starting in May 1st and ending in September 30th. This period was chosen in order to include not only the warmest

Table 2.1.1

Comparison between the TMY file data and the Chinese Design Handbook data.

Beijing	Summer MWS		% of hours with no wind (one year)	
	From TMY	From Handbook	From TMY	From Handbook
	1.85 m/s	1.9 m/s	19.6 %	20%
ShangHai	3.22 m/s	3.2 m/s	5.3%	6%

period of the year but also the warmest part of the mild season. Using an extended analysis period increases the number of warm days (and sequences of warm days) in which the system performance can be analyzed.

We start the evaluation of the climate conditions by looking at the typical design days. In figures 2.1.1, 2.1.2 and 2.1.3 we see temperature and humidity levels for the design days in Beijing, Shanghai and Tokyo respectively.
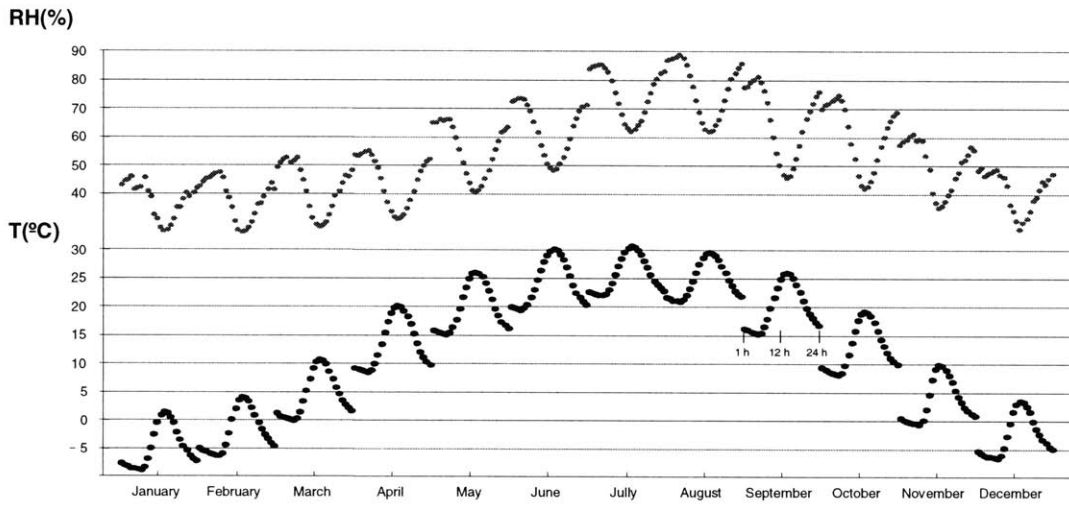
Figure 2.1.1

Relative humidity and temperature for the design day in each month, Beijing.
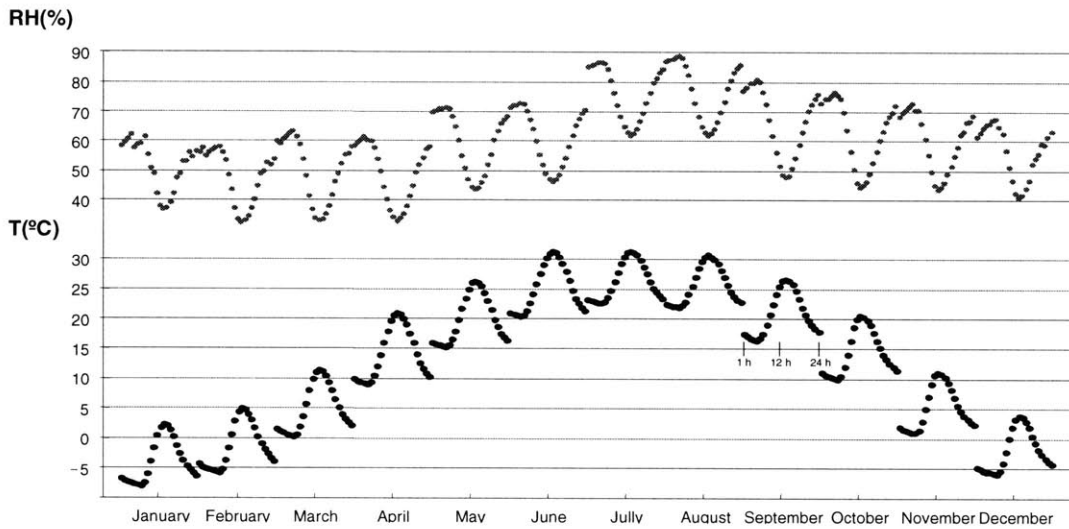
Figure 2.1.2

Relative humidity and temperature for the design day in each month, Shanghai.

82
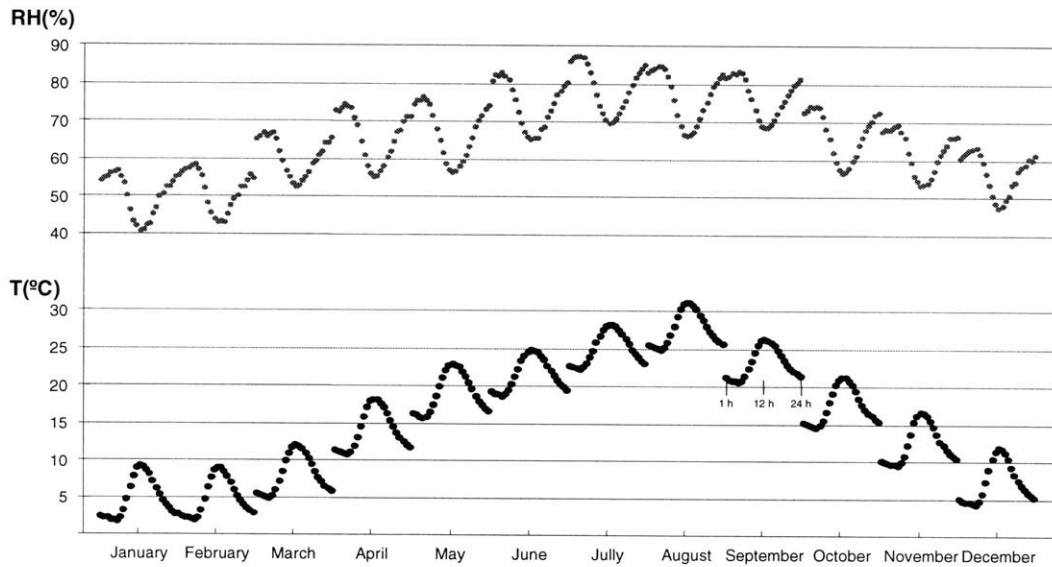
Figure 2.1.3

Relative humidity and temperature for the design day in each month, Tokyo.

Several simple conclusions can be taken from these figures. The three climates can be characterized as hot and humid. In the warm months, the humidity can be high, especially in the night (above 80% RH). The fact that the night is the coolest period of the day makes these high humidity levels more tolerable. Still, they are one of the main causes of thermal discomfort in these climates. For all cities, July and August are the months with the highest combination of heat and humidity. This combination makes them the months with the highest cooling load. There are no extremely warm (maximum temperature above 35 °C) months in any of the cities. This fact opens good possibilities to achieve thermal comfort using ventilative cooling.

In these charts it is possible to see that the temperature variation during the day is not very large (above 12ºC) for any of the cities. In all three cities, there is a need for a cooling system in order to keep indoor temperatures under control (below 30 °C, and preferably lower), and also overcome the thermal discomfort caused by humidity.

The simple analysis just presented is useful in a first stage to detect whether there is need for a cooling system. The next two sections present a set of climate parameters specific to passive systems.

2.1.1-Analysis of Climate Factors for Passive Cooling.

In order to evaluate summer weather conditions it is normal to consider the following climate parameters: temperature and humidity levels attained in the warmest parts of year, solar radiation level, and the average wind velocity and direction. In the case of passive systems, it is important to consider a set of other factors that can influence the success of a passive cooling strategy.

These weather factors are not as crucial to mechanical cooling systems as they are for passive systems. In the following pages of this subsection, an analysis of these specific climate factors is presented. This section ends with the conclusions from this analysis.

Both passive-cooling systems studied use the environment as a heat sink and, therefore, are sensitive to weather conditions. In particular the occurrence and persistence of warm and humid or no-wind periods. In the case of ventilative cooling, the additional determinant weather characteristic is the correlation between the warmest hours and the wind (velocity and direction). For night cooling systems, the following weather characteristics are important: daily temperature range, occurrence of high humidity periods during the day, which can lead to water condensation in the building structure.

In the present work, it is necessary to give closer attention to the warm days in the analysis period. The criterion used for defining warm days was based on the comfort equations. Simple calculations show that the PPD value will exceed 20% when the temperatures (air and radiant) go above 29°C (for 60% humidity and zero airflow velocity). For the apartment building in this study and for most of the cases analyzed the daytime indoor temperature is lower than outside (see section 2.3). In

order to take into account this temperature difference the following criteria is used to define the warm days:

$$T_{out} > 30°C \quad 2.1.1$$

Where T_{out} is the outdoor dry bulb temperature. The warm days will be the most challenging and deserve further attention. In these days, it is possible that the indoor temperature will rise to levels that can cause discomfort to the occupants. For this reason, the climate in and around these days is analyzed in more detail.

The remaining days in the warm season (with mild climate conditions outside maximum temperature not exceeding 30 °C and humidity below 75%) are not expected to be a problem for a properly designed passively cooled building. This is true whenever we have a well designed external shading system (in order to avoid direct solar gains in the warmest months) and enough exposed internal mass (which greatly dampens the daily variation of the building internal temperature see section 2.3).

The main challenge is then in the warmest days (with temperature above 30°C). In these days, the passive cooling system must handle a high cooling load and the climate factors mentioned above can greatly influence the its performance. We now proceed to analyzing the climates for application of the two systems. This section ends with the conclusions from this simple analysis.

Night Cooling.

As a starting point, we have in table 2.1.2 a set of simple indicators that can be used to assess night cooling potential. The night period is considered to range from 10 p.m. until 8 a.m. Depending on the outside weather conditions and on user needs, this period may vary. These variations are not considered in this first analysis.

From the climate parameters presented in table 2.1.2 it is possible to see that both Tokyo and Shanghai are not promising for night cooling. A temperature variation of five or six degrees is generally not sufficient to obtain any significant structural cooling (Givoni (1994)). For the same wind velocity and geometry, a temperature variation of 5 K or 6 K offers half the cooling potential of a 10 K temperature variation. When exposed to the cold night air, the walls always remain at a higher temperature than that air; during the day the situation is reversed. The higher this temperature difference, the more heat can be exchanged with the walls in a typical day.

Table 2.1.2

Important climatic parameters for nighttime ventilative cooling

Night Cooling	Average Temp. Variation From May to September	Average Wind Speed (from10 p.m. to 8 a.m.)	
		Simple Average	Corrected for N-S
Beijing	10.3 °C	1.6 m/s	1.2 m/s
Shanghai	6.8 °C	2.5 m/s	1.5 m/s
Tokyo	5.9 °C	3.3 m/s	2.8 m/s

The wind driven indoor air velocity in front of the wall determines the convective heat exchange coefficient (for air velocities ranging from 0.1 m/s to 3 m/s , h_{conv} will range from 4-14 W/(m^2 ^{o}C) – see section 1.4). The wind moves air, which is the energy transport media. It takes energy into the natural heat sink, the atmosphere. For these reasons it is necessary to consider also the wind velocity during the night period. In this aspect both Shanghai and Tokyo present the highest values (see column three in table 2.1.2).

Wind direction is another important factor. North-South orientation is usually preferred, it is ideal in terms of controlling the solar gains and obtaining adequate light levels throughout the year. The N-S orientation corrected average wind speed value is the most significant. After this correction the values for the different cities become more balanced. This simple and wind direction calculation is only possible because we are dealing with an isolated building. In case there were other buildings close to the our building this simple treatment would become invalid.

In table 2.1.2, the average temperature variation (second column) is calculated by subtracting the nighttime minimum temperature from the maximum daytime temperature. The average wind speed is calculated considering only the nighttime hours (from 10 p.m. until 8 a.m.). In the fourth column, a correct average wind velocity is presented. It is obtained by multiplying the wind velocity by $|cos(\theta)|$. The angle θ is the angle between the wind and the north-south direction.

The number of warm days (maximum temperature above 30°C) in the season is 41 for Beijing, 55 for Shanghai and 33 for Tokyo. Shanghai is the city with the highest number of warm days. Taking into consideration that the temperature variation is low and that the corrected wind velocity is similar to that of Beijing, one is lead to conclude that night cooling might not be an appropriate strategy for ShangHai. Compared to Beijing, Tokyo has lower cooling needs and a lower temperature spread, which is at least partially compensated by a much higher wind velocity. Clearly in order to proceed with this analysis, it is necessary to look further into the climate in the warm (most critical) days. Table 2.1.3 presents these additional factors.

In the second column, we see the number of days with maximum temperature above 30 ^{o}C. In parenthesis is the percentage of days in the warm season that fit this criterion. In the third column, we have the temperature variation for these days. It should be noted that this temperature variation is calculated by subtracting the

Table 2.1.3

A more detailed look at the application of night cooling to the warmer days.

| Night Cooling | Days With Maximum Temperature Above 30 °C | | | | | |
| | Number of Days | Temp. Variation | Average at Hour of Max. Temperature | | Avg. Wind Speed (10 p.m.-8 a.m.) | |
			Temp.	RH (%).	Simple Avg.	Corrected N-S
Beijing	41 (27%)	9.7 K	32.8 °C	42 %	1.4 m/s	1 m/s
ShangHai	55 (36%)	4.6 K	32.9 °C	66 %	2.6 m/s	1.6 m/s
Tokyo	33 (22%)	5.5 K	31.6 °C	57 %	4.4 m/s	3.9 m/s

minimum nighttime temperature from 30 °C. In this way a more correct assessment of the cooling potential from the previous night is obtained. If a simple subtraction from the maximum is used, larger temperature variations is obtained. These temperature variations are not representative (they would be unrealistically high due to the high daytime temperature maximum). In the fourth and fifth columns, we have the average temperature and relative humidity in the warmest hours of the each of the warm days (maximum temperature above 30 °C). In the six and seventh columns we have the nighttime wind data for the warm days. Again, simple and corrected averages are presented.

The temperature variations presented in this table are for the warm days only. Again, we see that Beijing has the highest value, Shanghai the lowest. Also notice that in Shanghai the warmer days are accompanied with high humidity content, which means that there is a risk of condensation in the high thermal mass partition surfaces.

Daytime Ventilative Cooling.

We now proceed to look at the daytime ventilative cooling case. After this subsection the conclusion is presented.

In table 2.1.4 presents a set of indicators relevant to daytime ventilative cooling. In the second column, we have the average wind speed during the warm period of the day (from 11 a.m. to 5 p.m.). In the third and fourth columns, we have the average temperature and relative humidity in the warmest hours of the each of the warm days (maximum temperature above 30ºC). In the sixth column, the average wind velocity in the warmest period of the daytime is presented.

Looking at table 2.1.4 we realize that Tokyo is the city with the highest potential when these parameters are used. This is due to the fact that the wind velocities are the highest and that the cooling load is the lowest. Shanghai might have enough wind velocity in the warm days to make a daytime ventilative cooling system feasible. This is a positive aspect since, as we saw above, the night cooling

Table 2.1.4

Important climatic parameters for daytime ventilative cooling

Daytime Ventilative Cooling	Whole Season Avg. Wind Speed (11 a.m.-5 p.m.)	Days With Max. Temp. > 30 ºC			
		Avg. at Hour of Max. Temperature		Number	Avg. Wind Speed
		Temp.	RH (%).	Of Days	(11 a.m.-5 p.m.)
Beijing	3.0 m/s	32.8 ºC	42	41 (27%)	2.8 m/s
ShangHai	4.0 m/s	32.9 ºC	66	33 (22%)	2.6 m/s
Tokyo	6.8 m/s	31.6 ºC	57	55 (36%)	4.4 m/s

90

potential for this city is quite low. Also worth noting is the fact that the daytime wind velocity in Beijing is twice the nighttime average value (the other two climates do not have such a high difference).

In a cross-ventilated building, orientation is a determinant factor. If the inlet-outlet axis is parallel to the predominant wind direction, we clearly will get higher ventilation rates. Normally, when we look at wind data, we either consider the probability distribution of wind directions or the wind velocities (generally the average).

Figure 2.1.3 (see below), shows a more detailed analysis of the wind potential. The six figures show the variations of the wind potential for different inlet-outlet orientation and period of the day in the warm season. These circular plots are obtained by calculating the average value of the product of the wind velocity and the cosine of the angle between the wind direction and the inlet-outlet axis. In this way, a clearer image of the ideal orientation of the inlet-outlet axis is displayed. The ideal "solar orientation" (north south) is another factor that must be considered when choosing the building orientation. It should be noted that these charts are not sufficient to obtain a complete picture of the wind potential. They must be used in conjunction with a standard wind rose chart. In this way a better evaluation of the relation between velocity and probability of occurrence of wind for each direction can be obtained.

A closer look at these charts shows that for Beijing and Tokyo, although the ideal ventilation orientation is not North-South, it is possible to use a N-S orientation and still use almost all the natural cross-ventilation potential. In both cases using N-S it is still possible to use 95% of the maximum available wind potential.

For Shanghai there is a reduction of approximately 30% in the average corrected (N-S) nighttime wind velocity when using a N-S orientation. For daytime ventilation, the loss is much smaller and the corrected average velocity obtained is higher (yet another factor pointing to the use of daytime ventilation in Shanghai).
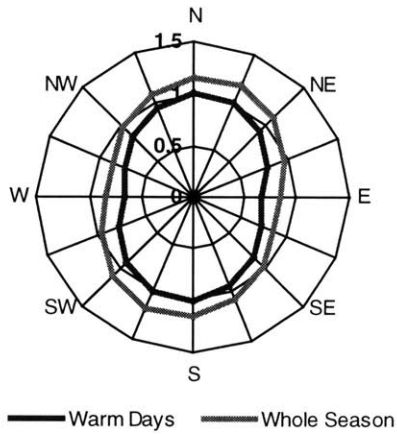
Beijing Night
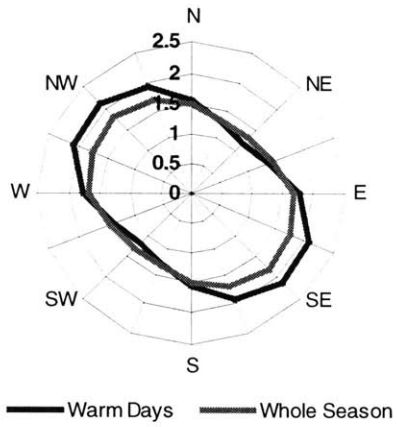
Beijing Day
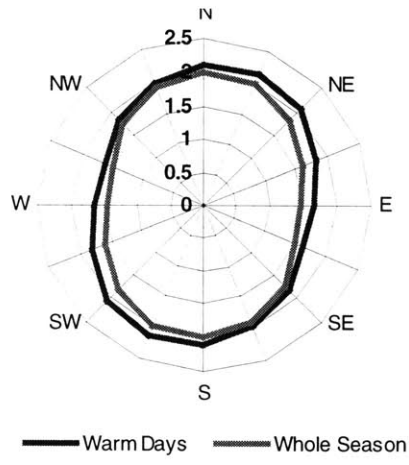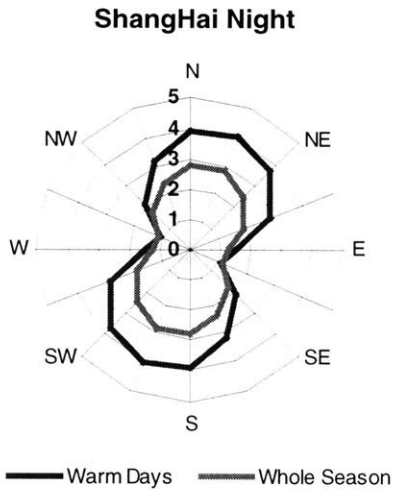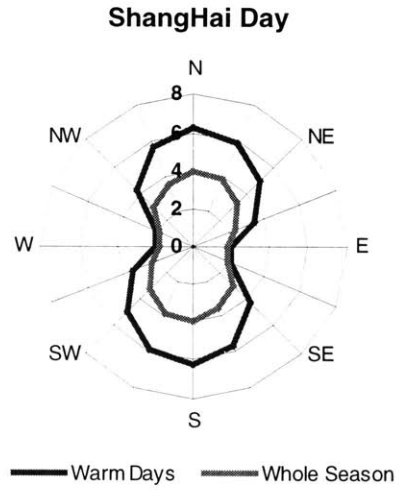
ShangHai Night

ShangHai Day

Tokyo Night

Tokyo Day

Figure 2.1.3
Average wind velocity obtained for different orientations of a cross-ventilated building.

Summary

The previous analysis leads to the following conclusions. The Beijing climate has a good potential for night cooling due to:
- Adequate daily temperature variation (9.7ºC in the warm days).
- No excessive humidity in the warmest days.
- Adequate wind level in the North-South direction both in the warmest days and in the warm season (although the average wind velocity should be considered low during the night (1m/s in the warm days)).

The Shanghai climate is the most challenging of the three and daytime ventilative cooling seems to be the most adequate strategy due to following:
- Low daily temperature variation in the warmest days.
- High relative humidity during the warmest days, which requires air movement in order to insure thermal comfort.
Adequate wind velocity during the daytime so that convective cooling with outside air can be done.

Tokyo has the least problematic climate (lower number of warm days). The best passive cooling strategy is daytime ventilative cooling. This conclusion is based on the following:
- Low daily temperature variation.
- High daytime average wind velocity.

The second part of this thesis continues with the description of the cases that will be analyzed in section 2.3.

2.2-Description of the Case Studied.

This section presents in detail the cases simulated in this thesis. The geometry and materials used in these cases is presented. In section 2.3 the results of the simulations of these cases are presented.

2.2.1-The Design.

This subsection presents the design of the building analyzed in this study. As mentioned in the introduction a generic six story apartment building is studied.

Figure 2.2.1 (in the next page) shows the geometry of this apartment building. It is a six-story apartment building with ten units (two per floor). Each unit has three bedrooms and a total floor area of $115m^2$.

Figure 2.2.2, shows the internal layout of the apartment units. In this figure we can see in dark gray the external surfaces and floors in medium gray the doors and in light gray the internal partitions. The middle compartment is the living room. Access to the apartments is done through an external corridor on the north side of the units (upper part in the drawing). People enter each apartment through the door that is visible on the upper part of the living room. On the south side of the living room there is an external balcony (in the figure the balcony starts were the living room internal wall turns dark gray). On the right hand side there are two identical bedrooms, one facing south and another one facing north. Between the two bedrooms, is the first restroom. On the lower left-hand side in this picture, we see the main bedroom, facing south. The compartment in the top left hand side is the kitchen. Between these two compartments, there is a second restroom.
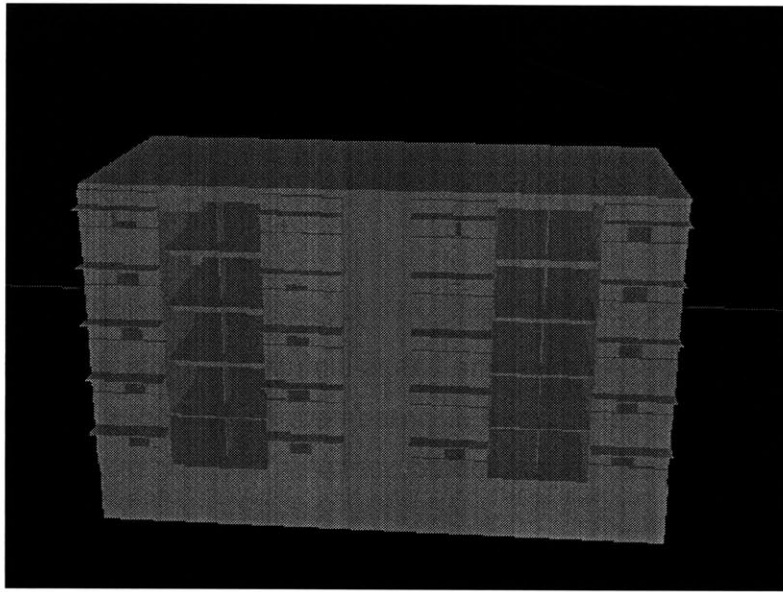
Figure 2.2.1

Representation in PHOENICS of the six story apartment building simulated.

North
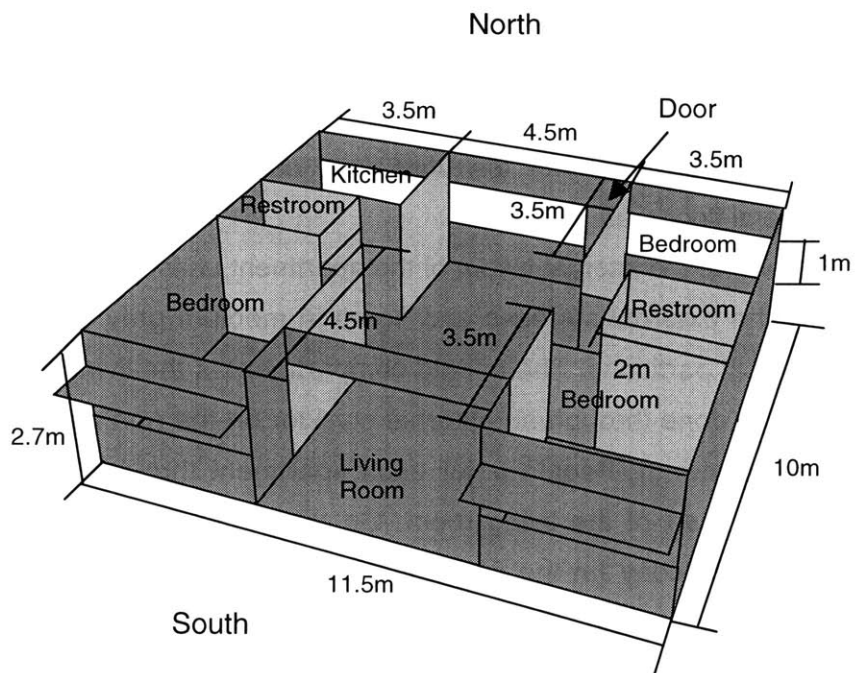
Figure 2.2.2

Interior configuration of the apartment units studied.

Several features in this design make it suitable for wind driven passive cooling. The main feature is the possibility to cross ventilate the living room separately from the three bedrooms. This allows for high nighttime ventilation rates, greatly enhancing nighttime heat release from the living room surfaces. Another feature that increases cross-ventilation are the large apertures above the internal doors. These apertures allow air to flow through the bedrooms even when the doors are closed. External shading is used in all the south windows. The balcony of the living room provides the shading for the living room balcony window.

When the apartment is in nighttime ventilation configuration both the balcony window in the living room and the north side windows of the living room are fully open. One square meter was considered to be a reasonable size of open windows in the night for the bedrooms. Using more than one square meter would be an unreasonable assumption since these windows will be open at night when the occupants are sleeping in the bedrooms. In order for the windows to be open at night the occupants are supposed to use protection steel bars on the north windows of the apartment. This security measure prevents intrusion from someone who gains access to the external access corridor. In the following paragraph a set of important details is explained.

During the day a set of ceiling fans is used in the apartment in order to promote mixing and enhance the convective heat transfer between the walls and the occupants. The apartment has double glass windows with 95mm air space, aluminum frame with no thermal break (DSA, 2.4mm glass). In order to calculate the heat gain from this window the SHGF method is used (ASHRAE (1997)). The window has a shading coefficient of 0.88. The living room windows are considered to be partially (50%) covered with light venetian blinds (shading coefficient 0.33). All the doors are panel doors with 11mm panels (ASHRAE, 24.13 (1997)).

2.2.2-The Cases Analyzed.

In table 2.2.1 we can see a description of the several cases studied. All cases have similar geometry (see figure 2.2.1). The numbering used reflects three main variations in the building structure and a ventilation strategy variation.

Case 1.1 is the base case; it has medium weight (10cm thickness) concrete

Table 2.2.1

Description of the cases studied.

Case (Name)	Flooring Material	Composition of the Partitions		Ventilation Strategy
		Floor	Internal Wall	
1.1 (Base)	Ceramic Tile	10 cm Concrete	10 cm Concrete	Wind Driven Night Cooling
1.2 (Reference)	Ceramic Tile	10 cm Concrete	10 cm Concrete,	Wind Driven, **Daytime heat removal** (30% of 2.2)
1.3 (Carpet)	**Carpet**	10 cm Concrete	10 cm Concrete	Wind Driven Night Cooling
2.1 (Lightweight)	Ceramic Tile	**10 cm Perforated Concrete**	**Lightweight (Gypsum Board)**	Wind Driven Night Cooling
2.2 (Daytime Ventilation)	Ceramic Tile	**10 cm Perforated Concrete**	**Lightweight (Gypsum Board)**	**Wind Driven, Daytime heat removal**
3	Ceramic	**14 cm Concrete**	**14 cm Concrete**	Wind Driven Night

Material	Density (Kg/m³)	Heat Capacity (J/(Kg K))	Conductivity (W/(m² K))	Width (m), if applicable.	Source of data
Insulation (Expanded Polystyrene)	43	1210	0.029	0.04	ASHRAE (1997)
Concrete	2100	880	1.4		Mills (1996)
Tile	2000	800	0.91	0,008	ASHRAE (1997)
Carpet (Nylon)	194	1200	0.42	0.005	The Carpet-Rug Institute -
Carpet Cushion	360	1200	0.55	0.006	Technical Information

Table 2.2.2
Material Characteristics

partitions. Case 2 is a lightweight structure case; it uses perforated concrete floor (see figure 2.2.3) and gypsum board low mass internal partitions. Case 3 is included to study the effects of a high thermal mass structure.

For cases number 1 and 2 the effect of varying the thermal mass of the partitions is analyzed. In case 1.3 the thermal mass decoupling effect of using an insulating floor covering (nylon carpet) is analyzed. In case 2 the ventilation strategy is varied. This is the only case where daytime natural ventilation is used. The reason for this is that in this type of ventilation strategy, there is limited use of thermal mass. Therefore, this strategy is applied to the low mass configuration (case 2.2). Case 2.1 was only used for Beijing and Tokyo (see section 2.3). It is meant to test the effectiveness of night cooling when there is limited thermal mass available (approximately 55% when compared with case one). In case 3 we have a 30% increase in thermal mass when compared with the base case. In all the cases the external walls are composed of 10 cm concrete with 4 cm of external insulation (ρ=43 Kg/m³; cp=1210 J/(Kg K);

k=0.029W/(m²K) ASHRAE (1997), expanded polystyrene extruded (smooth skin surface)). Figure 2.2.3 shows the perforated floor. This floor was modeled as bulk volume with an equivalent width of 6cm.
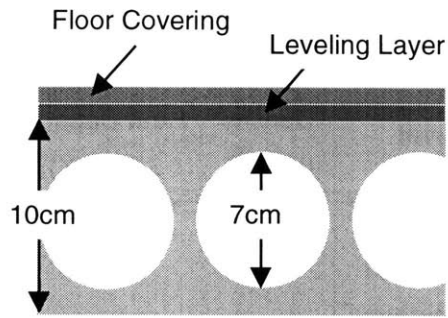
We now proceed to present the internal heat gains that were used in all the cases.

Figure 2.2.3

2.2.3-Internal Gains

The internal gains were calculated according to ASHRAE (1997) recommendations. Section 1.1.3 describes the that are used. Table 2.2.3 shows the values adopted. Notice tha variatin with day and night.

Table 2.2.3

Internal gains used in the calculation.

| Case | Internal Gains | | | |
| | Lighting and Appliances | | Occupants | |
	Day	Night	Day	Night
Standard	350 W	175 W	4x85 W	4x85 W

The following section of this report (section 2.3) presents the results of the simulations.

2.3- Results of the Simulations.

This section presents the results of applying the model introduced in section 1.4 to simulate the thermal performance of the apartment building described in section 2.2.

The analysis of these results will answer two main questions. The first question is whether it is possible to achieve adequate levels of thermal comfort in the warm season by using one of the two passive ventilative cooling systems: night cooling or daytime ventilation. The second question is weather daytime ventilation or night cooling is the best cooling strategy for each climate.

For each of the three cities the six simulation cases described in table 2.2.1 were performed. The first set of simulations evaluates the best ventilative cooling strategy (see subsection 2.3.1). One case represents each strategy. Case 1.1 for night cooling and case 2.2 for daytime ventilative cooling. Notice the fact that the daytime ventilation case uses lighter materials in the partitions. Thermal mass is not the main cooling system for daytime ventilation. In this way, it makes sense to test it with a lighter, and therefore less expensive, structure.

Each of the base ventilation cases (case 1.1 and case 2.2) is compared with the reference case (case 1.2) and with a scenario using outdoor conditions inside (temperature and humidity). After this a second set simulations is presented. It analyzes the impact of different structure and flooring material characteristics on the performance of the night cooling ventilation system.

Section 2.3.1 presents the flow simulation results. As explained in sections 1.3 and 1.4, the flow simulation is treated independently of the thermal simulation. Therefore, these results can be applied to all three cities. Subsections 2.3.2-2.3.4 present the results of the coupled model. Different features of the implementation are illustrated,

particularly the two ventilation strategies. The wall and room air temperature variations during the several days are plotted and analyzed, clarifying the results that are presented in the next subsection. Next, we have the main results of this analysis (subsection 2.3.3). This subsection presents the analysis of the performance of the two passive cooling systems and identifies best system. Subsection 2.3.3 presents the results of studying the impact of different internal partition compositions on the night cooling system performance. Finally the last subsection analyses possible humidity and condensation problems are.

2.3.1-Results of the Airflow Simulations.

Section 1.4 described the operation procedure of the coupled model. The results of the flow simulations are used in the coupled model as a database of flow cases that are accessed according to the wind conditions at each hour. Interpolations are used whenever the outside conditions are not identical to one of the simulated cases in the database.

In this subsection presents the results of the simulations. The validity of the interpolation procedure is discussed.

The coupled model uses the following information from CFD (obtained by reading the PHOENICS results file and making the necessary post processing):

-Airflow rates through each room.

-Average air velocities in the grid point adjacent to each wall surface of the apartment (indoor and outdoor)

-Average air velocity in the occupied area of the living room (for the calculation of convective cooling by daytime ventilation).

As explained in section 1.4 the flow simulations were performed for four different directions (due to the symmetry of the building this is equivalent to seven directions) and four different wind velocities (1, 2, 3 and 4m/s).

The results for all the directions showed a linear increase with wind velocity. This behavior makes the use of linear interpolation for obtaining the intermediate points an adequate approximation. In figures 2.3.1 and 2.3.2 in the next page we can see the flow rates and near wall velocities for the SW wind case. For this case simulations of 1, 2, and 4m/s wind were performed.
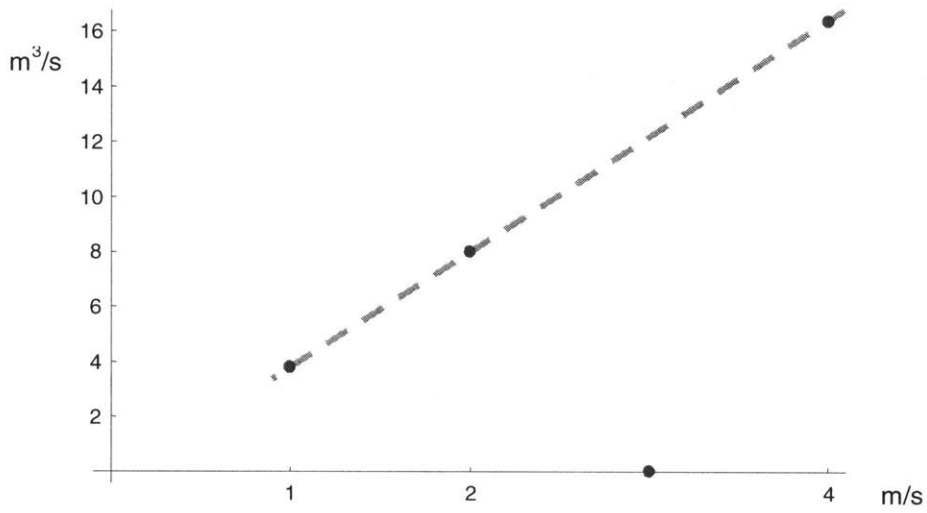
Figure 2.3.1

Airflow rates in the living room for wind coming from SW, three wind velocities, 2, 3 and 4m/s.
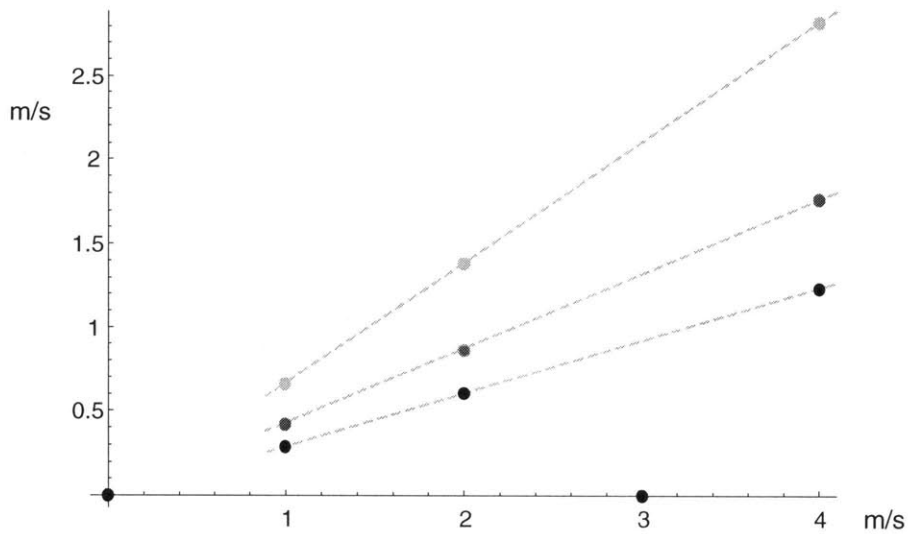

Figure 2.3.2

Average airflow velocities for three surfaces in the living roomwind coming from SW, three wind velocities, 2, 3 and 4m/s.

The **dark** dots are the velocities in the ceiling of the living room.

The dark gray dots are velocities in the internal partition between the living room and room 4.

The light gray points are the velocities in the wall plane below the north window of the living room
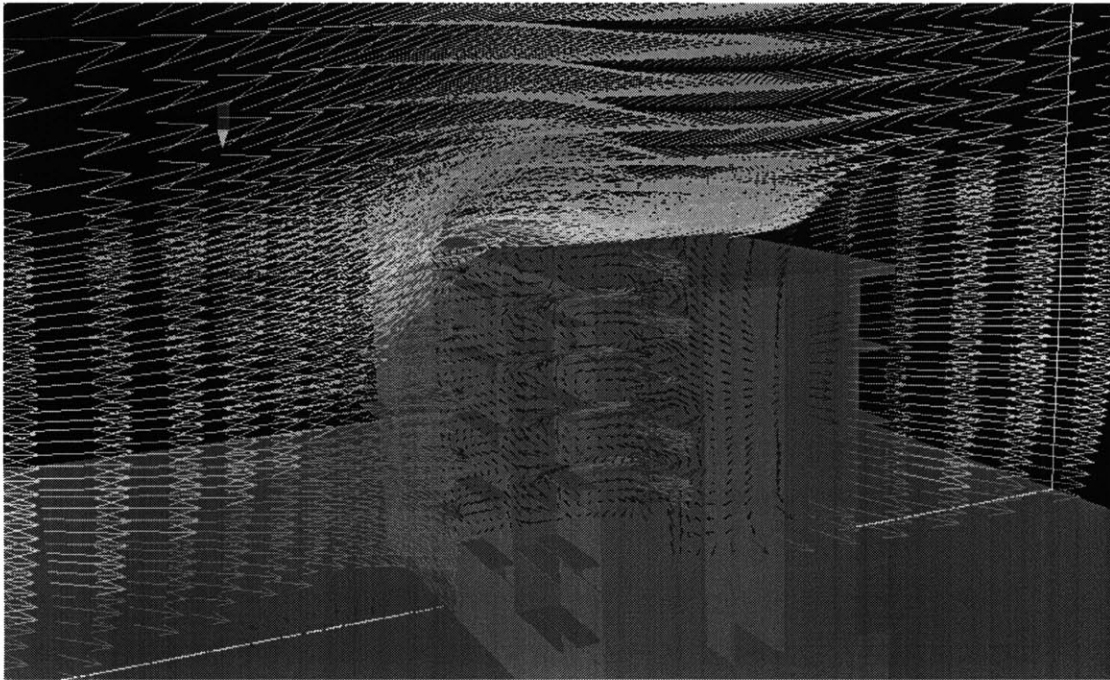
Figure 2.3.3
The airlflow in and around the buiding for SW 4m/s wind.

The fact that the 3m/s simulation was not performed is a consequence of the processing of the cases that was done before this case was calculated. This preliminary analysis showed a linear increase with wind velocity. This case was used for plotting these charts because the wind approaches the building with an angle of 45° making the flow pattern more complex than in the north or south wind direction cases.

The figure in the next page presents a set of simulated flow fields for the case used in the previous figures (SW, 4m/s). In figure 2.3.3, a general view of the velocity flow filed is shown. In figure 2.3.4, we can see a set of pictures of the airflow pattern for SW 4m/s wind. In the upper frame, we can see the airflow in the two units on the fifth floor of the building. In the lower left picture, we can see a section of the six-story building. The airflow enters the building from the south into the small south bedroom. On the left of this figure, we can see the air exiting the small north bedroom.
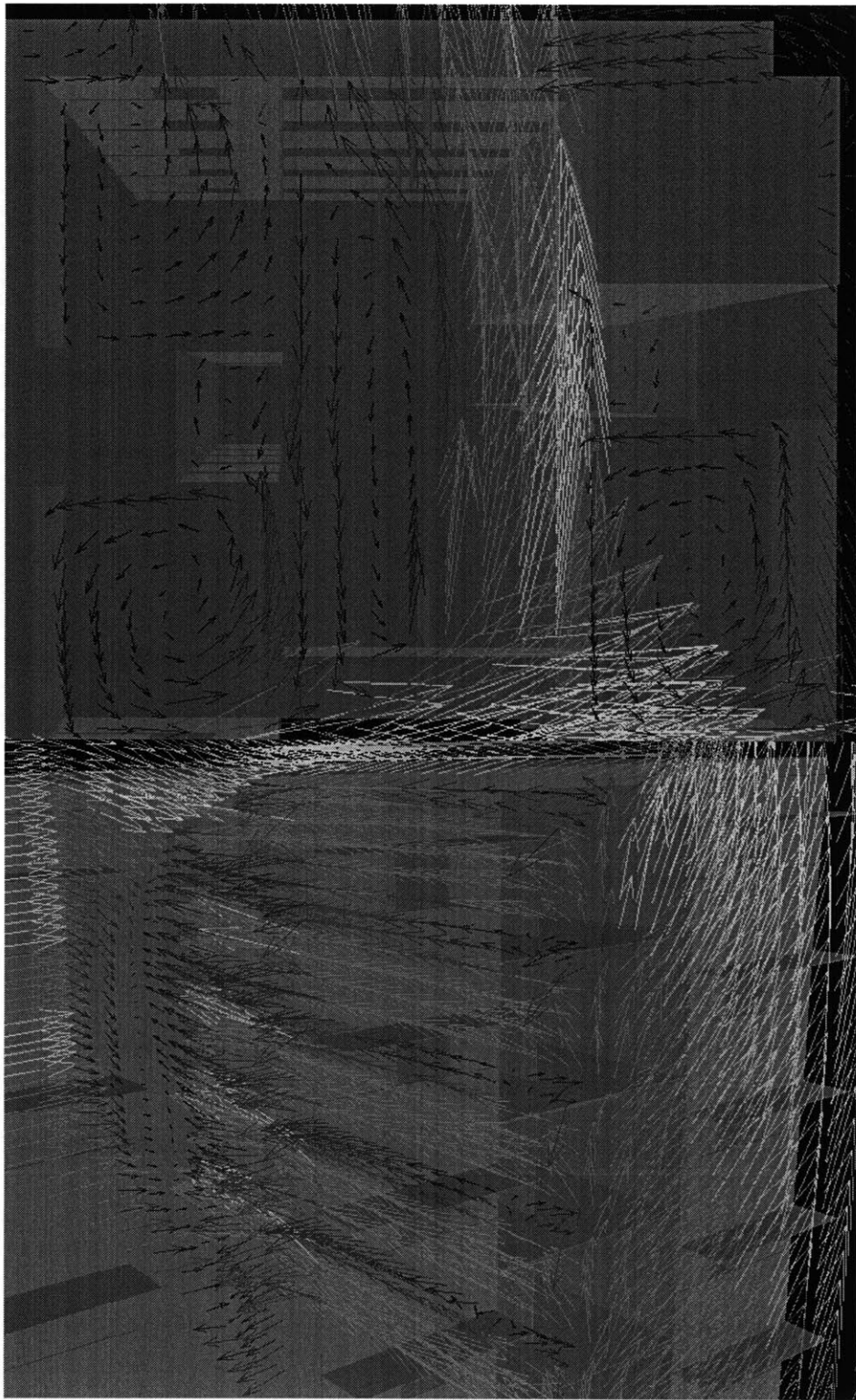
Figure 2.3.4

Several details of the airflow pattern in and around the building for SW 4m/s wind.

2.3.2- Detailed Analysis of the Hourly Temperature Variations.

Section 1.4 describes the general operation of the coupled thermal model. For the case being analyzed, this model predicts indoor air temperatures in intervals of two hundred seconds. When applied to the case described in section 2.2, the model produces 58 surface and glass temperatures as well as the air temperatures for each room. It is difficult to draw clear conclusions from such a large number of variables. However, the use of the Fanger comfort model allows us to have a unique parameter that characterizes the indoor environment (PPD). Still, it is useful to look at what is behind that parameter and analyze the predicted temperature variations in several parts of the system.

Inside the apartment, it is possible to observe two types of temperature variation, depending on the thermal inertia of the elements. The lightweight elements such as: doors, lightweight walls (these walls are only present in case 2.1 and 2.2), glass and the air inside the apartment have a low thermal storage capacity. For this reason, they have a fast response to changing conditions (such as solar radiation, airflow rates and outside temperature). The heavy walls and floors, due to their high thermal mass, have a much slower response.

In figure 2.3.5 we can see the temperature variation of the air and in the ceiling of the living room (room 1) for a period of three days (standard case, night cooling strategy). As expected, the indoor air temperature (black line) shows fast variations, depending on the outside temperature, solar gains and ventilation flow rate. The ceiling surface temperature shows a much slower temperature variation, with a noticeable lag in response.
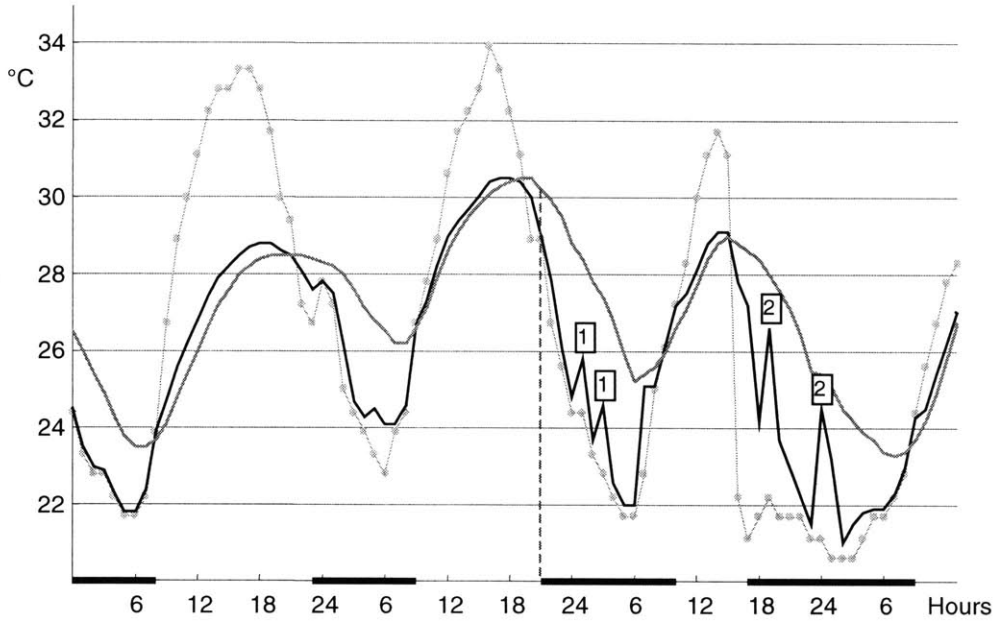
Figure 2.3.5

Hourly temperature variation for Beijing, night cooling (Case 1.1).

Light Gray, Outside Temp.. Medium Gray, Wall Temp.. **Black**, Indoor Temp..
The dark line in the horizontal axis indicates periods of high ventilation

This thermal lag (also called thermal inertia) effect is due to the presence of the heavy wall behind the surface. Since both the wall conductivity and its thermal capacity are high, when the air temperature decreases heat flows from the core of the wall into the surface, keeping its temperature stable for a period of time before it starts to follow the air temperature again. The fact that the daily temperature variation of the walls is much smaller than that of the outside air temperature is a direct consequence of this inertia.

One important component of the passive cooling system is the ceiling fans. During the day they promote convective heat transfer with the walls and increase convective cooling of the occupants. Due to the presence of these fans, the air temperature distribution inside each room is treated as isothermal. When the windows are closed, the indoor air temperature remains close to the wall temperature. During the ventilation periods (see dark line in the horizontal axis), the air temperature closely follows the outside temperature. During these periods it remains always slightly higher due to internal gains and heat transfer from the walls
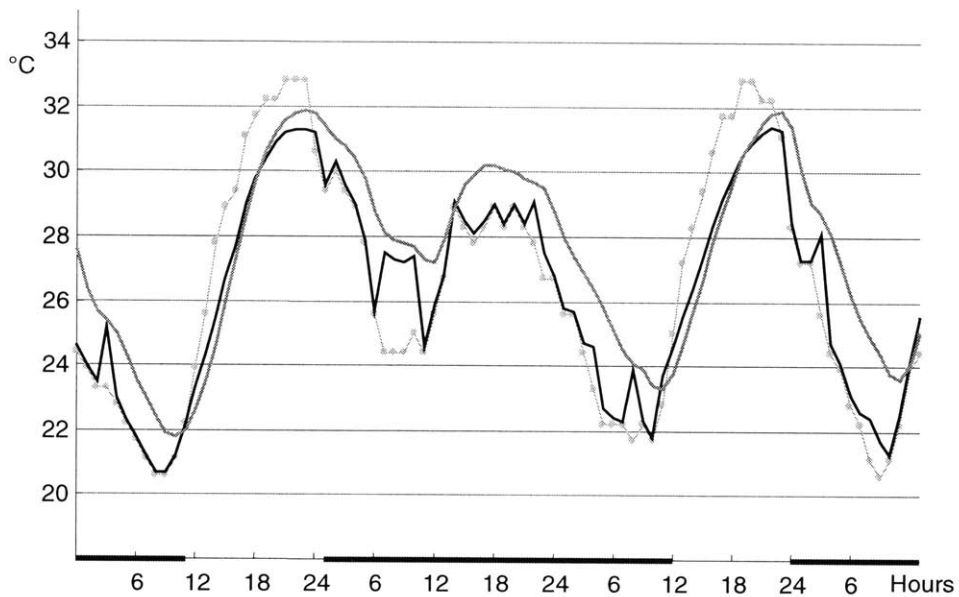
Figure 2.3.6

Hourly temperature variation in Beijing, daytime ventilation (Case 2.2).

Light Gray, Outside Temp.. Medium Gray, Wall Temp.. **Black**, Indoor Temp..

(for normal temperature variation periods the walls release heat into the air during the night).

There are several interesting features in figure 2.3.5. The simulated user behavior used for controlling the ventilation strategy is visible in the variation of the ventilation periods (see subsection 1.4.2). The vertical dashed line in the figure marks the moment when the users open the windows. The choice of this moment based on the criteria that, when the windows are opened, the inside temperature should not be too low (above 24°C) and the outside temperature should be lower than that of the inside (see part 2.2 for an extended explanation of the control strategies). The points labeled 1 and 2 in the figure correspond to low wind periods, when, due to the lower airflow rate, the air temperature becomes closer to the wall temperature. In points 2, the flow rate is lower than in points 1; therefore, the air temperature is even closer to the wall temperature for these points.

In figure 2.3.6, we can see the temperature variation for two and a half days in the natural ventilation lightweight structure case for Beijing (case 2.2). One noticeable difference when comparing with the previous figure is the fact that the indoor temperature closely follows the outdoor temperature. In this strategy, the

users are expected to open the window whenever it is cool outside (in this figure, the whole second day and first half of the third day). Another condition is that the windows should be open when, it being warm inside, the wind outside is such that the average airflow velocity that it causes in the indoor occupied zone with the windows open is higher than the ceiling fan generated airflow (see subsection 1.4.2). In this ventilation case, the users still leave the windows open during the night, but with only one fifth of the opening area used in the night cooling case. This number was chosen so a fairly sized aperture (1.8 m^2) would still exist during the night in the balcony.

The other differences between the two figures are due to the different structure compositions. In the second case we have a lightweight structure (perforated floor and internal partitions of negligible mass). The effect of this lighter structure is noticeable in two ways. First, there is a higher temperature variation of the walls during a day, due the lower overall thermal capacity. In addition, the air temperature remains closer to the ceiling temperature. At first, this second consequence is not obvious. This greater coupling between the ceiling, which still has some thermal mass, and the air is due to the light internal walls. These lighter elements exchange radiation with the floor and ceiling and they are in direct contact with the air. For this reason, they enhance heat transfer between the air and the thermal mass (the thermal mass in this case is mainly in the floors since the external walls have a relatively small area).

In this subsection, the impact of the two strategies in the daily temperature variations was shown. The next subsection presents the simulation results.

2.3.3- Comparison between Night and Daytime Ventilative Cooling Strategies.

The preliminary climate analysis presented in section 2.1 showed that Beijing was the city with the largest potential for using a night cooling strategy. The detailed analysis results presented in this section confirm this prediction. The other conclusions that came from that section, regarding the problems with ShangHai and the potential for ventilative cooling of the Tokyo climate, are also confirmed.

The present analysis uses two criteria to evaluate each of the ventilation strategies. The first criterion is the number of hours of thermal discomfort due to heat during the warm season, calculated using the Fanger equations. The second criterion is the maximum indoor temperature for each day in the analysis period. A supplementary criterion, only for the warmest days of the season (maximum $T_{out}>30°C$), is the average difference between the maximum indoor and outdoor temperatures.

For the first criterion, thermal discomfort conditions are considered to occur whenever the PPD indicator is above 20 (this is similar to ASHRAE standard 55). It should be noted that some calculation runs were performed with a more relaxed criterion (discomfort when PPD>30). This allows us to test the sensitivity of results to this criterion. This variation showed that this factor had no influence on which passive cooling solution was the best for each case.

Two additional cases were used for comparison purposes. The first case (labeled "outside" in the figures) is a scenario case that uses the comfort levels for outside conditions using the Fanger equation. For this scenario, the radiative temperature is set to the same value as the air temperature and the air velocity is set to zero. This case provides the analysis with a benchmark by which all cases

will be evaluated. This case was calculated for outside conditions, and therefore no solar or internal gains, were considered.

The second comparison case is case 1.2, a variation of case 1.1 using a daytime ventilation strategy, but with reduced flow. In this case the goal is to model a similar building but with a natural ventilation design of lower performance. Implementing and testing the modifications introduced in the airflow field by alterations in the fenestration would be very time-consuming. Therefore, it was chosen to run the same case with the constraint that this apartment would only achieve one third of the ventilation of the standard case.

Results for Beijing

In figure 2.3.7, we see the percentage of discomfort hours in the warm season (form May 1st to the end of September). Most of the discomfort hours (more than 95% of the total of discomfort hours for any of the cities) occur in the period from 7am to 12pm. On the right-hand side of the figure, we can see the different percentage of discomfort hours in this period of the day during the warm season. In
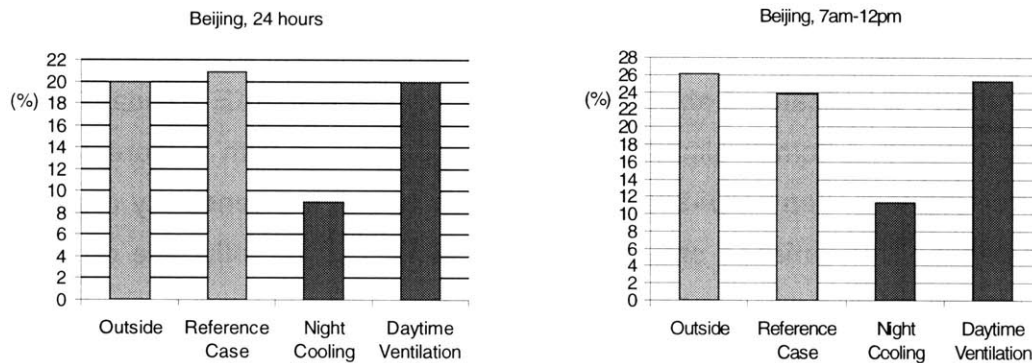

Figure 2.3.7

Comparison of the percentage of thermal discomfort hours using different strategies for Beijing climate.

Table 2.3.2

Maximum temperatures when using night cooling in Beijing.

Days with maximum temp. between 30 and 32 °C	10
Days with maximum temp. above 32°C	0
Maximum indoor temperature	31.6°C
Average difference between max. indoor and outdoor (in the warm days)	3.9 K

dark gray, we have the results of the two passive ventilation strategies; in light gray the base comparison cases.

From this figure, we can see that night cooling yields very encouraging results for the Beijing climate. Thermal discomfort only occurs in 330 hours (9% of the total number of hours in the warm season). The difference in performance between the two ventilation strategies is quite high, making night cooling undoubtedly the best one. Compared to the standard case, there is a 57% reduction in the number of discomfort hours (a reduction of 437 hours of thermal discomfort). The daytime ventilative cooling case shows only a small improvement over the base case.

In figures 2.3.8 and 2.3.9 (next page), we can see the maximum indoor and outdoor temperatures in the warm season for the two strategies. Again, the high effectiveness of the night cooling case is apparent in a noticeable lowering of the maximum temperatures. In the daytime ventilative cooling case, the control strategy opens the windows whenever it is warm inside (this conditions occurs in all the warm days for this case). For this reason the maximum indoor temperatures are very similar to outside, and go above 34°C on eight days.

From these results, we see that night cooling is undoubtedly the best of the two strategies. Further interesting data is displayed in table 2.3.2. Here we see a synthesis of figure 2.3.8. There are no indoor temperatures above 32°C and the night cooling system ensures an average difference between the maximum indoor and outdoor temperatures of 4°C.
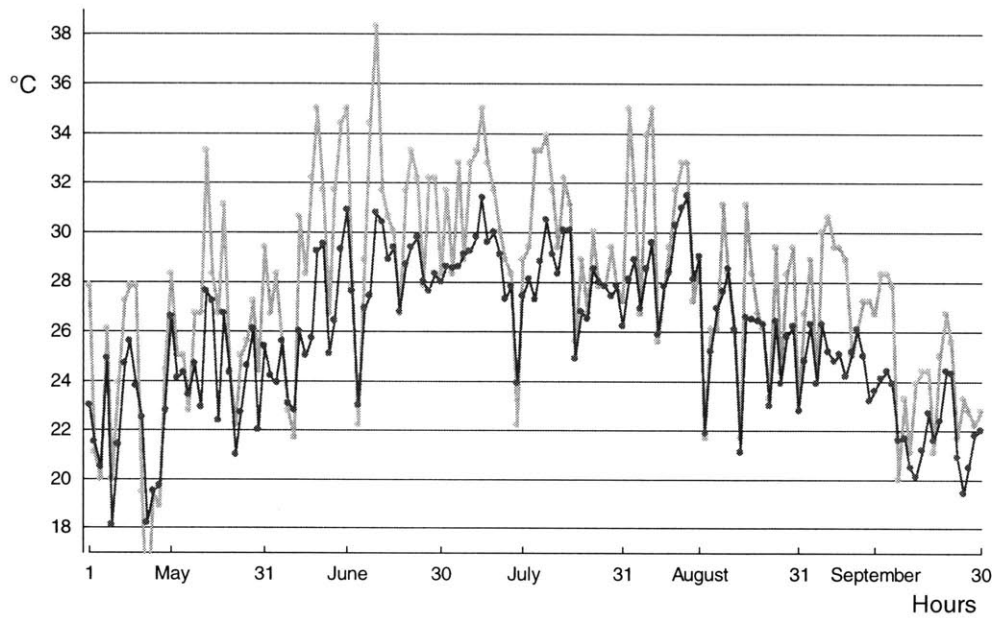
Figure 2.3.8

Beijing, Night Cooling (case 1.1).

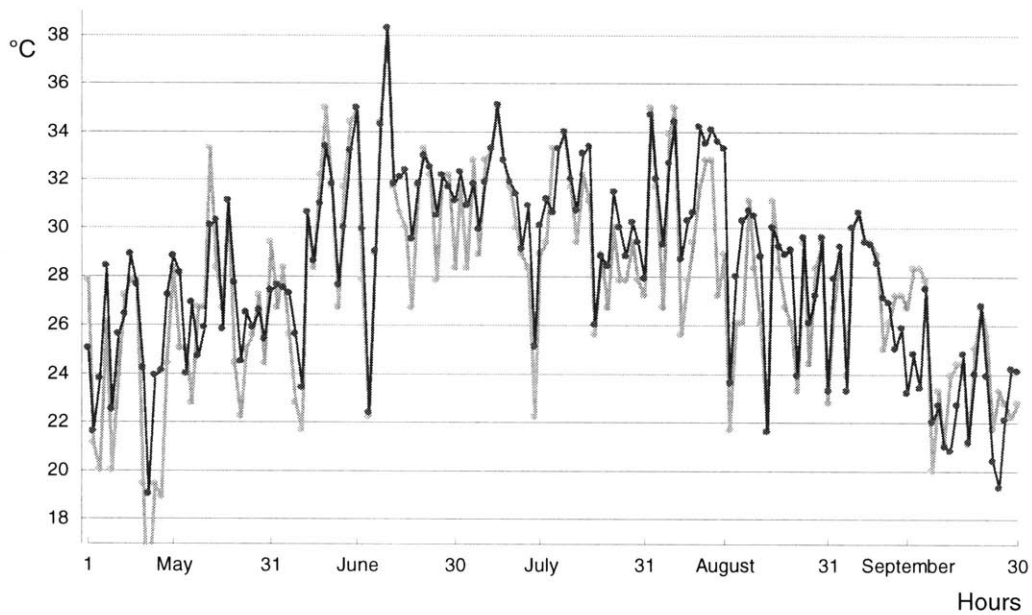Daily maximum temperature, in the **living room** (**dark** gray), and outside (light gray).

Figure 2.3.9

Beijing, Daytime Ventilative Cooling (case 2.2).

Daily maximum temperature, in the **living room** (**dark** gray), and outside (light gray).

Results for ShangHai.

In the analysis presented in section 2.1, Shanghai emerged as having the most problematic climate (see discussion in page 93). Shanghai had the worst values on all factors presented in table 2.1.3, particularly a low daily temperature variation and high daytime temperatures. The simulations using the coupled model confirmed these problems. In figure 2.3.10, we can see that the number of discomfort hours is always superior to one third for any of the strategies.

Night cooling is the best system but the improvements are not substantial when
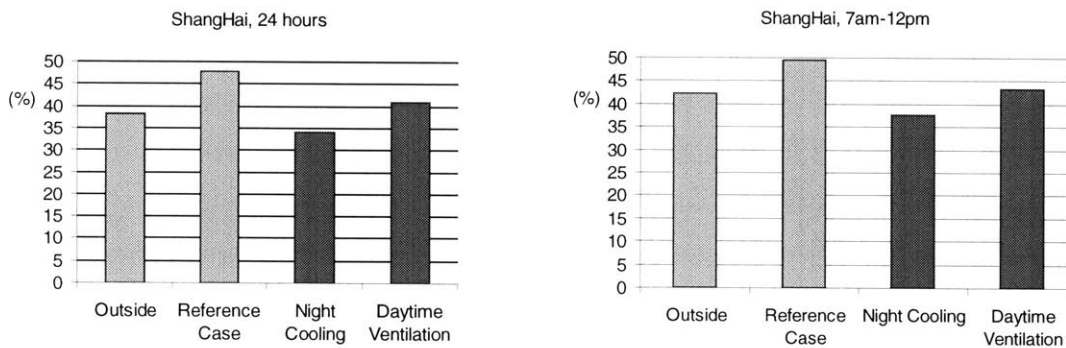
Figure 2.3.10

Comparison of the percentage of thermal discomfort hours using different strategies for Shanghai climate.

Table 2.3.3

Maximum temperatures when using night cooling in Shanghai.

Days with maximum temp. between 30 and 32 °C	32
Days with maximum temp. above 32 °C	29
Maximum indoor temperature	34.9°C
Average difference between max. indoor and outdoor (in the warm days)	0.9°C

compared with daytime ventilation or the base case. This is due to a small temperature variation between day and night. This characteristic of the climate does not allow for significant cooling of the thermal mass. The other climate parameters, such as wind velocity and orientation are not the problem (see figure 2.1.3). In this case, we can see that cooling by increased ventilation is always limited by the temperatures. If they are too high, it does not work.

Table 2.3 shows that even for the best case (case 1.1) there is a large number of days, totaling two months, when the indoor temperature exceeds 30°C. Also, the average difference between indoor and outdoor maximums is very low (0.9°C).

The lack of success of these passive-cooling systems for this climate is clearly visible in figures 2.3.11 and 2.3.12.
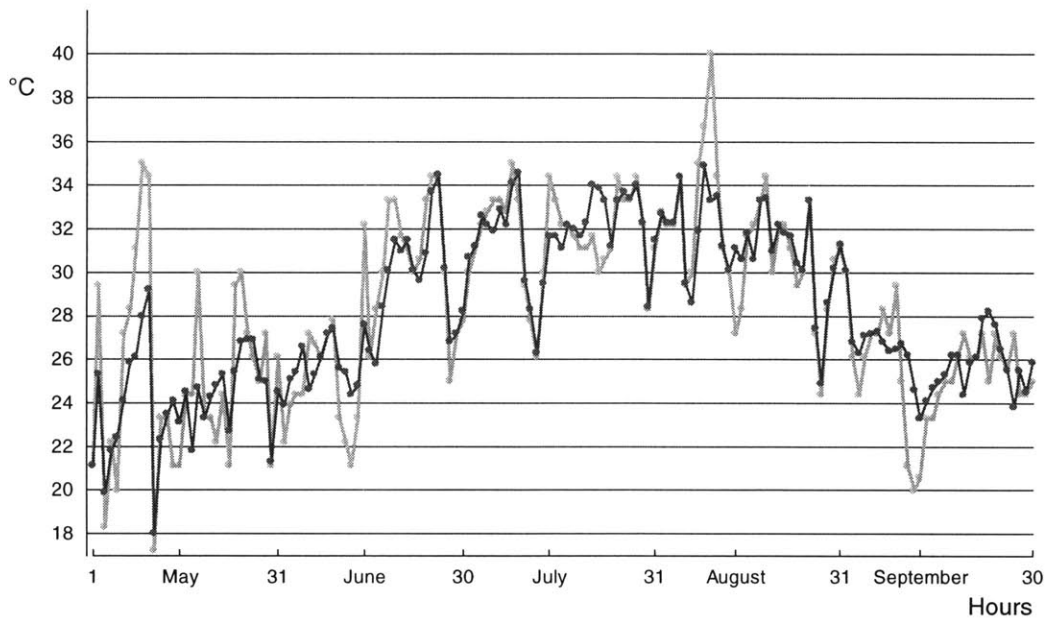
Figure 2.3.11

ShangHai, Night Cooling (case 1.1).

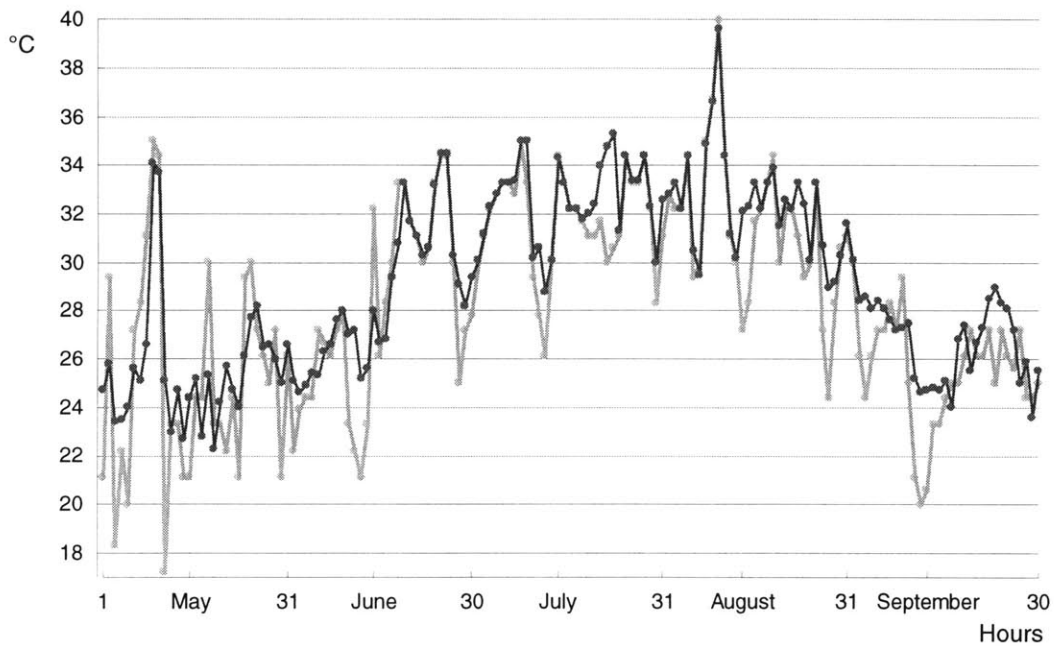Daily maximum temperature, in the living room (dark gray), and outside (light gray).

Figure 2.3.12

ShangHai, Daytime Ventilative Cooling (case 2.2).

Daily maximum temperature, in the **living room** (**dark** gray), and outside (light gray).

Results for Tokyo.

Tokyo has the mildest climate of the three cities, and results reflect this fact. Due to higher average wind velocity, the daytime ventilation strategy also works well, although it is inferior to the night cooling case in simple performance indicators. It should be noted that daytime ventilation is here tested with a lighter structure, as was done for Beijing. This structure makes the building less expensive. In addition, the condensation problems that might occur (see section 2.3.4) are mitigated.

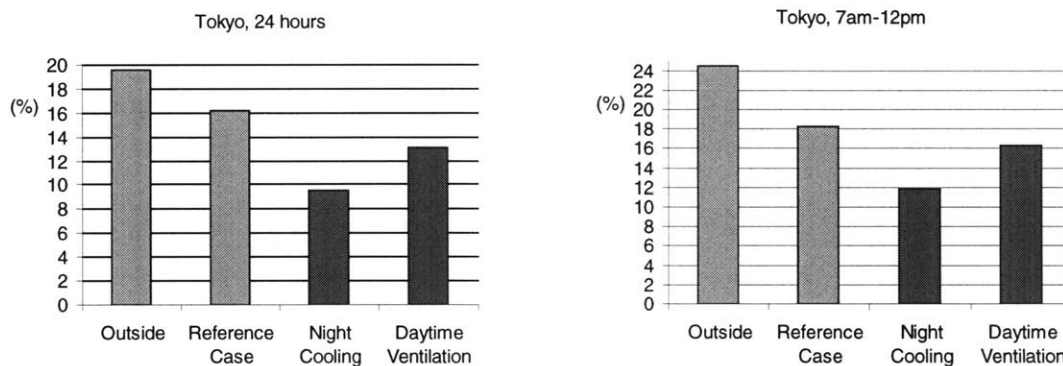The result for the best case in Tokyo is similar to Beijing, although Tokyo's

Figure 2.3.13

Comparison of the percentage of thermal discomfort hours using different strategies for Tokyo climate.

Table 2.3.4

Maximum temperatures when using night cooling in Tokyo.

Days with maximum temp. between 30 and 32 °C	9
Days with maximum temp. above 32 °C	0
Maximum indoor temperature	31.2 °C
Average difference between max. indoor and outdoor (in the warm days)	2.2 °C

climate is milder. This is due to the lower daily temperature variation, which reduces the efficiency of night cooling (and is not compensated by higher wind velocities, which increase the convective heat transfer). In table 2.3.4 we see that the difference between daily maximum temperatures is lower than in Beijing, which is also consistent with the result being similar, in spite of Beijing having a higher outside maximum average in the warm days.
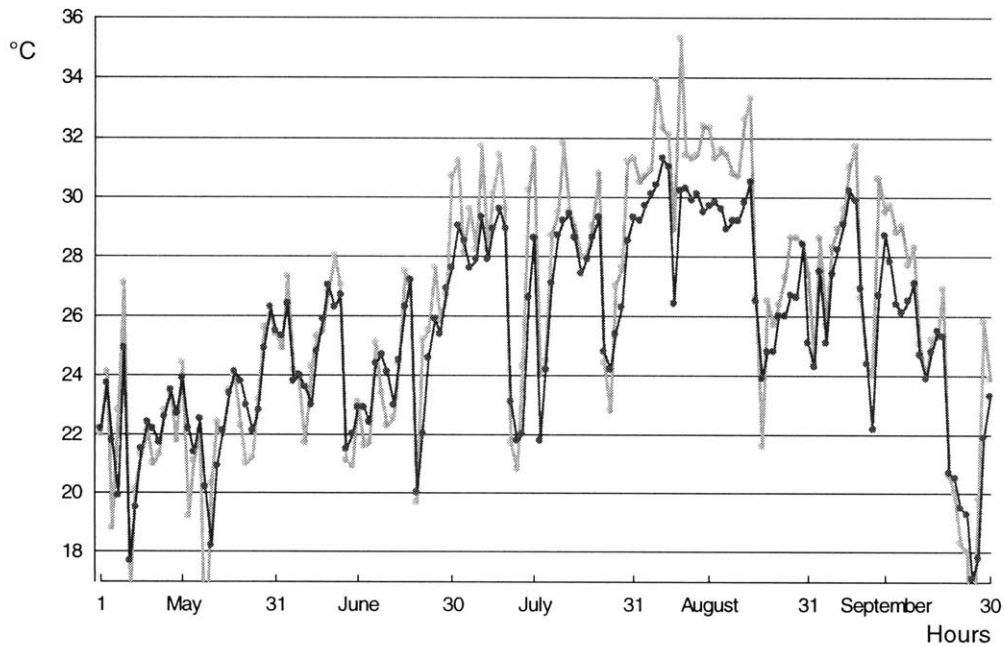
Figure 2.3.14

Tokyo, Daytime Ventilative Cooling (case 2.2).

Daily maximum temperature, in the living room (dark gray), and outside (light gray).
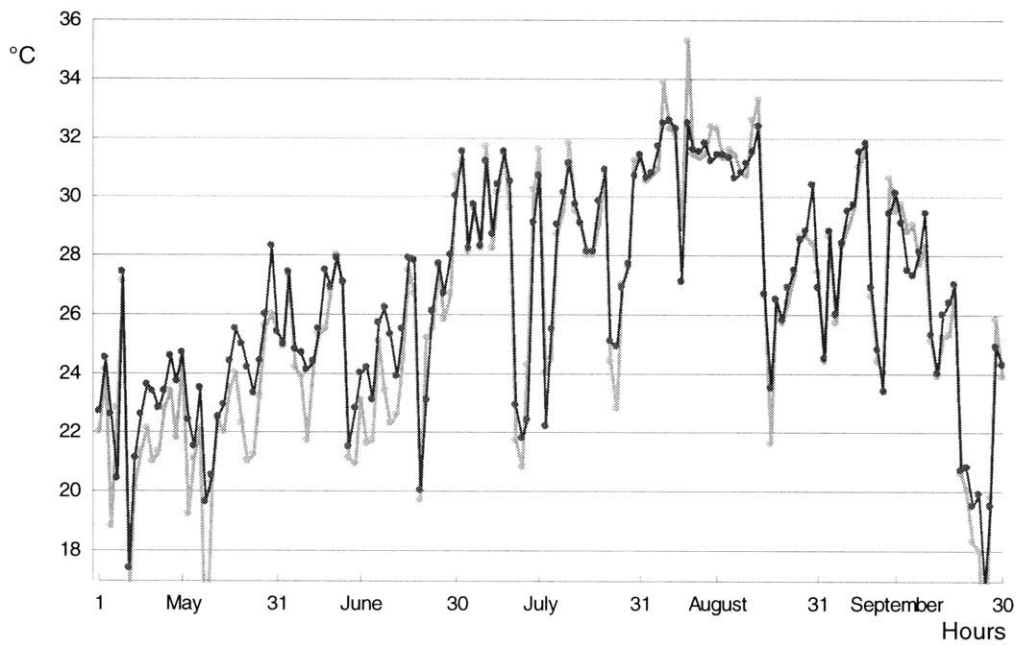

Figure 2.3.15

Tokyo, Daytime Ventilative Cooling (case 2.2).

Daily maximum temperature, in the living room (dark gray), and outside (light gray).

2.3.4- Impact of Different Structure Compositions on Night Cooling System Performance.

The building structure is an essential component of a night cooling system. In the previous section, we saw that the night cooling system is the best solution of the two ventilative cooling strategies analyzed. Therefore, it is important to further analyze the impact of different structural features on the performance of the system, in the three climates. Three structural configurations are considered (see section 2.2 for more details): normal (base case, 1.1), lightweight and heavyweight structure. The effect of covering the floor with carpet, in the normal structure case, is also analyzed.

As a first step we start by taking a closer look at the response of the normal and heavyweight case floors to a sequence of three warm days. The black lines in figure 2.3.16 (next page) are the living room floor temperature variations for the base case. The medium gray lines are the floor temperature point for the heavy structure case. The thick lines are the temperatures at the interior center point of the walls (in their "core"). The thin lines are the temperatures of the surface of the walls.

As should be expected, the normal case walls have a higher temperature fluctuation. In addition, we can see that the temperature difference between wall surface and wall core is never larger than 1 K. A noticeable increase in average temperature occurs in the whole wall during this three-day warm period. An interesting behavior during the first three nights can be observed. The lighter floor achieves a lower temperature during the night. In this way, it actually overcomes, although partially, its lower thermal mass when compared to the other cases. This
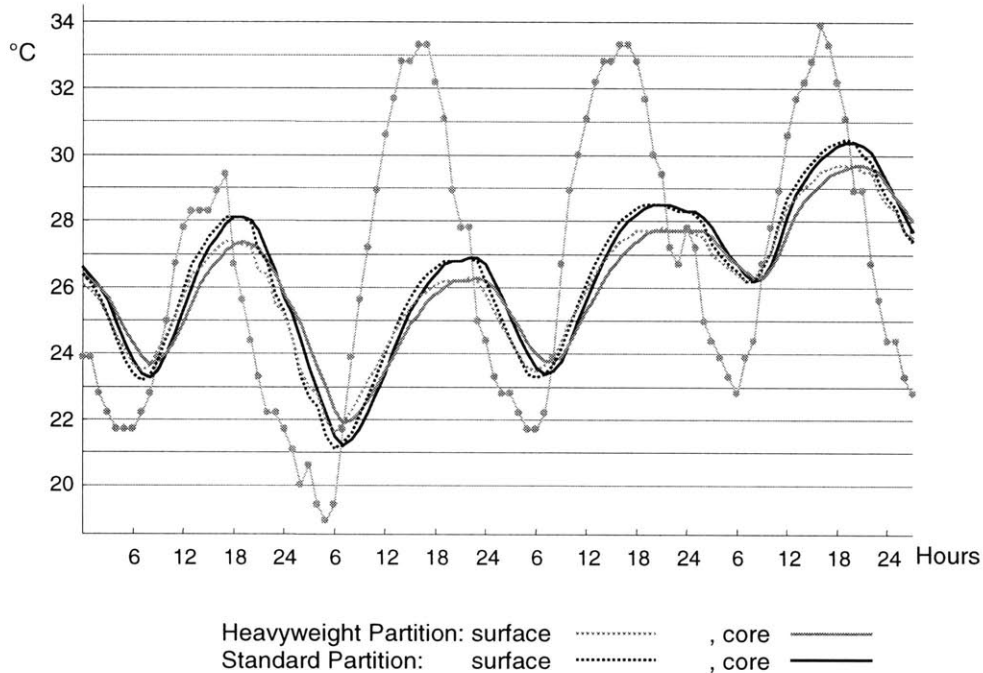
Figure 2.3.16

Hourly temperature variation, Beijing (Daytime Ventilation, Case 2.1).

Light Gray, Outside Temp.. Medium Gray, Wall Temp.. **Black**, Indoor Temp..

advantage disappears as we move along the sequence of days, because of the lighter walls tending to a higher average temperature than the heavy walls.

In figure, 2.3.17 we can see a detail of the previous chart showing the increased thermal inertia of the heavier wall.

The analysis of figures 2.3.18-2.3.20 leads us to an interesting set of conclusions. The first interesting result is the noticeably negative effect of the carpet on the system performance. Due to its thermal resistance, the carpet isolates the air room air from the floor. This effect is not compensated by the fact that the mass that is now inaccessible through the floor can be accessed by the ceiling (due to excessive depth, in this case). The different structural configurations produce different results for Beijing. For the other two cities, these changes have a smaller impact. This difference is a consequence of how much the system is actually affecting the indoor conditions for each city. Thus, in the case of ShangHai none of
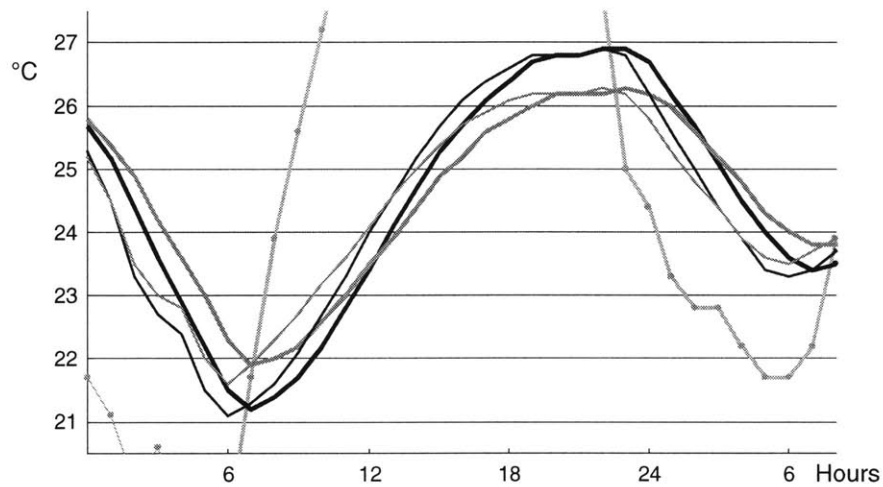
Figure 2.3.17

Hourly temperature variation, Beijing daytime ventilation (Case 2.1).

Light Gray, Outside Temp.. Medium Gray, Wall Temp.. **Black**, Indoor Temp..

the systems works, due to a too small daily temperature variation and too high average temperatures. Therefore, changing the structure has a limited impact, although the results show a qualitatively correct variation. For Tokyo, the variations are more noticeable, but still not as much as for Beijing. This is a direct consequence of the fact that the results for Tokyo are more related to the climate (which the mildest of the three) and less to system performance.

The main conclusions of this evaluation are then:

  - Using an isolating flooring material is highly unadvisable.

  - The use of increased thermal mass might not pay back above the level used in the normal case, if one takes into consideration the construction costs of increasing the building mass.
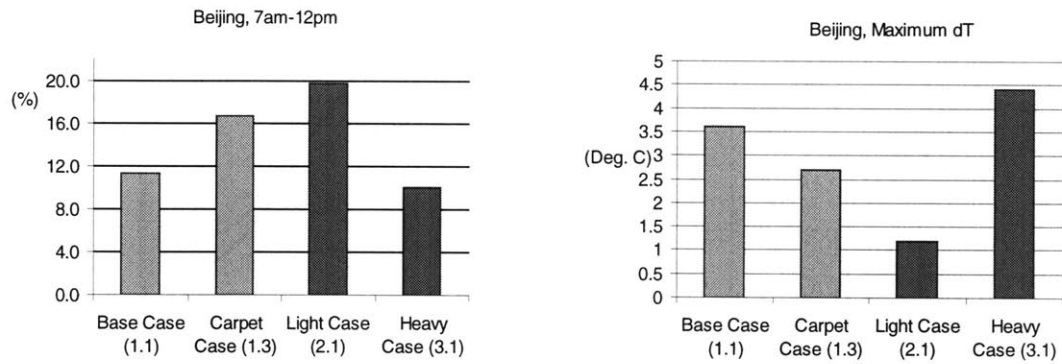
Beijing, 7am-12pm

Figure 2.3.18

Comparison of different structure types for Beijing, night cooling.
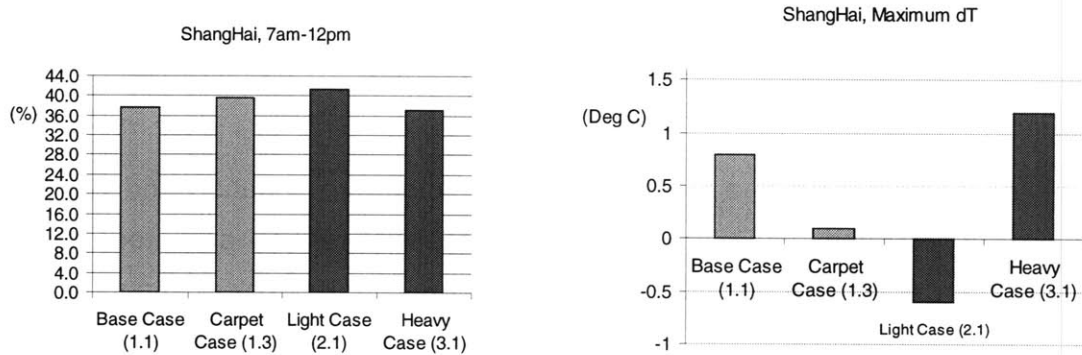
ShangHai, 7am-12pm

Figure 2.3.19

Comparison of different structure types for ShangHai, night cooling.
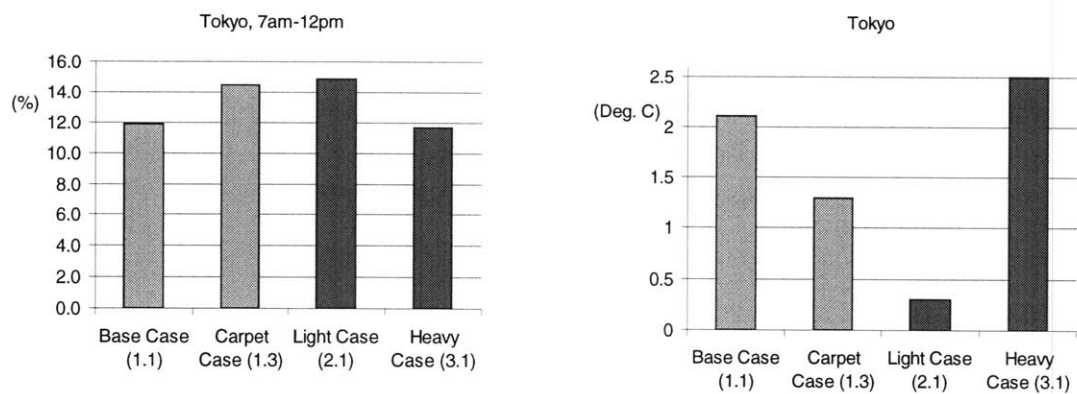
Tokyo, 7am-12pm

Figure 2.3.20

Comparison of different structure types for Tokyo, night cooling.

124

2.3.4- Analysis of the Humidity Levels and Condensation Problems.

The three climates analyzed in this study have high humidity levels (above 70%) in a major part of the warm season (see part 2.1). When moist air comes to contact with a surface at lower temperature condensation can occur. This undesirable effect happens whenever the water saturation pressure at the surface temperature is lower than the vapor pressure of the air in contact with that surface.

The high thermal mass partition elements generally have the lowest temperature during the day in a building. This is due to the high thermal capacity of their thermal mass. After this thermal mass is cooled by the night air it maintains a lower temperature than the air inside and outside the apartment (see figure 2.3.5 above). Although the highest relative humidity period is in the night hours (see figures 2.1.1-3) the daytime air can have a high water contend. During the day, there is infiltration of outside air (in this study, 1.5 ACH/hour). When this air infiltrates into the apartment and contacts with the colder surfaces of the high thermal mass elements condensation can occur (the temperature difference between inside and outside can as high as 6°C).

High humidity levels have a negative impact on thermal comfort. Condensation problems pose also obvious practical problems in an apartment. In this analysis condensation is considered to occur whenever the relative humidity of air at the surface temperature of the living room ceiling and with the water contend of living air goes above 98%. The ceiling of the living room is used here because it was found to be the surface with the lowest temperature).

Table 2.3.5

Average indoor relative humidity values in the warm days ($T_{out}>30°C$) during warmest period of the day (between 11am and 7pm).

City	Case	Average RH (%)	Maximum Average RH, (%)
Beijing	1.1(Night Cooling)	58	94
	2.2(Daytime Vent.)	46	76
ShangHai	1.1(Night Cooling)	69	84
	1.1(Daytime Vent.)	66	75
Tokyo	1.1(Night Cooling)	66	95
	2.2(Daytime Vent.)	58	81

Table 2.3.5 presents the average indoor RH in the warmest days (during the day). ShangHai has the highest average value. None of the average indoor RH values exceeds ASHRAE comfort recommendations (70% RH). In the case of the worst day (the column on the right in the table), very high values occur, especially in Beijing and Tokyo (above 90%). This is due to a combination of low indoor temperatures and high outside air water contends.

It can also be seen in this table that the use of daytime ventilation (second row in the table for each city) produces lower humidity levels. This can be understood if we recall that the indoor temperatures are generally higher for this case than for the night cooling case.

We now proceed to analyze possible condensation problems. In figure 2.3.20 (in the next page) shows the number of hours when condensation can occur in the ceiling of the living room for the two ventilative cooling systems. Beijing and Tokyo have the highest values. Again, in the case of daytime ventilation the problem is lower. For Shanghai condensation might not be major problem. In this city the nights are warmer; therefore, the daytime thermal mass surface temperatures are higher for this city.

126

Hours With Condensation
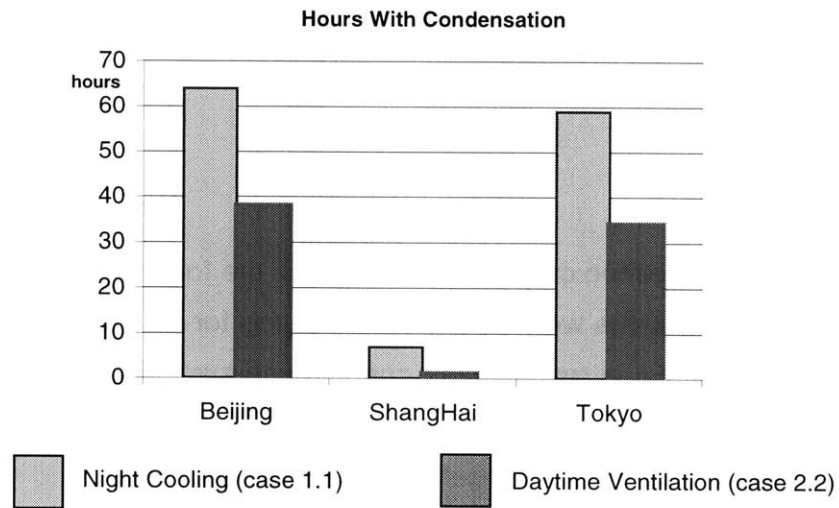

Figure 2.3.20

Number of hours with condensation for the two ventilation strategies.

From this analysis, it can be concluded that high humidity and consequent condensation can be a major problem when using night cooling in Beijing or ShangHai. It is not within the scope of this study to further analyze the impact of this problem on the applicability of this passive cooling solution.

Summary

The results of this section can be summarized in the following way: The daytime ventilation strategy performs worse than night cooling for all the three cities. Night cooling can be successful in replacing air conditioning systems in a substantial part

Table 2.3.5

Average indoor relative humidity values in the warm days ($T_{out}>30°C$) during warmest period of the day (between 11am and 7pm).

City	Case	Average RH (%)	Maximum Average RH, (%)
Beijing	1.1(Night Cooling)	58	94
	2.2(Daytime Vent.)	46	76
ShangHai	1.1(Night Cooling)	69	84
	1.1(Daytime Vent.)	66	75
Tokyo	1.1(Night Cooling)	66	95
	2.2(Daytime Vent.)	58	81

of the cooling season in both Beijing and Tokyo. In Shanghai, none of the the systems can ensure thermal comfort in the warm periods.

128

Conclusions

This thesis evaluates the performance of daytime and nighttime passive ventilative cooling systems for Beijing, Shanghai and Tokyo. A new simulation method for cross-ventilated wind driven airflow is presented. This method decouples the airflow model from the thermal model allowing for fast real weather simulation of the building thermal performance.

A six-story apartment building with three-bedroom units is simulated. This building does not have any contiguous buildings, and is located in a suburban area.

The performance of the two ventilation strategies is compared. The impact on the performance of the night cooling ventilation strategy of different building partition compositions (lightweight, normal (10cm concrete partitions) and heavyweight) and flooring materials (ceramic tile and carpet) is also simulated.

The performance of the two strategies is evaluated using the Fanger comfort equations. The results obtained show that night cooling is superior to daytime ventilative cooling in the three cities. Night cooling can successfully replace air conditioning systems for a major part of the cooling season in Beijing (91% of the time) and Tokyo (91% of the time). For Shanghai, none of the two passive ventilation systems is successful (comfort is assured only in 66% of the time). These results are for normal partition composition and ceramic tile floor covering (the normal case).

The performance of passive systems depends on the climate. Shanghai has the highest number of warm days. In addition, the average daily temperature variation is the smallest. Consequently, with any of the two ventilation strategies, the apartment in Shanghai heats up more during the day and cools down less during the night.

The results show that the daytime ventilation strategy is always worse than night cooling strategy. In Tokyo, however, the performance of daytime ventilation

can come quite close to that of night cooling. This is because this city has the highest average wind velocity and the lowest number of warm days. If the costs for constructing heavier buildings (needed for the night cooling case) are considered, daytime ventilation can, for this city, be considered competitive with night cooling.

In both Beijing and Tokyo, the night cooling strategy effectively reduces the daily indoor maximum temperature by 3.9 and 2.2 K respectively, when compared to the daily outdoor maximum temperature in the warm days (maximum outside temperature above 30°C). One problem was detected with the application of night cooling in these two cities, for the normal construction case. For a high number of hours in the cooling season, condensation can occur (60 hours) on the surface of the partitions. This condensation problem deserves further investigation.

The results for the simulation of the heavyweight partitions case do not show a noticeable improvement over the normal case. On the other hand, the lightweight case shows a noticeable degradation in system performance. Therefore, the normal structural system is the best option (or at least close to optimum). The use of carpet has a negative impact on night cooling performance.

References

Allard F., Inard C., Natural and Mixed Convection in Rooms: Prediction of Thermal Stratification and Heat Transfer by Zonal Models. Room Air Convection and Ventilation Effectiveness, ASHRAE 1992.

Aynsley, R. M., Melbourne W., Vickery B. J., Architectural Aerodynamics. Applied Science London (1977).

Aynsley, R. M., A Resistance Approach to Estimating Airflow Through Buildings with Large Openings Due to Wind. ASHRAE Transactions (1988), 1661-1668.

Balaras, C.A., The Role of Thermal Mass on the Cooling Load of Buildings. An Overview of Computational Methods. Energy and Buildings 24 (1996), 1-10.

Blomberg, T., Heat Conduction in Two and Three Dimensions. Department of Building Physics, Lund University Sweden (1996).

DiLaura, D.L., Santoro, S., Non-Diffuse Radiative Transfer 4: General Procedure for Planar Area Sources and Area Receivers. Journal of the Illuminating Engineering Society, Vol. 26, No. 1, Winter 1997.

Etheridge D.W., Nolan J.A., Ventilation Measurements at Model Scale in a Turbulent Flow. Building and Environment (1979) Vol. 14, 53-64.

Etheridge D.W., Sandberg M., Building Ventilation, Theory and Measurement. Wiley & Sons (1996), UK.

Ernest D.R., Bauman F.S., Arens E.A., The Prediction of Indoor Air Motion for Occupant Cooling in Naturally Ventilated Buildings. ASHRAE Transactions 1991.

Feustel H.E., A Survey of Airflow Models for Multizone Structures. Energy and Buildings, 18 (1992), 79-100.

Freskos G. O., Influence of Various Factors on the Prediction Furnished by CFD in Cross-Ventilation Simulations. Roomvent (1998).

Flourentzou F., Van der Maas J., Roulet C.-A., Natural Ventilation for Passive Cooling: Measurement of Discharge Coefficients. Energy and Buildings (1998), 283-292.

Givoni B., Climate Considerations in Building and Urban Design. Van Nostrand Reinhold (1998).

Givoni B., Passive and Low Energy Cooling of Buildings. Van Nostrand Reinhold (1994).

Haghighat F., Rao J., Fazio P., The Influence of Turbulent Wind on Air Change Rates-a Modeling Approach (1991) Vol.26 No.2, 95-109.

Inard C., Bouia H., Dalicieux P., Prediction of air temperature Distribution in Buildings with a Zonal Model. Energy and Buildings (1996), 125-132.

ISO, Moderate Thermal Environments – Determination of the PMV and PPD Indices and Specifications for Thermal Confort. International Standard 7730.

Landsberg H.E., The Urban Climate. Int. Geophys. Ser. 28. Academic Press, New York 1981.

Lino Y., et al. Study on Airflow Characteristics in and Around Building Induced by Cross Ventilation using Wind Tunnel Experiment and CFD Simulation. Roomvent (1998).

Mills A.F., Basic Heat and Mass Transfer. Irwin (1995), USA.

Murakami S., et al, Examining the k-ε Model by Means of a Wind Tunnel Test and Large Eddy Simulation of the Turbulence Structure Around a Cube. Journal of Wind Eng. And Industrial Aerodynamics., 41-44 (1990) 87-100.

Murakami S., et al, Wind Tunnel Test on Velocity-Pressure Field of Cross-Ventilation with Open Windows. ASHRAE Trasactions: Symposia (1991), USA.

Murakami S., Kato S., Akabayashi S., Mizutani K., Kim Y.-D., Wind Tunnel Test on Velocity-pressure Field of Cross-Ventilation with Open Windows. ASHRAE Transactions: Symposia (1991), 525-538.

Nielsen P.V., Tryggvason T., Computational Fluid Dynamics and Building Energy Performance Simulation. ROOMVENT'98.

Off F., Moser A., Suter P., Transient Numerical Modelling of Heat Transfer by Radiation and Convection in an Atrium with Thermal Inertia. ROOMVENT'96.

Panofsky H.A., Dutton J.A., Atmospheric Turbulence. John Wiley & Sons (1984).

Patankar S.V., Numerical Heat Transfer and Fluid Flow. Hemisphere (1980).

Roulet Cl.-A., Van der Maas J., Flourentzos F., A Planing Tool for Passive Cooling of Buildings. EPFL-LESO-PB 1997.

Santamouris M., Argiriou A.A., Balaras C.A.. Developments on Passive Cooling in Buildings-Results from Recent Research. ASHRAE Transactions Vol. 97, 15-2.

Shaw, C. T., Using Computational Fluid Dynamics, Prentice Hall, UK (1992).

Siegel, R., Howell, J.R., Thermal Radiation Heat Transfer, 2nd ed.. McGraw-Hill, New York (1981).

Straaten V., Thermal Performance of Buildings, Elsevier, Amsterdam (1967).

Van der Maas J., Roulet. Cl.-A, Nightime Ventilation by Stack Effect. ASHRAE Transactions (1991) Vol 97 Part1.

Kammerud R., Ceballos E., Curtis B., Place W., Anderson B., Ventilation Cooling of Residential Buildings. ASHRAE Transactions (1984) 05 No.2, 226-251.

Karabuchi T., et al, Application of Wind Tunnel Experiment and CFD Simulation on Estimation of Wind Environment Inside and Outside a Large-Scale Building Complex with an Atrium Space. Roomvent (1998).

Katatayama T., Full-sclae Measurements and Wind Tunnel Tests on Cross-ventilation. Journal of Wind Eng. And Industrial Aerodynamics., 41-44 (1992) 2553-2562.

Kato S., et al, Velocity-pressure Field of Cross Ventilation with Open Windows Analyzed by Wind Tunnel and Numerical Simulation. Journal of Wind Eng. And Industrial Aerodynamics., 41-44 (1992) 2575-2586.

Shaw C.T., Using Computational Fluid Dynamics. Prentice Hall (1992).

Togari S., Arai Y., Miura K., A Simplified Model for Predicting Vertical Temperature Distribution In a Large Space. ASHRAE Transactions: Research (1993), 84-99.

Appendix A - Validation

In this appendix, the explicit finite-difference technique used in this work for calculating heat conduction through building elements is compared with the exact analytical solutions for a semi-infinite heavy concrete wall.

Two boundary conditions were used. The first was a convective boundary layer with the air at a fixed temperature of 30°C. The second was an imposed constant surface heat flux of 50 W/m^2.

The analytical solutions for these two boundary conditions is given by the following expressions (Miells, 1995):

$$T(x,t) = T_{wi} + (T_{air} + T_{wi}) \left[\text{erfc}\left(\frac{x}{2\sqrt{t\alpha}} \right) - e^{\frac{t\alpha h_{aw}^2}{k_w^2} + \frac{x h_{aw}}{k_w}} \text{erfc}\left(\frac{\sqrt{t\alpha} h_{aw}}{k_w} + \frac{x}{2\sqrt{t\alpha}} \right) \right]$$

a) constant air temperature boundary condition:

$$T(x,t) = T_{wi} + \frac{Q \left[\frac{2 e^{-\frac{x^2}{4t\alpha}} \sqrt{t\alpha}}{\sqrt{\pi}} - x \, \text{erfc}\left(\frac{x}{2\sqrt{t\alpha}} \right) \right]}{k_w}$$

b) constant surface heat flux boundary condition:

The parameters used in the finite-difference analysis were (data for heavy concrete are from ASHRAE, 1997):

wall thermal conductivity: k_w=1.8 W/(m °C)

wall density: ρ_w=2430 kg/m3

wall specific heat: c_w=1085 J/(kg °C)

air specific heat: c_{air}=1000 J/(kg °C)

Figure A1.1

Comparison of the predicted transient response of the finite difference calculation and the exact solution, for a wall at 20 °C initial temperature, exposed to a convective boundary condition of 30 °C.

convection coefficient: h_{aw}=4 W/(m^2 °C)

discretization layer thickness: Lx=0.021 m

time step: Δt=300 s

initial wall temperature T_{wi}=20°C

number of layers: NLayer=20

A comparison between the finite-difference and the analytical solutions is in figures A1.1 and A1.2.
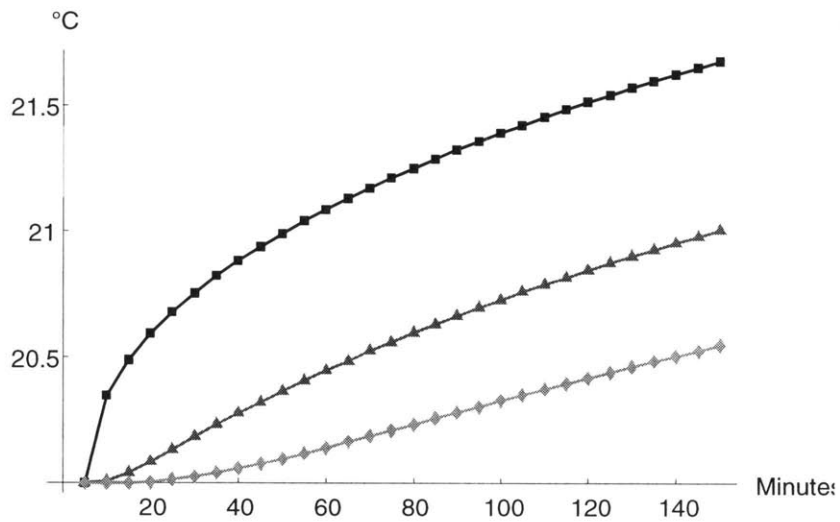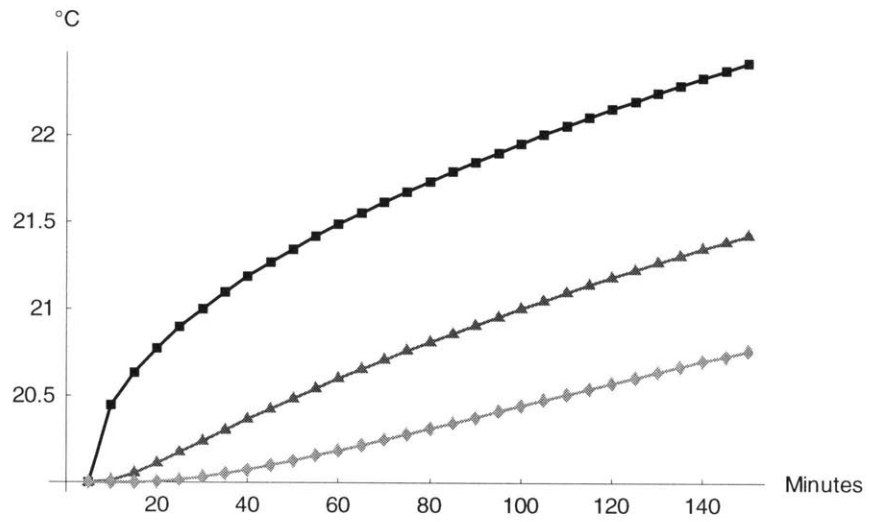
Figure A1.2

Comparison of the predicted transient response of the finite difference calculation and the exact solution, for a wall at 20 °C initial temperature, exposed to a constant heat flux boundary condition (Q=50 w/m^2).

Appendix B - Calculation Routine.

Initialization

```
Off[General::spell1];
<<Graphics`MultipleListPlot`
SetDirectory["D:\Calculation"];
$DefaultFont={"Arial",10};
```

Calculation of the flow rates and convective heat exchange coefficients with open windows

```
If[City==1,Temp=BT,If[City==2,Temp=ST,Temp=TT]];
Timing[LVentOpen=Table[0,{t,tmax},{r,4}];
    hawOpen=Table[{0,0},{t,tmax},{w,24}];
Do[{Drtn[City,t];LVentOpen[[t]]=RFlow[City,t];
            Do[{hawOpen[[t,w,f]]=
                hcor[WallSp[City,t][[w,f]]]*(5-hAddIn[[w,f]])/5+
                    hAddIn[[w,f]];},{w,24},{f,2}];},{t,400}];
            Do[If[LVentOpen[[t]]=={0,0,0,0},
    LVentOpen[[t]]={LVt*FF[[1]],LVt*FF[[2]],LVt*FF[[3]],LVt*FF[[4]]},],{t,400}];]
```

Night cooling iteration

```
hawBig=Table[{3+1.2*IsDay[[t]],3+1.2*IsDay[[t]]},{t,tmax},{w,24}];
LVent=Table[LVt*FF[[r]],{t,tmax},{r,4}];(*t,r*)

Results=Table[24.5,{t,tmax},{y,15}];
Timing[Do[{NV=0;If[(Hora<8||(Hora>18&&ColdOut)||ColdOut)&&Warm,
                {NV=1;LVent[[t]]=ρ*LVentOpen[[t]];haw=hawOpen[[t]]},
```

```
                haw=hawBig[[t]]];


Tr={TR1[t],TR2[t],TR3[t],TR4[t],Temp[[t]]};GlassTemp;ERE=ESG[t,City];
        RE=REe+ERE;SlG=SlGe;
IG[[t,1]]=4.5*2.7*GlassBack[[1]];IG[[t,2]]=3.5*GlassBack[[3]];
        IG[[t,3]]=3.5*GlassBack[[4]];Do[Basico,{ii,9}];
Tr={TR1[t],TR2[t],TR3[t],TR4[t],Temp[[t]]};GlassTemp;RE=REe+ERE;
Results[[t]]=
        Round[10*{Tr[[1]],Tr[[2]],Tr[[3]],Tr[[4]],Tr[[5]],MRT1,MRT2,MRT3,
                MRT4,NV,WR,WE[[t]],Two[[19,1]],Two[[10,1]],Two[[20,1]]}]/10.;
            Do[Basico,{ii,9}];
If[IntegerQ[t/168],Print[t," ",NV],]},{t,2,tmax}];]
```

Variables

```
City=2;(*1=Beijing; 2=Shanghai; 3=Tokyo*)


f=4; (*F L O O R*)


SC={0.5*(0.43+0.88),0.88};SCE={(1-0.52),(1-0.7)};Rwindow=0.082;
  αg=0.025;(*inner glass absortivity for solar*)
ρ=1.2;F=4;ss=1;
pa=1.2;met=58.2;M=1.2*met;Icl=0.5;fcl=1.1;Rcl:=0.155*Icl;CGF=0.3;
  haw=Table[6,{w,24},{p,2}];
tmax=3672;
kw=Table[1.4,{w,25},{p,10}];   rw=Table[2100,{w,25},{p,10}];
  cw=Table[880,{w,25},{p,10}]; cair=1000;
ε=Table[0.8,{w,25}];
Lair=0.01; kair=0.028; Lbrick=6*0.0254; kbrick=0.36; Lglass=0.008;
  kglass=1.38;
Lx=Table[0.02,{w,25}]; Lins=0.05;   dt=200;LVt=8*12.5*2.4*1.5/3600;
```

140

```
IsDay1={0,0,0,0,0,0,0,1,1,1,1,1,1,1,1,1,1,1,1,0,0,0,0,0};

IsDay={};Do[IsDay=Append[IsDay,IsDay1],{n,153}];IsDay=Flatten[IsDay];

DVnt=1*0.1*ρ;NRLoss=-20*6*0.30;

Hora:=t-Floor[(t-1)/24]*24;

Warm:=TrueQ[Results[[24*Floor[(t-1+12)/24]+18-24,1]]>24];

ColdOut:=TrueQ[Results[[t-1,5]]<Results[[t-1,1]]];

WR:=WE[[t]]+(Results[[t-1,11]]-WE[[t]])*

        E^(-(LVent[[t,1]]+LVent[[t,2]]+LVent[[t,3]])*3600/(2.7*115));


lB=ReadList["BF.txt",Number];

B=Partition[lB,7];BT=Transpose[B][[1]];BW=Transpose[B][[2]];

  Bws=Transpose[B][[3]];Do[If[Bws[[n]]>5,Bws[[n]]=5,],{n,3672}];

Bwd=Transpose[B][[4]];BB=Transpose[B][[5]];BF=Transpose[B][[6]];

  BP=Transpose[B][[7]];

lS=ReadList["SF.txt",Number];

S=Partition[lS,7];ST=Transpose[S][[1]];SW=Transpose[S][[2]];

  Sws=Transpose[S][[3]];Do[If[Sws[[n]]>5,Sws[[n]]=5,],{n,3672}];

Swd=Transpose[S][[4]];SB=Transpose[S][[5]];SF=Transpose[S][[6]];

  SP=Transpose[S][[7]];

lT=ReadList["TF.txt",Number];

T=Partition[lT,7];TT=Transpose[T][[1]];TW=Transpose[T][[2]];

  Tws=Transpose[T][[3]];Do[If[Tws[[n]]>5,Tws[[n]]=5,],{n,3672}];

Twd=Transpose[T][[4]];TB=Transpose[T][[5]];TF=Transpose[T][[6]];

  TP=Transpose[T][[7]];

If[City==1,Temp=BT,If[City==2,Temp=ST,Temp=TT]];

  If[City==1,WE=BW,If[City==2,WE=SW,WE=TW]];


WFM=Flatten[ReadList["DifRad.txt"],1];

WFAM=Flatten[ReadList["DifARad.txt"],1];

(*Total area for each room, fifth room with a large area is outside so the fraction
goes to zero in case of mistake*)
```

```
TtAreaRoom={2*8.5*2.7+2*2.7*4.5+2*4.5*8.5,2*5*2.7+2*3.5*2.7+2*3.5*5,

    2*2.7*3.5+2*4*2.7+2*4*3.5,2*2.7*3.5+2*4*2.7+2*4*3.5,1*^5};

WArea={5*2.7,3.5*1.7,2*2.7,1.5*2.7,3.5*2.7,3*2.7,4.5*1.7,

1.5*2.7,2.5*2.7,4*2.7,3.5*1.7,4*2.7,2*2.7,2*2.7,4*2.7,3.5*1.7,

5*3.5,5*3.5,8.5*4.5+2*1.5*2,8.5*4.5+2*1.5*2,3.5*4,3.5*4,3.5*4,3.5*4};


Belongs={{2,5},{2,5},{2,5},{2,5},{2,1},{1,5},{1,5},{3,5},{1,3},{1,4},{3,5},{3,

    5},{3,5},{4,5},{4,5},{4,5},{2,5},{2,5},{1,5},{1,5},{3,5},{3,5},{4,5},{4,5}};

AWF=Table[0,{w,24},{f,2}];

Do[AWF[[w,f]]=1/TtAreaRoom[[Belongs[[w,f]]]],{w,24},{f,2}];


FF={4.5*8.5/115,5*3.5/115,4*3.5/115,4*3.5/115,0};

hawBig=Table[{3+1.2*IsDay[[t]],3+1.2*IsDay[[t]]},{t,tmax},{w,24}];


houtMask={{0,1},{0,1},{0,0},{0,1},{0,0},{0,0},{0,1},{0,1},{0,0},{0,0},{0,1},{

    0,0},{0,0},{0,0},{0,0},{0,1},{0,0},{0,0},{0,0},{0,0},{0,0},{0,0},{0,0},{0,0}};

hAddIn={{0,0},{0,0},{0,5},{0,0},{0,0},{0,5},{0,0},{0,0},{0,0},{0,0},{0,0},{0,

    5},{0,0},{0,0},{0,5},{0,0},{0,0},{0,0},{0,0},{0,0},{0,0},{0,0},{0,0},{0,0}};

hFanIn={{5,5},{5,5},{5,5},{5,5},{5,5},{5,5},{5,5},{5,5},{5,5},{5,5},{5,

    5},{5,5},{5,5},{5,5},{5,5},{5,5},{5,5},{5,5},{5,5},{5,5},{5,5},{5,5},{5,5},};


(*R-values between inside and the room*)

UTR:={(1/5+Rwindow+1/haw[[2,2]])^-1,(1/5+Rwindow+1/haw[[7,2]])^-1,(

        1/5+Rwindow+1/haw[[2,2]])^-1,

        (1/5+Rwindow+1/haw[[2,2]])^-1,(1/5+Rwindow+1/haw[[16,2]])^-1};(*

        Resistance until glass*)


(*R values between inside and the glass*)

UTG:={(Rwindow+1/haw[[2,2]])^-1,(Rwindow+1/haw[[7,2]])^-1,(

        Rwindow+1/haw[[2,2]])^-1,

        (Rwindow+1/haw[[2,2]])^-1,(Rwindow+1/haw[[16,2]])^-1};(*

        Resistance untill glass*)
```

142

```
ESG[t_,City_]:={{0,
        α*(Ed[t+hi,City,4]+EB[t+hi,City,4])+(1-IsDay[[25]])*NRLoss},{0,
        α*(Ed[t+hi,City,1]+EB[t+hi,City,1])+(1-IsDay[[25]])*NRLoss},{0,
        0},{0,0},{0,0},{0,0},{0,
        α*(Ed[t+hi,City,2]+EB[t+hi,City,2])+(1-IsDay[[25]])*NRLoss},{0,
        0},{0,0},{0,0},{0,α*(Ed[t+hi,City,1]+EB[t+hi,City,1])+(1-
IsDay[[25]])*NRLoss},{0,0},{0,0},{0,0},{0,0},
{0,α*(Ed[t+hi,City,2]+EB[t+hi,City,2])+(1-
IsDay[[25]])*NRLoss},{0,0},{0,0},{0,0},{0,0},
{0,0},{0,0},{0,0},{0,0},{0,0},{0,0},{0,0},{0,0},{0,0},{0,0}};
```

Calculation engine (V10)

```
hcor[Vel_]:=Max[2.29+6.41*Min[Vel,3],3];(*C O R R E L A C A O*)

b[w_,p_]:=Sqrt[kw[[w,p]]*rw[[w,p]]*cw[[w,p]]];

alfa[w_,p_]:=kw[[w,p]]/(rw[[w,p]]*cw[[w,p]]);

Big[w_,p_]:=Lx[[w]]/kw[[w,p]];

FoT[w_,p_]:=0.99*(2*(1+Big[w,p]*haw[[w,1]]))^-1;

dtT[w_,p_]:=FoT[w,p]*Lx[[w]]^2/alfa[w,p];

Fo[w_,p_]:=alfa[w,p]*dt/(Lx[[w]]^2);

Results=Table[25,{t,tmax},{y,65}];

P[n_]:=Transpose[Results][[n]];


GlassTemp:={Two[[26,1]]=Tg1;Two[[27,1]]=Tg2;Two[[28,1]]=Tg3;Two[[29,1]]=Tg4;
        Two[[30,1]]=Tg5;Two[[25,1]]=Tg6;};

GArea={4.5*2.7,3.5*1,3.5*1,3.5*1,3.5*1,2*1};
```

```
(*Thermal functions for different boundary conditions, A->Adiabatic,

    CH->convective+fixed heat flux,

    Tfn->function for the internal nodes of the wall*)

Tf1CH[w_,r_,f_]:=2*Fo[w,1]*(Two[[w,2]]+haw[[w,f]]*Big[w,1]*Tr[[r]]+(RE[[w,f]]+SlG[[w
,f]]+AWF[[w,f]]*(1-CGF)*IG[[t,r]])*Big[w,1])+(1-2*Fo[w,1]-
2*Fo[w,1]*haw[[w,f]]*Big[w,1])*Two[[w,1]];(*B E G I N I N G, Convective + HeatFlux*)

TfNA[w_,p_]:=2*Fo[w,p-1]*Two[[w,p-1]]+(1-2*Fo[w,p-1])*Two[[w,p]];(*E      N      D,
ADIABATIC*)


TfNCH[w_,p_,r_,f_]:=2*Fo[w,p-1]*(Two[[w,p-1]]+haw[[w,f]]*Big[w,p-
1]*Tr[[r]]+(RE[[w,f]]+SlG[[w,f]]+AWF[[w,f]]*(1-CGF)*IG[[t,r]])*Big[w,p-1])+
 (1-2*Fo[w,p-1]-2*Fo[w,p-1]*haw[[w,f]]*Big[w,p-1])*Two[[w,p]];(*E  N  D, Convective +
HeatFlux*)


Tfn[w_,p_]:=2*dt/((rw[[w,p-1]]*cw[[w,p-1]]+rw[[w,p]]*cw[[w,p]])*Lx[[w]]^2)*
 (kw[[w,p-1]]*Two[[w,p-1]]+kw[[w,p]]*Two[[w,p+1]])+ (1-2*dt*(kw[[w,p-1]]+
kw[[w,p]])/((rw[[w,p-1]]*cw[[w,p-1]]+rw[[w,p]]*cw[[w,p]])*Lx[[w]]^2))*Two[[w,p]];


Sk=Table[0,{p,10}];Tr={25,25,25,25,30};Wr={15,15,15,15,15};

RE=Table[0,{w,30},{p,2}];IRG=RE;

SlG=RE;(*Wall, Face*)(*RE=RadiationExchange;IRG=InternalRadiativeGains;

SlG=SolarGains;*)

IG=Table[(4*85+350)*FF[[Room]],{time,tmax},{Room,5}];(*Table   with   the   internal
gains*)

Do[IG[[22+i+24*d]]={(4*85+200)*FF[[1]],(4*85+200)*FF[[2]],(4*85+200)*
FF[[3]],(4*85+200)*FF[[4]],0},{i,10},{d,0,Round[tmax/24]-2,1}];

LVt=ρ*1.5*115*2.7/3600;

LVent=Table[LVt*FF[[r]],{t,tmax},{r,4}];(*t,r*)


Two=Twn=Table[25,{w,30},{p,10}];(*Wall,Position*);

haw=Table[6,{w,30},{p,2}];(*Wall,Face*)
```

```
(*Explicit iteration base functions, for each layer of the wall*)

CHCH14[w_,r1_,r2_]:=

    Do[Sk={Tf1CH[w,r1,1],Tfn[w,2],Tfn[w,3],Tfn[w,4],Tfn[w,5],Tfn[w,6],

    Tfn[w,7],TfNCH[w,8,r2,2],0,TfNCH[w,8,r2,2]};

    Two[[w]]=Sk;];

CHCH12[w_,r1_,r2_]:=

    Do[Sk={Tf1CH[w,r1,1],Tfn[w,2],Tfn[w,3],Tfn[w,4],Tfn[w,5],Tfn[w,6],

    TfNCH[w,7,r2,2],0,0,TfNCH[w,7,r2,2]};Two[[w]]=Sk;];

CHCH10[w_,r1_,r2_]:=

    Do[Sk={Tf1CH[w,r1,1],Tfn[w,2],Tfn[w,3],Tfn[w,4],Tfn[w,5],TfNCH[w,6,r2,2],

    0,0,0,TfNCH[w,6,r2,2]};Two[[w]]=Sk;];

CHCH08[w_,r1_,r2_]:=

    Do[Sk={Tf1CH[w,r1,1],Tfn[w,2],Tfn[w,3],Tfn[w,4],    TfNCH[w,5,r2,2],0,

    0,0,0,TfNCH[w,5,r2,2]};Two[[w]]=Sk;];


CHCHPC[w_,r1_]:=Do[Sk={25,25,0,0,0,0,0,0,0,25};Two[[w]]=Sk;];

CHNA10[w_,r1_]:=

    Do[Sk={Tf1CH[w,r1,1],Tfn[w,2],Tfn[w,3],Tfn[w,4],Tfn[w,5],25,0,0,0,25};

       Two[[w]]=Sk;];


CHNA08F[w_,r1_]:=

    Do[Sk={Tf1CH[w,r1,1],Tfn[w,2],Tfn[w,3],Tfn[w,4],Tfn[w,5],Two[[w+1,4]],0,0,

    0,Tfn[w,5]};Two[[w]]=Sk;];

CHNA08C[w_,r1_]:=

    Do[Sk={Tf1CH[w,r1,1],Tfn[w,2],Tfn[w,3],Tfn[w,4],Two[[w-1,5]],0,0,0,0,

    Tn[w-1,5]};Two[[w]]=Sk;];


CHNA06F[w_,r1_]:=

    Do[Sk={Tf1CH[w,r1,1],Tfn[w,2],Tfn[w,3],Tfn[w,4],Two[[w+1,3]],0,0,0,0,
```

```
        Tfn[w,4]};Two[[w]]=Sk;];

CHNA06C[w_,r1_]:=

        Do[Sk={Tf1CH[w,r1,1],Tfn[w,2],Tfn[w,3],Two[[w-1,4]],0,0,0,0,0,Tfn[w-1,4]};

        Two[[w]]=Sk;];


CHNA04F[w_,r1_]:=

        Do[Sk={Tf1CH[w,r1,1],Tfn[w,2],Tfn[w,3],Two[[w+1,2]],0,0,0,0,0,Tfn[w,3]};

        Two[[w]]=Sk;];

CHNA04C[w_,r1_]:=

        Do[Sk={Tf1CH[w,r1,1],Tfn[w,2],Two[[w-1,3]],0,0,0,0,0,0,Tfn[w-1,3]};

        Two[[w]]=Sk;];


CHCH02[w_,r1_,r2_]:=

        Do[Sk={Tf1CH[w,r1,1],    TfNCH[w,2,r2,2],0,0,0,0,0,0,0,TfNCH[w,2,r2,2]};

        Two[[w]]=Sk;];
```

Base case

```
Basico:={CHCH12[1,2,5],CHCH12[2,2,5],CHCH10[3,2,1],CHCH12[4,2,5],CHCH10[5,2,1],

    CHCH10[6,1,5],CHCH12[7,1,5],CHCH12[8,3,5],CHCH10[9,1,3],CHCH10[10,1,4],

    CHCH12[11,3,5],CHCH12[12,3,5],CHCH10[13,3,1],CHCH10[14,4,1],CHCH12[15,4,5],

    CHCH12[16,4,5],CHNA06C[18,2],CHNA06F[17,2],CHNA06C[20,1],CHNA06F[19,1],

    CHNA06C[22,3],CHNA06F[21,3],CHNA06C[24,4],CHNA06F[23,4]};


kw=Table[1.4,{w,25},{p,10}];    rw=Table[2100,{w,25},{p,10}];

  cw=Table[880,{w,25},{p,10}];
```

146

```
cw[[17,1]]=848;cw[[19,1]]=848;cw[[21,1]]=848;cw[[23,1]]=848;

kw[[17,1]]=1.15;kw[[19,1]]=1.15;kw[[21,1]]=1.15;kw[[23,1]]=1.15;

rw[[17,1]]=2060;rw[[19,1]]=2060;rw[[21,1]]=2060;rw[[23,1]]=2060;

kw[[1,6]]=0.0145;kw[[2,6]]=0.0145;kw[[4,6]]=0.0145;kw[[7,6]]=0.0145;
   kw[[8,6]]=0.0145;

kw[[11,6]]=0.0145;kw[[16,6]]=0.0145;

rw[[1,6]]=200;rw[[2,6]]=200;rw[[4,6]]=200;rw[[7,6]]=200;rw[[8,6]]=200;
   rw[[11,6]]=200;rw[[16,6]]=200;

cw[[1,6]]=1300;cw[[2,6]]=1300;cw[[4,6]]=1300;cw[[7,6]]=1300;cw[[8,6]]=1300;
   cw[[11,6]]=1300;cw[[16,6]]=1300;
```

Carpet case

```
cw[[17,1]]=1056;cw[[19,1]]=1056;cw[[21,1]]=1056;cw[[23,1]]=1056;

kw[[17,1]]=0.085;kw[[19,1]]=0.085;kw[[21,1]]=0.085;kw[[23,1]]=0.085;

rw[[17,1]]=1102;rw[[19,1]]=1102;rw[[21,1]]=1102;rw[[23,1]]=1102;


Basico:={CHCH12[1,2,5],CHCH12[2,2,5],CHCH10[3,2,1],CHCH12[4,2,5],CHCH10[5,2,1],
    CHCH10[6,1,5],CHCH12[7,1,5],CHCH12[8,3,5],CHCH10[9,1,3],CHCH10[10,1,4],
    CHCH12[11,3,5],CHCH12[12,3,5],CHCH10[13,3,1],CHCH10[14,4,1],CHCH12[15,4,5],
    CHCH12[16,4,5],CHNA06C[18,2],CHNA06F[17,2],CHNA06C[20,1],CHNA06F[19,1],
    CHNA06C[22,3],CHNA06F[21,3],CHNA06C[24,4],CHNA06F[23,4]};


Vα1=DiagonalMatrix[{α,0.52,α,α,α,α,0.7,α,α,α,α,0.4,α}];
V1mα1=DiagonalMatrix[{1-α,1-0.52,1-α,1-α,1-α,1-α,1-0.7,1-α,1-α,1-α,1-α,1-0.4,1-α}];
Vα2=DiagonalMatrix[{0.4,α,α,0.52,α,α,α,α,α,α,α}];
V1mα2=DiagonalMatrix[{1-0.4,1-α,1-α,1-0.52,1-α,1-α,1-α,1-α,1-α,1-α,1-α}];
Vα3=DiagonalMatrix[{0.4,α,α,0.52,α,α,α,α,α,α,α}];
V1mα3=DiagonalMatrix[{1-0.4,1-α,1-α,1-0.52,1-α,1-α,1-α,1-α,1-α,1-α,1-α}];
Vα4=DiagonalMatrix[{0.4,α,α,0.7,α,α,α,α,α,α,α}];
V1mα4=DiagonalMatrix[{1-0.4,1-α,1-α,1-0.7,1-α,1-α,1-α,1-α,1-α,1-α}];
```

Low-mass case

```
Basico:={CHCH12[1,2,5],CHCH12[2,2,5],CHCHO2[3,2,1],CHCH12[4,2,5],CHCHO2[5,2,1],
    CHCHO2[6,1,5],CHCH12[7,1,5],CHCH12[8,3,5],CHCHO2[9,1,3],CHCHO2[10,1,4],
    CHCH12[11,3,5],CHCH12[12,3,5],CHCHO2[13,3,1],CHCHO2[14,4,1],CHCH12[15,4,5],
    CHCH12[16,4,5],CHNA04C[18,2],CHNA04F[17,2],CHNA04C[20,1],CHNA04F[19,1],
    CHNA04C[22,3],CHNA04F[21,3],CHNA04C[24,4],CHNA04F[23,4]};
```

```
Do[{rw[[3,p]]=950;cw[[3,p]]=820;kw[[3,p]]=0.16},{p,10}];
Do[{rw[[5,p]]=950;cw[[5,p]]=820;kw[[5,p]]=0.16},{p,10}];
Do[{rw[[6,p]]=950;cw[[6,p]]=820;kw[[6,p]]=0.16},{p,10}];
Do[{rw[[9,p]]=950;cw[[9,p]]=820;kw[[9,p]]=0.16},{p,10}];
Do[{rw[[10,p]]=950;cw[[10,p]]=820;kw[[10,p]]=0.16},{p,10}];
Do[{rw[[13,p]]=950;cw[[13,p]]=820;kw[[13,p]]=0.16},{p,10}];
Do[{rw[[14,p]]=950;cw[[14,p]]=820;kw[[14,p]]=0.16},{p,10}];
```

High mass case

```
Basico:={CHCH12[1,2,5],CHCH12[2,2,5],CHCH14[3,2,1],CHCH12[4,2,5],CHCH14[5,2,1],
    CHCH14[6,1,5],CHCH12[7,1,5],CHCH12[8,3,5],CHCH14[9,1,3],CHCH14[10,1,4],
    CHCH12[11,3,5],CHCH12[12,3,5],CHCH14[13,3,1],CHCH14[14,4,1],CHCH12[15,4,5],
    CHCH12[16,4,5],CHNA08C[18,2],CHNA08F[17,2],CHNA08C[20,1],CHNA08F[19,1],
    CHNA08C[22,3],CHNA08F[21,3],CHNA08C[24,4],CHNA08F[23,4]};
```

Phase change layer case

```
Basico:={CHCH12[1,2,5],CHCH12[2,2,5],CHCH10[3,2,1],CHCH12[4,2,5],CHCH10[5,2,1],
    [6,1,5],CHCH12[7,1,5],CHCH12[8,3,5],CHCH10[9,1,3],CHCH10[10,1,4],
    CHCH12[11,3,5],CHCH12[12,3,5],CHCH10[13,3,1],CHCH10[14,4,1],CHCH12[15,4,5],
    CHCH12[16,4,5],CHNA10[17,2],CHCHPC[18,2],CHNA10[19,1],CHCHPC[20,1],
    CHNA10[21,3],CHCHPC[22,3],CHNA10[23,4],CHCHPC[24,4]};
```

Natural ventilation iteration

```
hawBig=Table[{3+1.2*IsDay[[t]],3+1.2*IsDay[[t]]},{t,tmax},{w,24}];
LVent=Table[LVt*FF[[r]],{t,tmax},{r,4}];(*t,r*)


Results=Table[24.5,{t,tmax},{y,15}];
Timing[Do[{NV=0;
    If[(Hora<8||(Hora>18&&ColdOut)||(Tr[[1]]>28&&NatVSp[City,t][[1]]>0.3))&&
        Warm, {NV=1;LVent[[t]]=(0.8*IsDay[[t]]+0.2)*ρ*LVentOpen[[t]];Drtn[City,t];
        haw=Table[
            hcor[(0.8*IsDay[[t]]+0.2)*WallSp[City,t][[w,f]]]*(
                5-hAddIn[[w,f]])/5+hAddIn[[w,f]],{w,24},{f,2}];
            },haw=hawBig[[t]]];


Tr={TR1[t],TR2[t],TR3[t],TR4[t],Temp[[t]]};GlassTemp;ERE=ESG[t,City];RE=REe+ERE;SlG=
SlGe;
IG[[t,1]]=4.5*2.7*GlassBack[[1]];IG[[t,2]]=3.5*GlassBack[[3]];
    IG[[t,3]]=3.5*GlassBack[[4]];Do[Basico,{ii,9}];
Tr={TR1[t],TR2[t],TR3[t],TR4[t],Temp[[t]]};GlassTemp;RE=REe+ERE;
Results[[t]]=
    Round[10*{Tr[[1]],Tr[[2]],Tr[[3]],Tr[[4]],Tr[[5]],MRT1,MRT2,MRT3,MRT4,
        NV,WR,WE[[t]],Two[[19,1]],Two[[10,1]],Two[[20,1]]}]/10.;
```

```
Do[Basico,{ii,9}];

If[IntegerQ[t/72],Print[t," ",NV],]},{t,2,tmax}];]
```

Room temperatures

```
(*Glass Temperatures*)

Tg1:=-(-(RE[[26,1]]+0.5*SC[[1]]*WFAM[[t,City,1]])-haw[[2,1]]*Tr[[1]]-
        Temp[[t]]*UTG[[1]])/(haw[[2,1]]+UTG[[1]]);

Tg2:=-(-(RE[[27,1]]+0.5*SC[[2]]*WFAM[[t,City,2]]+GlassBack[[2]])-
        haw[[7,1]]*Tr[[1]]-Temp[[t]]*UTG[[2]])/(haw[[7,1]]+UTG[[2]]);

Tg3:=-(-(RE[[28,1]]+0.5*SC[[1]]*WFAM[[t,City,1]])-haw[[2,1]]*Tr[[2]]-
        Temp[[t]]*UTG[[3]])/(haw[[2,1]]+UTG[[3]]);

Tg4:=-(-(RE[[29,1]]+0.5*SC[[1]]*WFAM[[t,City,1]])-haw[[2,1]]*Tr[[3]]-
        Temp[[t]]*UTG[[4]])/(haw[[2,1]]+UTG[[4]]);

Tg5:=-(-(RE[[30,1]]+0.5*SC[[2]]*WFAM[[t,City,2]]+GlassBack[[5]])-
        haw[[16,1]]*Tr[[4]]-Temp[[t]]*UTG[[5]])/(haw[[16,1]]+UTG[[5]]);

Tg6:=-(-(RE[[25,1]]+SlG[[25,1]])-haw[[2,1]]*Tr[[1]]-Temp[[t]]*UTG[[1]])/(
        haw[[2,1]]+UTG[[1]]);


(*Solar radiation reabsorbed by the glass*)

GlassBack:={SCE[[1]]*(SC[[1]]*WFM[[t,City,1]]+SlGe[[26,1]]),
    SCE[[2]]*(SC[[2]]*WFM[[t,City,2]]+SlGe[[27,1]]),
    SCE[[1]]*(SC[[1]]*WFM[[t,City,1]]+SlGe[[28,1]]),
    SCE[[1]]*(SC[[1]]*WFM[[t,City,1]]+SlGe[[29,1]]),
    SCE[[2]]*(SC[[2]]*WFM[[t,City,2]]+SlGe[[30,1]])};


(*Mean Radiant Tmeperatures*)

MRT1:=(GArea[[1]]*Tg1+GArea[[2]]*Tg2+Two[[5,2]]*WArea[[5]]+2*2*2.7*Tr[[1]]+
        Two[[6,1]]*WArea[[6]]+
Two[[7,1]]*WArea[[7]]+Two[[9,1]]*WArea[[9]]+Two[[10,1]]*WArea[[10]]+
        Two[[19,1]]*WArea[[19]]+Two[[20,1]]*WArea[[20]])/
(WArea[[20]]+WArea[[19]]+WArea[[10]]+WArea[[9]]+WArea[[7]]+WArea[[6]]+
```

```
        WArea[[5]]+GArea[[1]]+GArea[[2]]+2*2*2.7);


MRT2:=(GArea[[3]]*Tg3+2*2.7*Tr[[2]]+Two[[1,1]]*WArea[[1]]+
        Two[[2,1]]*WArea[[2]]+
Two[[3,1]]*WArea[[3]]+Two[[4,1]]*WArea[[4]]+Two[[5,1]]*WArea[[5]]+
        Two[[17,1]]*WArea[[17]]+Two[[18,1]]*WArea[[18]])/
(GArea[[3]]+WArea[[1]]+2*2.7+WArea[[2]]+WArea[[3]]+WArea[[4]]+WArea[[5]]+
        WArea[[17]]+WArea[[18]]);


MRT3:=(GArea[[4]]*Tg4+2*2.7*Tr[[3]]+Two[[8,1]]*WArea[[8]]+
        Two[[9,2]]*WArea[[9]]+
Two[[11,1]]*WArea[[11]]+Two[[12,1]]*WArea[[12]]+Two[[13,1]]*WArea[[13]]+
        Two[[21,1]]*WArea[[21]]+Two[[22,1]]*WArea[[22]])/
(GArea[[4]]+WArea[[13]]+2*2.7+WArea[[8]]+WArea[[9]]+WArea[[11]]+WArea[[12]]+
        WArea[[21]]+WArea[[22]]);


MRT4:=(GArea[[5]]*Tg5+2*2.7*Tr[[4]]+Two[[10,2]]*WArea[[10]]+Two[[14,1]]*WArea[[14]]+
        Two[[15,1]]*WArea[[15]]+Two[[16,1]]*WArea[[16]]+Two[[23,1]]*WArea[[23]]+
        Two[[24,1]]*WArea[[24]])/
    (GArea[[5]]+2*2.7+WArea[[10]]+WArea[[14]]+WArea[[15]]+WArea[[16]]+WArea[[23]]+
        WArea[[24]]);



TR1[t_]:=(
        CGF*IG[[t,1]]+LVent[[t,1]]*cair*Temp[[t]]+GR1+
          GArea[[1]]*Two[[26,1]]*haw[[7,1]]+GArea[[2]]*Two[[27,1]]*haw[[7,1]]+
          GArea[[6]]*Two[[25,1]]*haw[[7,1]]
        +IsDay[[t]]*DVnt*cair*Tr[[2]]+IsDay[[t]]*DVnt*cair*Tr[[3]]+
          IsDay[[t]]*DVnt*cair*Tr[[4]]+1.61*2.7*1.5*Temp[[t]]+
        +Two[[5,10]]*WArea[[5]]*haw[[5,2]]+Two[[6,1]]*WArea[[6]]*haw[[6,1]]+
          Two[[7,1]]*WArea[[7]]*haw[[7,1]] +Two[[9,1]]*WArea[[9]]*haw[[9,1]]+
          Two[[10,1]]*WArea[[10]]*haw[[10,1]]+Two[[19,1]]*WArea[[19]]*haw[[19,1]]
        +Two[[20,1]]*WArea[[20]]*haw[[20,1]])/
```

```
            (1.61*2.7*1.5+LVent[[t,1]]*cair+WArea[[5]]*haw[[5,2]]+

              WArea[[6]]*haw[[6,1]]+WArea[[7]]*haw[[7,1]]

            +WArea[[9]]*haw[[9,1]]+WArea[[10]]*haw[[10,1]]+WArea[[19]]*haw[[19,1]]

            +WArea[[20]]*haw[[20,1]]+3*IsDay[[t]]*cair*DVnt+

              GArea[[1]]*haw[[7,1]]+GArea[[2]]*haw[[7,1]]+GArea[[6]]*haw[[7,1]]);


TR2[t_]:=(

            CGF*IG[[t,2]]+LVent[[t,1]]*cair*Temp[[t]]+GR2+

              IsDay[[t]]*DVnt*cair*Tr[[1]]+GArea[[3]]*Two[[28,1]]*haw[[2,1]]

            +Two[[1,1]]*WArea[[1]]*haw[[1,1]]+Two[[2,1]]*WArea[[2]]*haw[[2,1]]+

              Two[[3,1]]*WArea[[3]]*haw[[3,1]]

            +Two[[4,1]]*WArea[[4]]*haw[[4,1]]+Two[[5,1]]*WArea[[5]]*haw[[5,1]]+

              Two[[17,1]]*WArea[[17]]*haw[[17,1]]+Two[[18,1]]*WArea[[18]]*haw[[18,1]])/

              (LVent[[t,1]]*cair+WArea[[1]]*haw[[1,1]]+WArea[[2]]*haw[[2,1]]+

                WArea[[3]]*haw[[3,1]]

            +WArea[[4]]*haw[[4,1]]+WArea[[5]]*haw[[5,1]]+WArea[[17]]*haw[[17,1]]

            +WArea[[18]]*haw[[18,1]]+IsDay[[t]]*cair*DVnt+GArea[[3]]*haw[[2,1]]);


TR3[t_]:=(

            CGF*IG[[t,3]]+LVent[[t,1]]*cair*Temp[[t]]+GR3+

              IsDay[[t]]*DVnt*cair*Tr[[1]]+GArea[[4]]*Two[[29,1]]*haw[[11,1]]

                +Two[[9,10]]*WArea[[9]]*haw[[9,2]]+Two[[11,1]]*WArea[[11]]*haw[[11,1]]+

              Two[[12,1]]*WArea[[12]]*haw[[12,1]]

            +Two[[13,1]]*WArea[[13]]*haw[[13,1]]+Two[[21,1]]*WArea[[21]]*haw[[21,1]]

            +Two[[22,1]]*WArea[[22]]*haw[[22,1]])/ (

            LVent[[t,1]]*cair+WArea[[9]]*haw[[9,2]]+WArea[[11]]*haw[[11,1]]+

            WArea[[12]]*haw[[12,1]]+WArea[[13]]*haw[[13,1]]+WArea[[21]]*haw[[21,1]]

            +WArea[[22]]*haw[[22,1]]+IsDay[[t]]*cair*DVnt+GArea[[4]]*haw[[11,1]]);


TR4[t_]:=(

            CGF*IG[[t,4]]+LVent[[t,1]]*cair*Temp[[t]]+GR4+

              IsDay[[t]]*DVnt*cair*Tr[[1]]+GArea[[5]]*Two[[30,1]]*haw[[16,1]]
```

```
+Two[[10,10]]*wArea[[10]]*haw[[10,2]]+Two[[14,1]]*wArea[[14]]*haw[[14,1]]+

   Two[[15,1]]*wArea[[15]]*haw[[15,1]]+Two[[16,1]]*wArea[[16]]*haw[[16,1]]+

   Two[[23,1]]*wArea[[23]]*haw[[23,1]]+Two[[24,1]]*wArea[[24]]*haw[[24,1]])/

  (LVent[[t,1]]*cair+wArea[[10]]*haw[[10,2]]+wArea[[14]]*haw[[14,1]]+

   wArea[[15]]*haw[[15,1]]+wArea[[16]]*haw[[16,1]]+wArea[[23]]*haw[[23,1]]+

   wArea[[24]]*haw[[24,1]]+IsDay[[t]]*cair*DVnt+GArea[[5]]*haw[[16,1]]);
```

Radiative exchange matrix

```
ε=0.94;σ=5.6697*^-8;α=0.25;
```

```
Matrix MA, MB, MC view factors of the surfaces.
```

```
MVF1=MB;MI1=IdentityMatrix[13];
  AreaB={1/AB[[1,1]],1/AB[[2,2]],1/AB[[3,3]],1/AB[[4,4]],1/AB[[5,5]],
     1/AB[[6,6]],1/AB[[7,7]],1/AB[[8,8]],1/AB[[9,9]],1/AB[[10,10]],
     1/AB[[11,11]],1/AB[[12,12]],1/AB[[13,13]]};
MVF2=MA;MI2=IdentityMatrix[11];
  AreaA={1/AA[[1,1]],1/AA[[2,2]],1/AA[[3,3]],1/AA[[4,4]],1/AA[[5,5]],
     1/AA[[6,6]],1/AA[[7,7]],1/AA[[8,8]],1/AA[[9,9]],1/AA[[10,10]],,
     1/AA[[11,11]]};
MVF3=MD;MI3=IdentityMatrix[11];
  AreaD={1/AD[[1,1]],1/AD[[2,2]],1/AD[[3,3]],1/AD[[4,4]],1/AD[[5,5]],
     1/AD[[6,6]],1/AD[[7,7]],1/AD[[8,8]],1/AD[[9,9]],1/AD[[10,10]],
     1/AD[[11,11]]};
MVF4=MC;MI4=IdentityMatrix[10];
  AreaC={1/AC[[1,1]],1/AC[[2,2]],1/AC[[3,3]],1/AC[[4,4]],1/AC[[5,5]],
     1/AC[[6,6]],1/AC[[7,7]],1/AC[[8,8]],1/AC[[9,9]],1/AC[[10,10]]};
```

```
Vε1=DiagonalMatrix[{ε,ε,ε,ε,ε,ε,ε,ε,ε,ε,ε,ε,ε}];
V1mε1=DiagonalMatrix[{1-ε,1-ε,1-ε,1-ε,1-ε,1-ε,1-ε,1-ε,1-ε,1-ε,1-ε,1-ε,1-ε}];
Vα1=DiagonalMatrix[{α,0.52,α,α,α,α,0.7,α,α,α,α,α,α}];
```

```
V1mα1=DiagonalMatrix[{1-α,1-0.52,1-α,1-α,1-α,1-α,1-0.7,1-α,1-α,1-α,1-α,1-α,1-α}];

Vε2=DiagonalMatrix[{ε,ε,ε,ε,ε,ε,ε,ε,ε,ε,ε}];

V1mε2=DiagonalMatrix[{1-ε,1-ε,1-ε,1-ε,1-ε,1-ε,1-ε,1-ε,1-ε,1-ε,1-ε}];

Vα2=DiagonalMatrix[{α,α,α,0.52,α,α,α,α,α,α,α}];

V1mα2=DiagonalMatrix[{1-α,1-α,1-α,1-0.52,1-α,1-α,1-α,1-α,1-α,1-α,1-α}];

Vε3=DiagonalMatrix[{ε,ε,ε,ε,ε,ε,ε,ε,ε,ε,ε}];

V1mε3=DiagonalMatrix[{1-ε,1-ε,1-ε,1-ε,1-ε,1-ε,1-ε,1-ε,1-ε,1-ε,1-ε}];

Vα3=DiagonalMatrix[{α,α,α,0.52,α,α,α,α,α,α,α}];

V1mα3=DiagonalMatrix[{1-α,1-α,1-α,1-0.52,1-α,1-α,1-α,1-α,1-α,1-α,1-α}];

Vε4=DiagonalMatrix[{ε,ε,ε,ε,ε,ε,ε,ε,ε,ε}];

V1mε4=DiagonalMatrix[{1-ε,1-ε,1-ε,1-ε,1-ε,1-ε,1-ε,1-ε,1-ε,1-ε}];

Vα4=DiagonalMatrix[{α,α,α,0.7,α,α,α,α,α,α}];

V1mα4=DiagonalMatrix[{1-α,1-α,1-α,1-0.7,1-α,1-α,1-α,1-α,1-α,1-α}];


ME1=Inverse[MI1-Transpose[Transpose[MVF1].(V1mε1)]];

MS1=Inverse[MI1-Transpose[Transpose[MVF1].(V1mα1)]];

ME2=Inverse[MI2-Transpose[Transpose[MVF2].(V1mε2)]];

MS2=Inverse[MI2-Transpose[Transpose[MVF2].(V1mα2)]];

ME3=Inverse[MI3-Transpose[Transpose[MVF3].(V1mε3)]];

MS3=Inverse[MI3-Transpose[Transpose[MVF3].(V1mα3)]];

ME4=Inverse[MI4-Transpose[Transpose[MVF4].(V1mε4)]];

MS4=Inverse[MI4-Transpose[Transpose[MVF4].(V1mα4)]];


IE1:=ε*σ*{{(Two[[25,1]]+273.15)^4},{(Two[[27,1]]+273.15)^4},{(
        Two[[10,1]]+273.15)^4},{(Two[[7,1]]+273.15)^4},
        {(Tr[[1]]+273.15)^4},{(Two[[9,1]]+273.15)^4},{(
        Two[[26,1]]+273.15)^4},{(Two[[6,1]]+273.15)^4},
        {(Tr[[1]]+273.15)^4},{(Two[[5,10]]+273.15)^4},{(Two[[20,1]]+273.15)^4},
        {(Two[[19,1]]+273.15)^4},{(Two[[7,1]]+273.15)^4}};


IE2:=ε*σ*{{(Two[[17,1]]+273.15)^4},{(Two[[5,1]]+273.15)^4},{(
        Two[[1,1]]+273.15)^4},{(Two[[2,1]]+273.15)^4},
        {(Two[[28,1]]+273.15)^4},{(Two[[2,1]]+273.15)^4},{(
```

```
        Two[[3,1]]+273.15)^4},{(Tr[[2]]+273.15)^4},
    {(Tr[[1]]+273.15)^4},{(Two[[18,1]]+273.15)^4},{(Two[[4,1]]+273.15)^4}};


IE3:=ε*σ*{{(Two[[21,1]]+273.15)^4},{(Two[[12,1]]+273.15)^4},{(
    Two[[11,1]]+273.15)^4},{(Two[[29,1]]+273.15)^4},
      {(Two[[11,1]]+273.15)^4},{(Two[[13,1]]+273.15)^4},{(
      Tr[[3]]+273.15)^4},{(Tr[[1]]+273.15)^4},
      {(Two[[22,1]]+273.15)^4},{(Two[[9,10]]+273.15)^4},{(Two[[8,1]]+273.15)^4}};


IE4:=ε*σ*{{(Two[[23,1]]+273.15)^4},{(Two[[10,10]]+273.15)^4},{(
     Two[[16,1]]+273.15)^4},{(Two[[30,1]]+273.15)^4},
    {(Two[[16,1]]+273.15)^4},{(Two[[14,1]]+273.15)^4},{(
     Tr[[4]]+273.15)^4},{(Tr[[1]]+273.15)^4},
    {(Two[[24,1]]+273.15)^4},{(Two[[15,1]]+273.15)^4}};


SE1:={{0},{SC[[2]]*WFM[[t,City,2]]},{0},{0},{0},{0},{
        SC[[1]]*WFM[[t,City,1]]},{0},{0},{0},{0},{0},{0}};
SE2:={{0},{0},{0},{0},{SC[[1]]*WFM[[t,City,1]]},{0},{0},{0},{0},{0},{0}};
SE3:={{0},{0},{0},{SC[[1]]*WFM[[t,City,1]]},{0},{0},{0},{0},{0},{0},{0}};
SE4:={{0},{0},{0},{SC[[2]]*WFM[[t,City,2]]},{0},{0},{0},{0},{0},{0}};


RE1[n_]:=Vε1[[n,n]]/V1mε1[[n,n]]*(ME1.IE1-IE1/Vε1[[n,n]])[[n,1]];
SG1[n_]:=Vα1[[n,n]]/V1mα1[[n,n]]*(MS1.SE1-SE1/Vα1[[n,n]])[[n,1]];
RE2[n_]:=Vε2[[n,n]]/V1mε2[[n,n]]*(ME2.IE2-IE2/Vε2[[n,n]])[[n,1]];
SG2[n_]:=Vα2[[n,n]]/V1mα2[[n,n]]*(MS2.SE2-SE2/Vα2[[n,n]])[[n,1]];
RE3[n_]:=Vε3[[n,n]]/V1mε3[[n,n]]*(ME3.IE3-IE3/Vε3[[n,n]])[[n,1]];
SG3[n_]:=Vα3[[n,n]]/V1mα3[[n,n]]*(MS3.SE3-SE3/Vα3[[n,n]])[[n,1]];
RE4[n_]:=Vε4[[n,n]]/V1mε4[[n,n]]*(ME4.IE4-IE4/Vε4[[n,n]])[[n,1]];
SG4[n_]:=Vα4[[n,n]]/V1mα4[[n,n]]*(MS4.SE4-SE4/Vα4[[n,n]])[[n,1]];


GR1:=2*1*(RE1[1]+SG1[1])+2*2.7*(RE1[5]+SG1[5])+2*2.7*(RE1[9]+SG1[9])+1.5*0.7*(
        RE2[9]+SG2[9])+1.5*0.7*(RE3[8]+SG3[8])+1.5*0.7*(RE4[8]+SG4[8]);
GR2:=(RE2[8]+SG2[8])*2*1.5;GR3:=(RE3[7]+SG3[7])*2*1.5;
```

```
GR4:=(RE4[7]+SG4[7])*2*1.5;


REe:={{RE2[3],0},{1/(2*(1*3.5+0.7*3.5))*(1*3.5*RE2[4]+0.7*3.5*RE2[6]),0},{
        RE2[7],0},{RE2[11],0},{RE2[2],RE1[10]},
        {RE1[8],0},{1/(2*(0.7*4.5+3.5))*(0.7*4.5*RE1[4]+3.5*RE1[13]),0},{RE3[11],
        0},{RE1[6],RE3[10]},{RE1[3],RE4[2]},
        {RE3[3],0},{1/(2*(1*3.5+0.7*3.5))*(1*3.5*RE3[2]+0.7*3.5*RE3[5]),0},{
        RE3[6],0},{RE4[6],0},{RE4[10],0},
        {1/(2*(1*3.5+0.7*3.5))(1*3.5*RE4[3]+0.7*3.5*RE4[5]),0},{RE2[1],0},{
        RE2[10],0},{RE1[12],0},{RE1[11],0},
        {RE3[1],0},{RE3[9],0},{RE4[1],0},{RE4[9],0},{RE1[1],0},
        {RE1[7],0},{RE1[2],0},{RE2[5],0},{RE3[4],0},{RE4[4],0}};


SlGe:={{SG2[3],0},{1/(2*(1*3.5+0.7*3.5))*(1*3.5*SG2[4]+0.7*3.5*SG2[6]),0},{
        SG2[7],0},{SG2[11],0},{SG2[2],SG1[10]},
        {SG1[8],0},{1/(2*(0.7*4.5+3.5))*(0.7*4.5*SG1[4]+3.5*SG1[13]),0},{SG3[11],
        0},{SG1[6],SG3[10]},{SG1[3],SG4[2]},
        {SG3[3],0},{1/(2*(1*3.5+0.7*3.5))*(1*3.5*SG3[2]+0.7*3.5*SG3[5]),0},{
        SG3[6],0},{SG4[6],0},{SG4[10],0},
        {1/(2*(1*3.5+0.7*3.5))(1*3.5*SG4[3]+0.7*3.5*SG4[5]),0},{SG2[1],0},{
        SG2[10],0},{SG1[12],0},{SG1[11],0},
        {SG3[1],0},{SG3[9],0},{SG4[1],0},{SG4[9],0},{SG1[1],0},
        {SG1[7],0},{SG1[2],0},{SG2[5],0},{SG3[4],0},{SG4[4],0}};
```

Ventilation flow rates

```
LFR08=ReadList["LFR08f.txt"];LFR10=ReadList["LFR10f.txt"];
LFR12=ReadList["LFR12f.txt"];
LFR14=ReadList["LFR14f.txt"];LFR16=ReadList["LFR16f.txt"];
LFR09=0.5*(LFR08+LFR10);LFR11=0.5*(LFR10+LFR12);LFR13=0.5*(LFR12+LFR14);
LFR15=0.5*(LFR14+LFR16);
```

```
LMV08=ReadList["LMV08f.txt"];LMV10=ReadList["LMV10f.txt"];

LMV12=ReadList["LMV12f.txt"];

LMV14=ReadList["LMV14f.txt"];LMV16=ReadList["LMV16f.txt"];

LMV09=0.5*(LMV08+LMV10);LMV11=0.5*(LMV10+LMV12);LMV13=0.5*(LMV12+LMV14);

LMV15=0.5*(LMV14+LMV16);


NV08=ReadList["NV08f.txt"];NV10=ReadList["NV10f.txt"];

NV12=ReadList["NV12f.txt"];

NV14=ReadList["NV14f.txt"];NV16=ReadList["NV16f.txt"];

NV09=0.5*(NV08+NV10);NV11=0.5*(NV10+NV12);NV13=0.5*(NV12+NV14);

NV15=0.5*(NV14+NV16);


NVMax08=ReadList["NVMax08f.txt"];NVMax10=ReadList["NVMax10f.txt"];

NVMax12=ReadList["NVMax12f.txt"];

NVMax14=ReadList["NVMax14f.txt"];NVMax16=ReadList["NVMax16f.txt"];

NVMax09=0.5*(NVMax08+NVMax10);NVMax11=0.5*(NVMax10+NVMax12);

NVMax13=0.5*(NVMax12+NVMax14);NVMax15=0.5*(NVMax14+NVMax16);


NVMaxPos08=ReadList["NVMaxPos08f.txt"];NVMaxPos10=ReadList["NVMaxPos10f.txt"];

NVMaxPos12=ReadList["NVMaxPos12f.txt"];

NVMaxPos14=ReadList["NVMaxPos14f.txt"];

NVMaxPos16=ReadList["NVMaxPos16f.txt"];


BSide=Table[0,{n,3672}];BwdS=Bwd;
Do[If[1<=Bwd[[n]]<=7,BSide[[n]]=2,BSide[[n]]=1],{n,3672}]


Do[If[Bwd[[n]]==1,BwdS[[n]]=15,If[Bwd[[n]]==2,BwdS[[n]]=14,

        If[Bwd[[n]]==3,BwdS[[n]]=13,If[Bwd[[n]]==4,BwdS[[n]]=12,

        If[Bwd[[n]]==5,BwdS[[n]]=11,If[Bwd[[n]]==6,BwdS[[n]]=10,

        If[Bwd[[n]]==7,BwdS[[n]]=9,0]]]]]]],{n,3672}];


SSide=Table[0,{n,3672}];SwdS=Swd;
Do[If[1<=Swd[[n]]<=7,SSide[[n]]=2,SSide[[n]]=1],{n,3672}]
```

```
Do[If[Swd[[n]]==1,SwdS[[n]]=15,If[Swd[[n]]==2,SwdS[[n]]=14,

        If[Swd[[n]]==3,SwdS[[n]]=13,If[Swd[[n]]==4,SwdS[[n]]=12,

        If[Swd[[n]]==5,SwdS[[n]]=11,If[Swd[[n]]==6,SwdS[[n]]=10,

        If[Swd[[n]]==7,SwdS[[n]]=9,0]]]]]]],{n,3672}];


TSide=Table[0,{n,3672}];TwdS=Twd;

Do[If[1<=Twd[[n]]<=7,TSide[[n]]=2,TSide[[n]]=1],{n,3672}]


Do[If[Twd[[n]]==1,TwdS[[n]]=15,If[Twd[[n]]==2,TwdS[[n]]=14,

        If[Twd[[n]]==3,TwdS[[n]]=13,If[Twd[[n]]==4,TwdS[[n]]=12,

        If[Twd[[n]]==5,TwdS[[n]]=11,If[Twd[[n]]==6,TwdS[[n]]=10,

        If[Twd[[n]]==7,TwdS[[n]]=9,0]]]]]]],{n,3672}];


Drtn[1,t_]:=

If[BwdS[[t]]==08,{LFRt=LFR08;LMVt=LMV08;NVt=NV08;NVMaxt=NVMax08;},

If[BwdS[[t]]==09,{LFRt=LFR09;LMVt=LMV09;NVt=NV09;NVMaxt=NVMax09;},

If[BwdS[[t]]==10,{LFRt=LFR10;LMVt=LMV10;NVt=NV10;NVMaxt=NVMax10;},

If[BwdS[[t]]==11,{LFRt=LFR11;LMVt=LMV11;NVt=NV11;NVMaxt=NVMax11;},

If[BwdS[[t]]==12,{LFRt=LFR12;LMVt=LMV12;NVt=NV12;NVMaxt=NVMax12;},

If[BwdS[[t]]==13,{LFRt=LFR13;LMVt=LMV13;NVt=NV13;NVMaxt=NVMax13;},

If[BwdS[[t]]==14,{LFRt=LFR14;LMVt=LMV14;NVt=NV14;NVMaxt=NVMax14;},

If[BwdS[[t]]==15,{LFRt=LFR15;LMVt=LMV15;NVt=NV15;NVMaxt=NVMax15;},

If[BwdS[[t]]==16,{LFRt=LFR16;LMVt=LMV16;NVt=NV16;NVMaxt=NVMax16;},]]]]]]]]];

Drtn[2,t_]:=

If[SwdS[[t]]==08,{LFRt=LFR08;LMVt=LMV08;NVt=NV08;NVMaxt=NVMax08;},

If[SwdS[[t]]==09,{LFRt=LFR09;LMVt=LMV09;NVt=NV09;NVMaxt=NVMax09;},

If[SwdS[[t]]==10,{LFRt=LFR10;LMVt=LMV10;NVt=NV10;NVMaxt=NVMax10;},

If[SwdS[[t]]==11,{LFRt=LFR11;LMVt=LMV11;NVt=NV11;NVMaxt=NVMax11;},

If[SwdS[[t]]==12,{LFRt=LFR12;LMVt=LMV12;NVt=NV12;NVMaxt=NVMax12;},

If[SwdS[[t]]==13,{LFRt=LFR13;LMVt=LMV13;NVt=NV13;NVMaxt=NVMax13;},

If[SwdS[[t]]==14,{LFRt=LFR14;LMVt=LMV14;NVt=NV14;NVMaxt=NVMax14;},

If[SwdS[[t]]==15,{LFRt=LFR15;LMVt=LMV15;NVt=NV15;NVMaxt=NVMax15;},
```

```
If[SwdS[[t]]==16,{LFRt=LFR16;LMVt=LMV16;NVt=NV16;NVMaxt=NVMax16;},]]]]]]]]];
Drtn[3,t_]:=

If[TwdS[[t]]==08,{LFRt=LFR08;LMVt=LMV08;NVt=NV08;NVMaxt=NVMax08;},

If[TwdS[[t]]==09,{LFRt=LFR09;LMVt=LMV09;NVt=NV09;NVMaxt=NVMax09;},

If[TwdS[[t]]==10,{LFRt=LFR10;LMVt=LMV10;NVt=NV10;NVMaxt=NVMax10;},

If[TwdS[[t]]==11,{LFRt=LFR11;LMVt=LMV11;NVt=NV11;NVMaxt=NVMax11;},

If[TwdS[[t]]==12,{LFRt=LFR12;LMVt=LMV12;NVt=NV12;NVMaxt=NVMax12;},

If[TwdS[[t]]==13,{LFRt=LFR13;LMVt=LMV13;NVt=NV13;NVMaxt=NVMax13;},

If[TwdS[[t]]==14,{LFRt=LFR14;LMVt=LMV14;NVt=NV14;NVMaxt=NVMax14;},

If[TwdS[[t]]==15,{LFRt=LFR15;LMVt=LMV15;NVt=NV15;NVMaxt=NVMax15;},

If[TwdS[[t]]==16,{LFRt=LFR16;LMVt=LMV16;NVt=NV16;NVMaxt=NVMax16;},]]]]]]]]];


RFlow[City_,t_]:=
If[City==1,RctB[t,LFRt],If[City==2,RctS[t,LFRt],RctT[t,LFRt]]];


WallSp[City_,t_]:=
If[City==1,RctB[t,LMVt],If[City==2,RctS[t,LMVt],RctT[t,LMVt]]];


NatVSp[City_,t_]:=
If[City==1,RctB[t,NVt],If[City==2,RctS[t,NVt],RctT[t,NVt]]];


NatVSpMax[City_,t_]:=
If[City==1,RctB[t,NVMaxt],If[City==2,RctS[t,NVMaxt],RctT[t,NVMaxt]]];


RctB[t_,Vector_]:=
  Abs[(Vector[[2*(f-1)+1+(BSide[[t]]-1)+10*(2-1)]]-Vector[[2*(f-1)+1+(BSide[[t]]-
1)]])*Bws[[t]]+Vector[[2*(f-1)+1+(BSide[[t]]-1)+10*(2-1)]]-4*(Vector[[2*(f-
1)+1+(BSide[[t]]-1)+10*(2-1)]]-Vector[[2*(f-1)+1+(BSide[[t]]-1)]])];


RctS[t_,Vector_]:=
  Abs[(Vector[[2*(f-1)+1+(SSide[[t]]-1)+10*(2-1)]]-Vector[[2*(f-1)+1+(SSide[[t]]-
1)]])*Sws[[t]]+Vector[[2*(f-1)+1+(SSide[[t]]-1)+10*(2-1)]]-4*(Vector[[2*(f-
1)+1+(SSide[[t]]-1)+10*(2-1)]]-Vector[[2*(f-1)+1+(SSide[[t]]-1)]])];
```

```
RctT[t_,Vector_]:=
  Abs[(Vector[[2*(f-1)+1+(TSide[[t]]-1)+10*(2-1)]]-Vector[[2*(f-1)+1+(TSide[[t]]-
1)]])*Tws[[t]]+Vector[[2*(f-1)+1+(TSide[[t]]-1)+10*(2-1)]]-4*(Vector[[2*(f-
1)+1+(TSide[[t]]-1)+10*(2-1)]]-Vector[[2*(f-1)+1+(TSide[[t]]-1)]])];
```

Solar radiation

```
ETfit=InterpolatingPolynomial[{-11.2,-13.9,-7.5,1.1,3.3,-1.4,-6.2,-2.4,7.5,
      15.4,13.8,1.6}, x];
Declifit=InterpolatingPolynomial[{-20,-10.8,0,11.6,20,23.45,20.6,12.3,
      0,-10.5,-19.8,-23.45}, x];
Ccfit=InterpolatingPolynomial[{0.058,0.060,0.071,0.097,0.121,0.134,0.136,
      0.122,0.092,0.073,0.063,0.057}, x];;
Long[1]=116.28;Lat[1]=39.93;Long[2]=121.43;Lat[2]=31.17;Long[3]=139.46;
Lat[3]=35.41;
a[0]=0.01154;a[1]=0.77674;a[2]=-3.94657;a[3]=8.57881;a[4]=-8.38135;
a[5]=3.01188;
tv={-0.00885,2.71235,-0.62062,-7.07329,9.75995,-3.89922};
ρg=0.3;


ψ[1]=0;ψ[2]=180;ψ[3]=-90;ψ[4]=90;Σ[1]=90;
Σ[2]=90;Σ[3]=90;Σ[4]=90;


ET[h_]:=ETfit/.x->(4+9/30+h/(30.6*24));
Decli[h_]:=Declifit/.x->(4+9/30+h/(30.6*24));
Cc[h_]:=Ccfit/.x->(4+9/30+h/(30.6*24));
H[h_,City_]:=
  Abs[0.25*(720-(60*(h-Floor[(h-1)/24]*24)+ET[h]-4*(120-Long[City])))];


β[h_,City_]:=
  Max[Re[(180/Pi)*ArcSin[Cos[Pi*Lat[City]/180]*Cos[Pi*Decli[h]/180]*
```

160

```
                    Cos[Pi*H[h,City]/180]+Sin[Pi*Lat[City]/180]*Sin[Pi*Decli[h]/180]]],0];
φ[h_,City_]:=(180/Pi)*

    ArcCos[(Sin[Pi*Lat[City]/180]*Sin[β[h,City]*Pi/180]-

    Sin[Pi*Decli[h]/180])/(Cos[β[h,City]*Pi/180]*Cos[Pi*Lat[City]/180])];
γ[h_,City_,S_]:=

  If[h-Floor[(h-1)/24]*24<12,

    φ[h,City]+ψ[S],-φ[h,City]+ψ[S]];
θ[h_,City_,S_]:=(180/Pi)*

    ArcCos[(Cos[β[h,City]*Pi/180]*Cos[γ[h,City,S]*Pi/180]+

    Sin[β[h,City]*Pi/180]*Cos[Σ[S]*Pi/180])];


Y[h_,City_,S_]:=

  Re[If[Re[Cθ[h,City,S]]>-0.2,0.55+0.437*Cθ[h,City,S]+0.313*Cθ[h,City,S]^2,0.45]];


Cθ[h_,City_,S_]:=

  Max[Re[Cos[β[h,City]*Pi/180]*Cos[γ[h,City,S]*Pi/180]],0];
hi=(31+28+31+30)*24;


Eds[h_,City_,S_]:=

  If[City==1,Y[h,City,S]*BF[[h-hi]],

    If[City==2,Y[h,City,S]*SF[[h-hi]],Y[h,City,S]*TF[[h-hi]]]];
EdgB[h_,City_,S_]:=

  If[City==1,BB[[h-hi]],If[City==2,SB[[h-hi]],TB[[h-hi]]]]*ρg*Sin[Pi*β[h,City]/180];
Ed[h_,City_,S_]:=Eds[h,City,S]*(1+ρg)+EdgB[h,City,S];


EB[h_,City_,S_]:=

  If[City==1,BB[[h-hi]],If[City==2,SB[[h-hi]],TB[[h-hi]]]]*Cθ[h,City,S];


Usellerrr[t_]:=If[t==1,If[,,]];
```

PHOENICS airflow simulation file reading and pre-processing

```
Nx=75;Ny=59;Nz=46;miu=16*^-6;Slice=(Nx-1)*(Ny-1);NG=11 ;Ola=Nx+Ny+Nz-3;

SetDirectory["D:\FlowResults"];ll=ReadList["F2012.txt",Number];

PrMf[nx_,ny_,nz_]:=ll[[Ola+(nx-2)*(Ny-1)+ny-1+(Nz-2-(nz-2))*NG*Slice]];

VxMf[nx_,ny_,nz_]:=ll[[Ola+(nx-2)*(Ny-1)+ny-1+Slice+(Nz-2-(nz-2))*NG*Slice]];

VyMf[nx_,ny_,nz_]:=ll[[Ola+(nx-2)*(Ny-1)+ny-1+2*Slice+(Nz-2-(nz-2))*NG*Slice]];

VzMf[nx_,ny_,nz_]:=-ll[[Ola+(nx-2)*(Ny-1)+ny-1+3*Slice+(Nz-2-(nz-2))*NG*Slice]];

KeMf[nx_,ny_,nz_]:=ll[[Ola+(nx-2)*(Ny-1)+ny-1+4*Slice+(Nz-2-(nz-2))*NG*Slice]];

EtMf[nx_,ny_,nz_]:=ll[[Ola+(nx-2)*(Ny-1)+ny-1+5*Slice+(Nz-2-(nz-2))*NG*Slice]];

MtMf[nx_,ny_,nz_]:=ll[[Ola+(nx-2)*(Ny-1)+ny-1+8*Slice+(Nz-2-(nz-2))*NG*Slice]];


WArea={5*2.7,3.5*1.7,2*2.7,1.5*2.7,3.5*2.7,3*2.7,4.5*1.7,1.5*2.7,2.5*2.7,
    4*2.7,3.5*1.7,4*2.7,2*2.7,2*2.7,4*2.7,3.5*1.7,5*3.5,5*3.5,8.5*4.5+2*1.5*2,
    8.5*4.5+2*1.5*2,3.5*4,3.5*4,3.5*4,3.5*4};



AP[F_,S_,A_]:={{42,22+26*(S-1),29+26*(S-1),13+6*(5-F),18+6*(5-F)},
    {19,18+26*(S-1),19+26*(S-1),15+6*(5-F),16+6*(5-F)},
    {19,32+12*(S-1),33+12*(S-1),15+6*(5-F),16+6*(5-F)},
    {42,32+12*(S-1),33+12*(S-1),15+6*(5-F),16+6*(5-F)},
    {23,22+26*(S-1),29+26*(S-1),13+6*(5-F),18+6*(5-F)},
    {31,19+37*(S-1),21+37*(S-1),13+6*(5-F),14+6*(5-F)},
    {29,30+15*(S-1),32+15*(S-1),13+6*(5-F),14+6*(5-F)},
    {33,30+15*(S-1),32+15*(S-1),13+6*(5-F),14+6*(5-F)}}[[A]];


NVntP[F_,S_,r_]:={{23+26*(S-1),28+26*(S-1),21,41,16+6*(5-F),17+6*(5-F)},
    {16+41*(S-1),20+41*(S-1),21,30,16+6*(5-F),17+6*(5-F)},
    {31+11*(S-1),35+11*(S-1),21,28,16+6*(5-F),17+6*(5-F)},
    {31+11*(S-1),35+11*(S-1),35,41,16+6*(5-F),17+6*(5-F)}}[[r]];


WP[F_,S_,w_,f_,p_]:={
{{15+47*(S-1),15+47*(S-1),21,31,13+6*(5-F),18+6*(5-F)},
    {14+49*(S-1),14+49*(S-1),21,31,13+6*(5-F),18+6*(5-F)}},
    {{15+41*(S-1),21+41*(S-1),20,20,13+6*(5-F),18+6*(5-F)},
```

```
{15+41*(S-1),21+41*(S-1),19,19,13+6*(5-F),18+6*(5-F)}},

{{15+44*(S-1),18+44*(S-1),31,31,13+6*(5-F),18+6*(5-F)},{0,0,0,0,0,0}},

{{21+35*(S-1),21+35*(S-1),20,23,13+6*(5-F),18+6*(5-F)},

{22+33*(S-1),22+33*(S-1),20,23,13+6*(5-F),18+6*(5-F)}},

{{21+35*(S-1),21+35*(S-1),24,31,13+6*(5-F),18+6*(5-F)},

{22+33*(S-1),22+33*(S-1),24,31,13+6*(5-F),18+6*(5-F)}},

{{22+33*(S-1),22+33*(S-1),36,42,13+6*(5-F),18+6*(5-F)},{0,0,0,0,0,0}},

{{22+26*(S-1),29+26*(S-1),42,42,13+6*(5-F),18+6*(5-F)},

{22+26*(S-1),29+26*(S-1),43,43,13+6*(5-F),18+6*(5-F)}},

{{30+17*(S-1),30+17*(S-1),20,23,13+6*(5-F),18+6*(5-F)},

{29+19*(S-1),29+19*(S-1),20,23,13+6*(5-F),18+6*(5-F)}},

{{29+19*(S-1),29+19*(S-1),24,29,13+6*(5-F),18+6*(5-F)},

{30+17*(S-1),30+17*(S-1),24,29,13+6*(5-F),18+6*(5-F)}},

{{29+19*(S-1),29+19*(S-1),34,42,13+6*(5-F),18+6*(5-F)},

{30+17*(S-1),30+17*(S-1),34,42,13+6*(5-F),18+6*(5-F)}},

{{30+11*(S-1),36+11*(S-1),20,20,13+6*(5-F),18+6*(5-F)},

{30+11*(S-1),36+11*(S-1),19,19,13+6*(5-F),18+6*(5-F)}},

{{36+5*(S-1),36+5*(S-1),20,29,13+6*(5-F),18+6*(5-F)},

{37+3*(S-1),37+3*(S-1),20,29,13+6*(5-F),18+6*(5-F)}},

{{33+8*(S-1),36+8*(S-1),29,29,13+6*(5-F),18+6*(5-F)},{0,0,0,0,0,0}},

{{33+8*(S-1),36+8*(S-1),34,34,13+6*(5-F),18+6*(5-F)},{0,0,0,0,0,0}},

{{36+5*(S-1),36+5*(S-1),34,42,13+6*(5-F),18+6*(5-F)},

{37+3*(S-1),37+3*(S-1),34,42,13+6*(5-F),18+6*(5-F)}},

{{30+11*(S-1),36+11*(S-1),42,42,13+6*(5-F),18+6*(5-F)},

{30+11*(S-1),36+11*(S-1),43,43,13+6*(5-F),18+6*(5-F)}},

{{15+41*(S-1),21+41*(S-1),20,31,18+6*(5-F),18+6*(5-F)},{0,0,0,0,0,0}},

{{15+41*(S-1),21+41*(S-1),20,31,13+6*(5-F),13+6*(5-F)},{0,0,0,0,0,0}},

{{22+26*(S-1),29+26*(S-1),24,42,18+6*(5-F),18+6*(5-F)},{0,0,0,0,0,0}},

{{22+26*(S-1),29+26*(S-1),24,42,13+6*(5-F),13+6*(5-F)},{0,0,0,0,0,0}},

{{30+11*(S-1),36+11*(S-1),20,29,18+6*(5-F),18+6*(5-F)},{0,0,0,0,0,0}},

{{30+11*(S-1),36+11*(S-1),20,29,13+6*(5-F),13+6*(5-F)},{0,0,0,0,0,0}},

{{30+11*(S-1),36+11*(S-1),34,42,18+6*(5-F),18+6*(5-F)},{0,0,0,0,0,0}},

{{30+11*(S-1),36+11*(S-1),34,42,13+6*(5-F),13+6*(5-F)},{0,0,0,0,0,0}}}[[w,f,p]];
```

```
WAxis={{2,2},{1,1},{1,0},{2,2},{2,2},{2,0},{1,1},{2,2},{2,2},{2,2},{1,1},{2,
    2},{1,0},{1,0},{2,2},{1,1},{3,0},{3,0},{3,0},{3,0},{3,0},{3,0},{3,0},{3,0}};


AFlow[F_,S_,A_]:=Sum[VyMf[x,AP[F,S,A][[1]],z]*Lxf[[x]]*Lzf[[z]],{x,AP[F,S,A][[2]],
    AP[F,S,A][[3]]},{z,AP[F,S,A][[4]],AP[F,S,A][[5]]}];


MedVel[F_,S_,w_,f_]:=
If[WAxis[[w,f]]==2,
    Sum[Sqrt[((VyMf[x,y,z]+VyMf[x,y-1,z])/2)^2+((VzMf[x,y,z]+VzMf[x,y,z+1])/
        2)^2]*Lyf[[y]]*Lzf[[z]]*1/WArea[[w]],
        {x,WP[F,S,w,f,1],WP[F,S,w,f,2]},{y,WP[F,S,w,f,3],WP[F,S,w,f,4]},{z,
        WP[F,S,w,f,5],WP[F,S,w,f,6]}],


If[WAxis[[w,f]]==3,
        Sum[Sqrt[((VxMf[x,y,z]+VxMf[x-1,y,z])/2)^2+((VyMf[x,y,z]+VyMf[x,y-1,z])/
        2)^2]*Lxf[[x]]*Lyf[[y]]*1/WArea[[w]],
        {x,WP[F,S,w,f,1],WP[F,S,w,f,2]},{y,WP[F,S,w,f,3],WP[F,S,w,f,4]},{z,
        WP[F,S,w,f,5],WP[F,S,w,f,6]}],


If[WAxis[[w,f]]==1,
        Sum[Sqrt[((VxMf[x,y,z]+VxMf[x-1,y,z])/
        2)^2+((VzMf[x,y,z]+VzMf[x,y,z+1])/2)^2]*Lxf[[x]]*
        Lzf[[z]]*1/WArea[[w]],
        {x,WP[F,S,w,f,1],WP[F,S,w,f,2]},{y,WP[F,S,w,f,3],WP[F,S,w,f,4]},{z,
        WP[F,S,w,f,5],WP[F,S,w,f,6]}],0]]];


NVntVel[F_,S_,r_]:=
  Sum[Sqrt[((VxMf[x,y,z]+VxMf[x-1,y,z])/2)^2+((VyMf[x,y,z]+VyMf[x,y-1,z])/
    2)^2+((VzMf[x,y,z]+VzMf[x,y,z+1])/2)^2]*Lxf[[x]]*Lyf[[y]]*
    Lzf[[z]]*1/Sum[Lxf[[x]]*Lyf[[y]]*Lzf[[z]], {x,NVntP[F,S,r][[1]],
    NVntP[F,S,r][[2]]},{y,NVntP[F,S,r][[3]],NVntP[F,S,r][[4]]},{z,
    NVntP[F,S,r][[5]],NVntP[F,S,r][[6]]}],
```

```
{x,NVntP[F,S,r][[1]],NVntP[F,S,r][[2]]},{y,

NVntP[F,S,r][[3]],NVntP[F,S,r][[4]]},{z,NVntP[F,S,r][[5]],NVntP[F,S,r][[6]]}};


PosNVntVmax[F_,S_,r_]:=

  Flatten[Position[

    Table[Sqrt[VxMf[x,y,z]^2+VyMf[x,y,z]^2+VzMf[x,y,z]^2],{x,

        NVntP[F,S,r][[1]],NVntP[F,S,r][[2]]},

      {y,NVntP[F,S,r][[3]],NVntP[F,S,r][[4]]},{z,

      NVntP[F,S,r][[5]],NVntP[F,S,r][[6]]}},

      Max[Table[

      Sqrt[VxMf[x,y,z]^2+VyMf[x,y,z]^2+VzMf[x,y,z]^2],{x,

      NVntP[F,S,r][[1]],NVntP[F,S,r][[2]]},

      {y,NVntP[F,S,r][[3]],NVntP[F,S,r][[4]]},{z,

      NVntP[F,S,r][[5]],NVntP[F,S,r][[6]]}]]]];


NVntVmax[F_,S_,r_]:=

  Max[Table[

    Sqrt[VxMf[x,y,z]^2+VyMf[x,y,z]^2+VzMf[x,y,z]^2],{x,NVntP[F,S,r][[1]],

      NVntP[F,S,r][[2]]},{y,NVntP[F,S,r][[3]],NVntP[F,S,r][[4]]},{z,

      NVntP[F,S,r][[5]],NVntP[F,S,r][[6]]}]];
```